

# Gait shape control for 2-D.O.F bipedal robots using hybrid virtual holonomic constraints

by

Mohamed Al Lawati

A thesis  
presented to the University of Waterloo  
in fulfillment of the  
thesis requirement for the degree of  
Master of Applied Science  
in  
System Design Engineering

Waterloo, Ontario, Canada, 2014

© Mohamed Al Lawati 2014

I hereby declare that I am the sole author of this thesis. This is a true copy of the thesis, including any required final revisions, as accepted by my examiners.

I understand that my thesis may be made electronically available to the public.

## Abstract

Motion control for bipedal robots is an active research area because bipedal robots can perform tasks and work in terrain where wheeled robots cannot. Researchers have developed bipedal robots that are able to walk, run and perform predefined tasks such as stair climbing. Mimicking human motion is one of the potential benefits of bipedal robots. In the robotics and control literature, many controllers have been presented that achieve dynamically stable gait motions (i.e. stable walking). This thesis studies virtual holonomic constraint (VHC) based control laws that generate stable gaits for 2-DOF bipedal robots.

The planar 2-DOF robot under study is modelled as a hybrid automaton and consists of three physical components: a stance leg, a swing leg and a hip mass. The robot is actuated by a hip torque and an ankle torque. For the continuous phase, the dynamics of the robot are similar to a rigid double pendulum except that the robot has an “extra” mass attached to its hip position. At ground impact events, the system’s configuration variables are redefined and the associated velocities change instantaneously. The ground is modelled as an inclined surface with no curvature.

Due to the hybrid nature of 2-DOF bipedal robots, this thesis extends the notion of VHC to hybrid VHC for a general Euler-Lagrange system with impacts and applies it to a 2-DOF bipedal robot. For any desired gait of the 2-DOF robot, the motion of the swing leg can be expressed as a function of the stance leg. Using this function, a hybrid VHC is generated and the control objective becomes enforcing the hybrid VHC. A design procedure is developed that returns a feasible hybrid VHC for the 2-DOF bipedal robot.

The concept of VHC motivates the design of feedback linearizing controllers that drive the states of the robot to a constraint manifold. Feedback linearizing controllers are designed that enforce the hybrid VHC. In this framework, two possible control laws are presented. The first control law generates a fully actuated robot in closed-loop configuration. Sufficient conditions for stability are given and proven. The second control law yields an under-actuated system in closed-loop configuration. This control design is shown to consume no energy as long as the hybrid VHC that models a passive gait is enforced. The stability of this controller is studied numerically through the method of Poincaré sections.

## **Acknowledgements**

All my thanks and gratitude are to God, the Almighty, for his guidance throughout my whole life. This work wouldn't have been possible without the support from the Almighty.

I would like to thank Dr. Christopher Nielsen for his excellent supervision and guidance throughout my MASc. research. I learned lots of new and interesting stuff from him through this wonderful journey.

I am also thankful to Dr. Eihab Abdel-Rahman for his guidance especially in the early stages of my MASc. program.

Finally, I would like to thank my readers: Professor David Wang and Professor Glenn Heppler for their time and efforts reviewing my thesis.

## **Dedication**

I dedicate this work to the most beloved people I ever know.

My parents,

My brothers and sisters,

My uncles, and

My wife and son.

# Table of Contents

List of Tables	viii
List of Figures	ix
<b>1 Introduction</b>	<b>1</b>
1.1 Motivation and problem statement . . . . .	2
1.1.1 Problem statement . . . . .	3
1.2 Literature review . . . . .	5
1.3 Organization and contributions . . . . .	14
<b>2 Modelling</b>	<b>16</b>
2.1 Hybrid dynamical systems . . . . .	16
2.2 Hybrid model of 2-D.O.F. bipedal robot . . . . .	21
2.2.1 Continuous-time dynamics . . . . .	22
2.2.2 Discrete-time dynamics . . . . .	27
2.2.3 The hybrid model . . . . .	33
<b>3 Open-loop gaits</b>	<b>36</b>
3.1 Orbital stability . . . . .	37
3.2 Passive 2-D.O.F. bipedal robot . . . . .	40
3.2.1 Numerical stability test using Poincaré’s method . . . . .	42
3.2.2 Modelling passive gaits as hybrid virtual holonomic constraints . . . . .	47

<b>4</b>	<b>Hybrid virtual holonomic constraints</b>	<b>49</b>
4.1	Virtual holonomic constraints . . . . .	49
4.2	Hybrid virtual holonomic constraints . . . . .	51
4.3	Virtual holonomic constraints applied to the 2-D.O.F bipedal robot . . . . .	55
4.3.1	Polynomial design generating a hybrid V.H.C. . . . .	59
4.4	State transformation . . . . .	62
4.5	Feedback linearization yielding a fully actuated closed-loop configuration . . . . .	67
4.5.1	Simulation results . . . . .	67
4.5.2	Stability analysis . . . . .	70
4.6	Feedback linearization yielding an under-actuated closed-loop configuration . . . . .	74
4.6.1	Stability study . . . . .	76
4.6.2	Optimal control effort . . . . .	82
<b>5</b>	<b>Conclusions and future work</b>	<b>85</b>
	<b>APPENDICES</b>	<b>87</b>
<b>A</b>	<b>Appendix A</b>	<b>88</b>
<b>B</b>	<b>Appendix B</b>	<b>90</b>
	<b>References</b>	<b>92</b>

# List of Tables

1.1	The choices made for $\phi_1$ and $\phi_2$ in [25]. . . . .	10
1.2	The human-behaviours studied in [32]. . . . .	12
2.1	Input torque vector components. . . . .	25
3.1	Parameters used in simulations. . . . .	40
4.1	Values of gains in Equation (4.30). . . . .	68
4.2	Values of gains in Equation (4.35). . . . .	75
4.3	Eigenvalues of the linearized Poincaré map near fixed points. . . . .	80

# List of Figures

1.1	Passive runner. . . . .	6
1.2	All forces and moments acting on foot. . . . .	7
1.3	The 5-degrees-of-freedom bipedal robot studied in [32]. . . . .	13
2.1	Graphical representation of the bouncing ball hybrid system. . . . .	19
2.2	Water cooling system using a bang-bang controller. . . . .	20
2.3	Graphical representation of water cooling hybrid system. . . . .	21
2.4	The actuation torques, $\tau_1$ and $\tau_2$ , of the 2-DOF bipedal robot. In Figure 2.4a, the $x'$ -axis is parallel to the walking surface. . . . .	23
2.5	Two models for the continuous dynamics of the 2-DOF bipedal robot. . . . .	24
2.6	Ground modelled in local coordinate system. . . . .	28
2.7	Collision event. . . . .	30
2.8	Graphical representation of the 2-DOF bipedal robot hybrid system. . . . .	34
3.1	From rimless wheel to passive 2-DOF bipedal robot. . . . .	37
3.2	An illustration of Poincaré’s method for determining orbital stability of a closed-orbit $\gamma$ . . . . .	39
3.3	A typical closed-orbit for the the 2-DOF bipedal robot. . . . .	41
3.4	Angular position and angular velocity of leg 2 as functions of time. . . . .	41
3.5	The passive gait is sensitive to initial conditions. . . . .	42
3.6	Poincaré map of the passive 2-DOF bipedal robot (leg 2). . . . .	45
3.7	Poicaré sections. . . . .	46

3.8	Functional relation between the swing and stance legs over a gait cycle. . .	47
4.1	Feasible versus non-feasible VHCs. . . . .	50
4.2	A $p$ polynomial satisfying (4.11) results in a gait pattern not necessarily the same as the passive gait pattern. . . . .	69
4.3	The regulation of $\xi_1$ using a VHC based controller, VHC approximating passive-gait based controller and a hVHC based controller. . . . .	69
4.4	Location of the ZMP for the fully actuated closed-loop configuration utilizing different constraints. . . . .	70
4.5	This figure shows the tracking of $\eta_1$ to $\eta_1^{\text{ref}}$ , which <i>approximates</i> a passive gait. . . . .	71
4.6	The controller increases the region of attraction of the passive HLC. . . . .	72
4.7	The polynomial $p$ satisfying (4.11). . . . .	75
4.8	The regulation of $\xi_1$ using a VHC-based controller and a hVHC-based controller. . . . .	76
4.9	The regulation of $\xi_1$ using a VHC-based controller and a hVHC-based controller. . . . .	77
4.10	The dynamics on $\hat{\Gamma}$ are divided into three regions. Region 1 yield stable solutions whereas Region 2 yields marginally stable solutions. Region 3 could lead to stable or marginally stable solutions. . . . .	77
4.11	Regions 1 and 2 on $\hat{\Gamma}$ . . . . .	79
4.12	Region 3 on $\hat{\Gamma}$ . . . . .	79
4.13	Poincaré map $\mathbf{g}$ restricted to $\hat{\Gamma}$ for all three regions. . . . .	80
4.14	Phase-portrait of rimless wheel with solutions. . . . .	81
4.15	Optimal controller utilizing an approximation of the passive gait shape. . .	84
A.1	Alternative models found in literature. . . . .	88

# Chapter 1

## Introduction

Imagine you want to draw a circle on a sheet of paper. You can either do so by using a guide like, for example, a coin. Otherwise, you can do a free-hand drawing of the circle. In the former case, you have a physical object that “enforces” the motion of your hand. In other words, the object constrains the movement of your hand. In the latter, your hand is physically free to move in any direction on the plane of the paper since there is no physical constraint acting on the motion. It is still possible to draw the circle in this case because your brain and motor control system “enforce” your hand to follow the desired shape. The enforcement by your brain and motor control system can be viewed “as if” a physical constraint is present. This type of constraint is what we call a “virtual constraint”. Virtual constraints, unlike physical constraints, can be easily and quickly changed depending on the application.

In this thesis, the “virtual holonomic constraint” (VHC) approach is taken to dynamically stabilize a 2-degrees of freedom (2-D.O.F.) walking bipedal robot. In simple words, dynamic stability of walking robots means “stable-while-walking”. The word “holonomic” simply means that the constraint depends only on the coordinates (i.e. positions) and not on the velocities.

Following the framework of Teel et al. [1], the 2-DOF bipedal robot under study is modelled as a “hybrid system”. A hybrid model captures the continuous-time behaviour of a system as well as its discrete-time behaviour, which makes it a powerful modelling tool for many real-life systems. Further discussion on hybrid systems is presented in Chapter 2.

This thesis extends the notion of VHC of [2] to “hybrid VHC” for an Euler-Lagrange system with impacts. Due to the flexibility that virtual constraints based controllers offer,

a large family of gait “shapes” can be easily achieved. In addition, invariance of these gait shapes is guaranteed by properly designing a hybrid VHC (Chapter 4).

## 1.1 Motivation and problem statement

This work is motivated by the idea of passive walkers pioneered by McGeer in early 1990s [3]. The gravitational field is the only source of energy in passive walkers, thus, generating “free” gaits. These gaits can be viewed as hybrid limit cycles in the state-space of these systems. However, being an open-loop system, the limit cycles in free gaits have relatively small regions of attraction. Furthermore, there is no ability to change the stable motion induced by the gravitational field. This naturally suggests the use of feedback control to increase the region of attraction and stabilize alternate, non-free, gaits.

The approach taken in this thesis is to view a hybrid limit cycle in the state-space of a 2-DOF bipedal robot as a constraint imposed between the two legs: stance and swing. The constraint is modelled as a functional relationship between the configuration variables of the robot. In general, the functional constraint can be any sufficiently smooth function, but in practice it is convenient to use constant coefficient polynomials. The functional constraint defines a subset of the robot’s state space which we call the constraint manifold. When the system is restricted to evolve on the constraint manifold, the robot follows the desired gait. The control design problem then reduces to the problem of stabilizing the constraint manifold. We achieve this objective by using feedback linearization.

Recently, the notion of VHC has been formalized in the literature [2] for continuous-time Euler-Lagrange systems. Our work differs from [2] on virtual constraints because the systems we consider are naturally modelled as hybrid systems. Hence we call our constraints hybrid virtual holonomic constraints. In this thesis, we define the idea of feasible hybrid virtual holonomic constraints and introduce a design procedure that systematically creates feasible constraints that produce desired gaits for a 2-DOF bipedal robots. Finally, we use feedback linearizing controllers in order to enforce our hybrid VHC yielding two possible close loop configuration: fully actuated and under-actuated configurations.

### 1.1.1 Problem statement

Consider an Euler-Lagrange system with an  $N$ -dimensional configuration space<sup>1</sup>  $\mathcal{Q}$  and  $m$  control inputs  $\tau \in \mathbb{R}^m$ . The model is given by

$$\frac{d}{dt} \frac{\partial L}{\partial \dot{q}} - \frac{\partial L}{\partial q} = B(q)\tau \quad (1.1)$$

where  $L(q, \dot{q})$  is the Lagrangian function. We assume that  $L$  is smooth and has the form  $L(q, \dot{q}) = K(q, \dot{q}) - P(q)$  where  $K(q, \dot{q}) = (1/2)\dot{q}^\top M(q)\dot{q}$  is the system's kinetic energy and  $P : \mathcal{Q} \rightarrow \mathbb{R}$  is the system's potential energy. The inertia matrix  $M(q)$  is positive definite for all  $q \in \mathcal{Q}$ . Furthermore,  $B : \mathcal{Q} \rightarrow \mathbb{R}^{N \times m}$  is assumed to be smooth and full rank for all  $q \in \mathcal{Q}$ . The system can be rewritten in the standard vector form

$$M(q)\ddot{q} + C(q, \dot{q})\dot{q} + G(q) = B(q)\tau \quad (1.2)$$

where  $C(q, \dot{q}) \in \mathbb{R}^{N \times N}$  represents the centripetal and Coriolis terms and  $G(q) = \nabla P(q) \in \mathbb{R}^N$  represents the gravitation effects [6]. In this thesis, we assume that  $\mathcal{Q} \simeq \mathbb{R}^N$ . System (1.2) models a very large class of physical systems including the bipedal robots studied in this thesis.

When a bipedal robot's feet hit the ground, the dynamical model (1.2) undergoes an instantaneous change in its states  $(q, \dot{q}) \in \mathcal{Q} \times \mathbb{R}^N$ . We assume single support at impact instants, i.e. only one leg touches the ground at impacts. This observation motivates us to define an "impact surface"  $\mathcal{S} \subset \mathcal{Q} \times \mathbb{R}^N$ . The impact surface has the property that when  $(q, \dot{q}) \in \mathcal{S}$ , the states instantaneously change to  $(q^+, \dot{q}^+) = J(q, \dot{q})$  where  $J : \mathcal{Q} \times \mathbb{R}^N \rightarrow \mathcal{Q} \times \mathbb{R}^N$  is smooth. The "+" superscript refers to states just after impact.

These observations motivate us to define special class of hybrid Euler-Lagrange system, denoted  $\text{EL}_{\mathcal{H}}$ , given by

$$\text{EL}_{\mathcal{H}} : \quad \begin{cases} M(q)\ddot{q} + C(q, \dot{q})\dot{q} + G(q) = B(q)\tau, & (q, \dot{q}) \notin \mathcal{S} \\ (q^+, \dot{q}^+) = J(q, \dot{q}), & (q, \dot{q}) \in \mathcal{S}. \end{cases} \quad (1.3)$$

The topic of virtual holonomic constraints for Euler-Lagrange systems was investigated in [2]. We recall the definition below.

---

<sup>1</sup> In mechanics, a configuration of an arbitrary object is the specification of the position of every point in this object relative to a fixed reference frame [4]. A configuration space of a robot is the space of all configurations of the robot [5].

**Definition 1.1.1** ([2]). A virtual holonomic constraint (VHC) of order  $k$  for System (1.2) is a relation  $h(q) = 0$  where  $h : \mathcal{Q} \rightarrow \mathbb{R}^k$  is smooth,  $\text{rank}(dh_q) = k$  for all  $q \in h^{-1}(0)$ , and the set

$$\Gamma := \{(q, \dot{q}) : h(q) = dh_q \dot{q} = 0\} \quad (1.4)$$

is controlled invariant. That is, there exists a smooth feedback  $\tau(q, \dot{q})$  such that  $\Gamma$  is positively invariant for the closed-loop system. The set  $\Gamma$  is called the **constraint manifold** associated with the VHC  $h(q) = 0$ . A VHC is **stabilizable** if there exists a smooth feedback  $\tau(q, \dot{q})$  that asymptotically stabilizes  $\Gamma$ . In this case  $\tau(q, \dot{q})$  is said to **enforce the VHC**  $h(q) = 0$ .

It is convenient to adopt a parametric description of the VHC in which the first  $k$  configuration variables are expressed as smooth functions of the remaining  $N - k$  configuration variables

$$\begin{aligned} q_1 &= \phi_1(q_{k+1}, \dots, q_N) \\ q_2 &= \phi_2(q_{k+1}, \dots, q_N) \\ &\vdots \\ q_k &= \phi_k(q_{k+1}, \dots, q_N). \end{aligned} \quad (1.5)$$

Here,  $h(q) = \text{col}(q_1 - \phi_1(q), \dots, q_k - \phi_k(q))$ . If  $q_{k+1}, \dots, q_N$  are angular variables, then the set  $h^{-1}(0)$  is an  $(N - k)$ -dimensional torus. We are now ready to state the general problem considered in this thesis.

**Hybrid VHC enforcement problem :** Given a hybrid Euler-Lagrange system (1.3) and a virtual holonomic constraint of order  $k$ , find if possible, a feedback control law  $\tau(q, \dot{q})$  such that.

- (i) The feedback enforces the VHC for the continuous-time dynamics in (1.3) in the sense of Definition 1.1.1.
- (ii) The constraint manifold is invariant under the discrete-time dynamics in (1.3), i.e.,

$$J(\mathcal{S} \cap \Gamma) \subseteq \Gamma. \quad (1.6)$$

- (iii) The dynamics (1.3) restricted to  $\Gamma$  satisfy application specific constraints such as boundedness, no finite-escape time, trajectory tracking, etc.

•

The above problem is quite general. In this thesis we study a specialized version of the problem applied to a simple bipedal walker. As we show in Chapter 2, the bipedal walker is a system of the form (1.3) with  $N = 2$ ,  $m = 2$  and where the impact surface  $\mathcal{S}$  is determined by the terrain on which the bipedal robot is walking on. We will consider VHC of order 1 parameterized as in (1.5). In this case, the function  $\phi_1 : \mathbb{R} \rightarrow \mathbb{R}$  that defines the VHC  $h(q) = q_1 - \phi_1(q_2)$  will be chosen so that the robot walks with a desired gait. By changing the function  $\phi_1$  we can stabilize different “gait shapes” including the shape associated with passive motion.

## 1.2 Literature review

Planar 2-DOF bipedal robots have been extensively studied in the literature in both open-loop and closed-loop configurations. For open-loop configurations, also known as compass-gaits, the idea of 2-DOF planar passive walking was introduced by McGeer [3]. A passive 2-DOF walker consists of two rigid links connected by a revolute joint at the hip position. On gentle slopes, the walker can achieve stable dynamic walking provided its inertial parameters are designed carefully and it has been given the right “push” initially.

A 2-DOF bipedal robot can be modelled as a hybrid system. This thesis utilizes the framework of Goebel et al. [1] to model hybrid systems (Chapter 2). In [1], hybrid dynamical systems are generally written as differential and difference inclusions. Reference [7] also models mechanical Lagrangian systems with frictionless impacts using differential inclusions, where the dynamics belong to some admissible set. In their work, they design an observer for estimating velocities using position measurement for mechanical Lagrangian systems with frictionless impacts.

As an extension to the idea of passive 2-DOF bipedal robots, kneed passive walkers were analyzed and built [8]. Using a linear spring at each leg and a torsional spring at the hip joint, the 2-DOF bipedal robot can accomplish passive running [9]. Figure 1.1 roughly illustrates passive running stages. Stage (a) shows when the walker has landed on the ground. The compression of the linear spring in the green leg causes the robot to jump off-ground and enter stage (b). At stage (b), the torsional spring at the hip “corrects” the position of the legs making the red leg ready to land. Once the red leg lands in stage (c), the stages (a) – (c) are repeated. Subsequently, further studies on open-loop passive walkers were carried out by Goswami et al. [10], [11] and [12]. Reference [10] presents detailed modelling of a compass-gait assuming point-mass model for the two legs. However, our

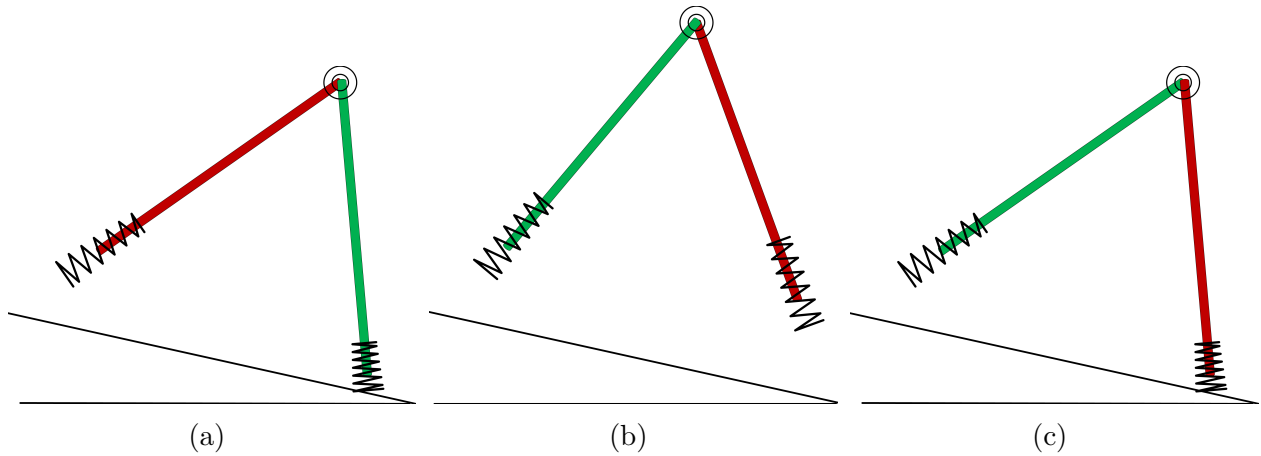


Figure 1.1: Passive runner.

model (Chapter 2) accounts for geometry of the two legs. Bifurcation of hybrid limit cycles is numerically studied in [12] using the ideas of a Poincaré map and chaos was reported.

Several control methodologies have been developed and applied to bipedal robots. Zero moment point (ZMP) is one of the earliest attempts in achieving stable gaits. The notion of ZMP was first explicitly introduced in 1972 [13] and appeared in practice in Japan in 1984. The idea of ZMP requires a robot to have a foot for each leg and can be described as follows. Consider Figure 1.2, which shows only a foot in equilibrium during single-support phase. The applied load from the rest of the mechanism reduces to a force and moment about the center of mass (CoM) acting on the foot, denoted by  $\vec{F}_A$  and  $\vec{M}_A$ . The weight of the foot,  $\vec{W}$ , acts at CoM and the reaction ( $\vec{R}$  and  $\vec{M}$ ) is applied at  $P$ . Physically, the ground is able to support the foot due to the presence of pressure *by* the ground *on* the foot and the presence of static friction.

The pressure always acts along the vertical direction towards the positive  $z$  axis. As known in mechanics, pressure is a distributed force that acts at all contact points between the foot and ground. Therefore, the effect of the pressure can be described by a single vertical force applied at point  $P$ , where  $P$  being the center of pressure (CoP). Also, the effect of the friction can be described by a force and moment at point  $P$ . The combined effect of pressure and friction is reaction force  $\vec{R}$  and reaction moment  $\vec{M}$  (Figure 1.2). In static equilibrium, the pressure balances (i) the vertical component of  $\vec{F}_A$  ( $F_{A_z}$ ) (ii) horizontal components of  $\vec{M}_A$  ( $M_{A_x}$  and  $M_{A_y}$ ) (iii) the horizontal components of moments induced by  $\vec{F}_A$  about CoM. It is noted that an increase in the magnitude of (i), (ii) or (iii) results

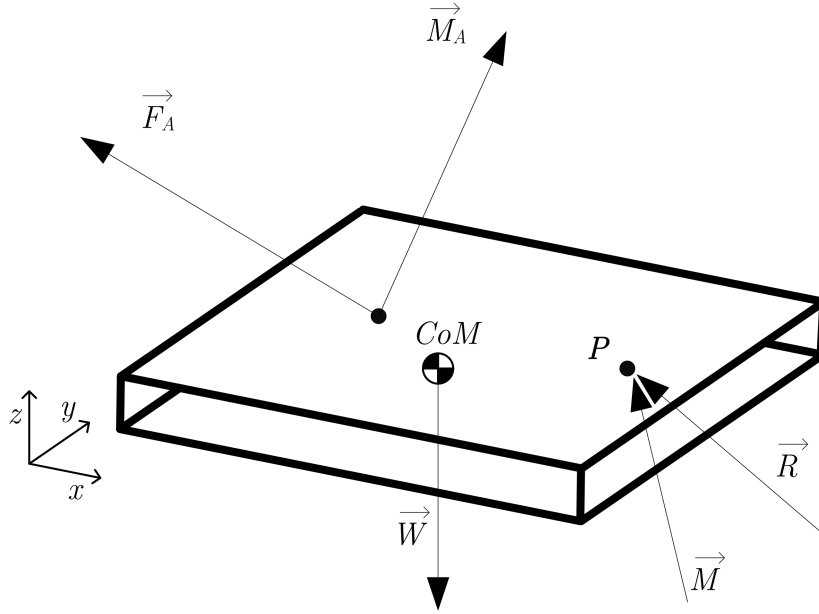


Figure 1.2: All forces and moments acting on foot.

in increasing the distance between CoM and  $P$ , i.e.  $P$  shifts further. The static friction is acting on the foot at all ground contact points and lies in the horizontal plane. Its effect can be described by

- the horizontal components of  $\vec{R}$ , namely,  $R_x$  and  $R_y$ , and
- the vertical component of  $\vec{M}$ , namely,  $M_z$ .

In static equilibrium, these components balance horizontal components of the applied forces  $\vec{F}_A$ , applied moments  $\vec{M}_A$  and the induced moments by  $\vec{F}_A$ . Now, since all the applied forces on the foot are balanced by the reaction components  $R_x, R_y, R_z$  and  $M_z$ , static equilibrium implies that

$$M_x = M_y = 0 \quad (1.7)$$

Therefore, the necessary and sufficient condition for the static equilibrium is that the point  $P$  (or called ZMP) must remain inside the foot contact surface. In this case,  $ZMP \equiv CoP$ .

ZMP can be viewed as the point where the normal “pressure force” should act in order to balance all applied vertical forces and horizontal moments. As the normal applied force

and/or applied horizontal moment on the foot increase, ZMP shifts further from CoM to balance the effect of the additional load in order to keep the foot statically balanced. Obviously, the foot contact area may not be large enough to accommodate this point. As a result, the point  $P$  may exist outside the foot contact area and is referred to as **fictitious zero moment point (FZMP)** [14]. It becomes clear that if FZMP exists, the foot can no more support the total applied vertical moments causing a net overturning moment on the foot. As a final note, FZMP is not equivalent to CoP.

ZMP based controllers ensure that the point  $P$  remains within the foot contact area by calculating pre-defined trajectories for the whole mechanism. Among the drawbacks of ZMP based controllers is that the calculation of pre-defined trajectories may be computationally expensive. Adding to that, the larger load on the foot requires larger foot area in contact with ground. The control approach taken in this thesis assumes point contact with the ground and does *not* need any pre-computed trajectories in order to achieve stable walking (Chapter 4). However, the bipedal robot model in this thesis assumes the presence of ankle torque and, hence, requires feet (Chapter 2). For all closed-loop configurations presented in this thesis, the ZMP is shown through simulation to stay within a reasonable range.

Several control designs have been developed that do not rely on pre-computed trajectories. Asano et al. proposed “virtual passive” walking on level ground [15]. The idea is as follows. Consider a 2-DOF passive bipedal robot. Although no applied torque is acting, the force by gravity (which is conservative) applies “virtual” torques at the joints, denoted by  $\tau_g$ . The expression of  $\tau_g$  is straightforward to evaluate and is explicitly shown in [15], which depends on the current states of the robot. Now, to make this robot walk actively on level-ground,  $\tau_g$  is applied at the ankle and hip positions mimicking the effect of a virtual gravity field. This approach avoids computation of pre-defined trajectories since the control law depends on the actual states. The drawback is that only passive gait patterns are possible.

As an extension to this work, Asano et al. constrain the total mechanical energy  $E$  of the robot in order to generate a wider range of gait patterns [16]. Their fundamental idea is based on two observations:

- In a passive gait cycle,  $E$  is monotonically increasing in the single-support phase.
- At ground impact,  $E$  drops instantly. This drop in the value of  $E$  is restored again at the end of the single-support phase.

As another approach to control design of bipedal robots, *virtual holonomic constraint* (VHC) is one of the most recent and popular approaches in the field. This approach for bipedal robots control was pioneered by Grizzle et al. [17]. The theory is well developed and established in [17]. Among the advantages of VHC approach is that it does *not* require a pre-computed trajectory and allows for a large variety of gait “shapes” to be accomplished.

Aside to bipedal robots, Shiriaev et al. used the notion of VHC to find an integral of motion of the “reduced system” (or “zero dynamics” as called by others) of a class of  $n$ -DOF mechanical systems subject to  $n - 1$  VHC [19]. The idea is summarized as follows. Consider an under-actuated Euler-Lagrange system with configuration variables  $q \in \mathbb{R}^n$  and input  $u \in \mathbb{R}^{n-1}$ . Define the relations which relates  $n - 1$  configuration variables to the remaining one as

$$q_1 = \phi_1(\theta), q_2 = \phi_2(\theta), \dots, q_{n-1} = \phi_{n-1}(\theta), q_n = \theta \quad (1.8)$$

These relations (1.8) constitute the VHC. Now, suppose that there exists some control input that enforces the given Euler-Lagrange system to (1.8). Then, the dynamics of the Euler-Lagrange system restricted to the surface defined by (1.8) are second order and are given by [18]

$$\alpha(\theta)\ddot{\theta} + \beta(\theta)\dot{\theta}^2 + \gamma(\theta) = 0. \quad (1.9)$$

It is worth noting that the dynamics (1.9) have several names in the bipedal robot literature such as “virtual limit system” as in [18], “zero dynamics” as in [17] and “reduced dynamics” as in [2].

System (1.9) has an integral of motion (also called a first integral of the system) of the form  $I(\theta, \dot{\theta}, \theta_0, \dot{\theta}_0)$  that preserves its initial value. An explicit expression for  $I(\theta, \dot{\theta}, \theta_0, \dot{\theta}_0)$  is given in [19], [20] and [18]. Reference [21] further studies the properties of Equation (1.9). A similar integral of motion is independently developed by Maggiore et al. in [2].

The integral of motion is useful to study qualitative behaviour of the zero dynamics of a given system. However, the expression of the zero dynamics of the system studied in this thesis is quite complicated making it difficult to evaluate and use an analytical expression of the integral of motion. In the bipedal robots literature, the integral of motion is used to analyze the closed-loop stability of under-actuated Euler-Lagrange systems. References [22] and [23] introduce a procedure to find the “correct” initial conditions that converge to a hybrid limit cycle of a compass-gait. Their procedure is based on the calculation of integral motion and a solution to a minimization problem for the system parameters.

For closed-loop configurations, the integral of motion is used to come up with transverse coordinates of a three-link bipedal robot (with the third link being the torso) [24]. The

work of [24] is described and summarized as follows. Let  $q = \text{col}(q_1, q_2, q_3)$  be the configuration variable vector of the three-link bipedal robot where  $q_1, q_2, q_3$  represent the angular positions of the stance leg, the swing leg and the torso, respectively. Also, let  $y_1 : \mathbb{R} \rightarrow \mathbb{R}$  and  $y_2 : \mathbb{R} \rightarrow \mathbb{R}$  be two output functions such as

$$\begin{aligned} y_1 &= q_2 - \phi_1(q_1) \\ y_2 &= q_3 - \phi_2(q_1) \end{aligned} \tag{1.10}$$

where  $\phi_1$  and  $\phi_2$  represent a VHC that defines a desired periodic hybrid trajectory  $q_\star = \text{col}(q_{1\star}, q_{2\star}, q_{3\star})$ . On the desired periodic hybrid trajectory, we have

$$\begin{aligned} y_1 &= 0 \\ y_2 &= 0 \\ I(q_{1\star}(t), \dot{q}_{1\star}(t), q_{1\star}(0), \dot{q}_{1\star}(0)) &= 0 \end{aligned} \tag{1.11}$$

Furthermore, if a trajectory stays on the desired periodic hybrid orbit then (1.11) holds with  $\dot{y}_1 = \dot{y}_2 \equiv 0$ . This discussion motivates the following transformed states

$$z := \text{col}(q_1, y_1, \dot{y}_1, y_2, \dot{y}_2, I) \in \mathbb{R}^6 \tag{1.12}$$

The last 5 states in (1.12) are transversal to the desired orbit whereas the first state in (1.12) is tangential to desired orbit. Since a periodic hybrid trajectory is assumed to exist, the stability of this periodic trajectory is equivalent to the stability of the origin of the transversal coordinates  $\zeta := \text{col}(y_1, \dot{y}_1, y_2, \dot{y}_2, I) \in \mathbb{R}^5$ . Stability is studied by calculation of the eigenvalues of the linearized transversal system.

Reference [25] designs controllers based on VHC for a three-link bipedal robot with the third link being the torso as follows. Let  $\theta_1(t), \theta_2(t)$  and  $\theta_3(t)$  represent the stance leg angle, swing leg angle and torso angle, respectively. The VHC is formed by writing  $\theta_2$  and  $\theta_3$  as smooth functions of  $\theta_1$  (i.e.  $\theta_2 = \phi_1(\theta_1(t))$  and  $\theta_3 = \phi_2(\theta_1(t))$ ). Table 1.1 describes the choices made for  $\phi_1$  and  $\phi_2$ . Then, two output functions  $h_1 : \mathbb{R} \rightarrow \mathbb{R}$  and  $h_2 : \mathbb{R} \rightarrow \mathbb{R}$  are

Table 1.1: The choices made for  $\phi_1$  and  $\phi_2$  in [25].

Constraint	Description
$\phi_1(t) := -\theta_1(t)$	Motion of stance leg is a mirror image of swing leg.
$\phi_2(t) := \theta_3^d$	$\theta_3^d$ is constant meaning that the torso is desired to be at a fixed height.

defined yielding a well defined relative degree of 2 for each output function. This allows

for feedback-linearizing controllers to be designed. In this thesis, this approach is taken for control design (Chapter 4). In [25], gait stability in closed-loop configuration is studied numerically using the method of Poincaré sections. We adapt similar Poincaré analysis for an open-loop 2-DOF bipedal robot (Chapter 3). In addition to that, reference [26] proposes and proves the following result. Given a  $n$ -DOF bipedal robot and a VHC of order  $k$ , let  $P$  be a Poincaré map for the full-order robot model and  $\rho$  be the associated Poincaré map of the dynamics restricted to the constrain manifold. Then the following two statements are equivalent:

- $x^* \in \mathbb{R}^n$  is an exponentially stable fixed point of  $P$ ,
- $x^* \in \mathbb{R}^n$  is an exponentially stable fixed point of  $\rho$ .

This result is used in Section 4.6.1 to discuss stability of the proposed controller.

It is left to note that a formal explicit definition of VHC was missing in the literature until Maggiore et al. formalized the definition of VHC of order  $k$  [2] in 2013. They further introduced the notion of **regular VHC**, which yields an input-output linearizable system [2]. This thesis extends the notion of regular VHC presented in [2] to **hybrid regular VHC** for hybrid Euler-Lagrange systems of form (1.3). Hybrid regular VHC are then applied to a 2-DOF bipedal robot.

Among the recent experimental bipedal robot platforms is MABEL [27]. MABEL is a 2D five-link bipedal robot that consists of two kneed legs and a torso. The robot has no feet and its legs encounter point contact with ground. MABEL is an under-actuated robot with one degree of under-actuation. For each leg, the two actuated degrees of freedom are the angular position of the virtual line connecting the hip to the toe and the length of this virtual line [27]. It has been shown in [28] that using virtual constraints, MABEL is able to walk and to reject disturbances when ground steps down for upto 5.08 cm. A down-step more than 5.08 cm caused the swing leg of MABEL to be destroyed. Video available at [29]. The main reason for breaking the swing leg after stepping down was the rapid oscillations of the torso [30]. On the other hand, stepping-up caused lots of oscillations in the vertical ground reaction, which caused the robot to fall after the step-up [30].

To tackle the problem of MABEL passing through uneven terrain, reference [30] characterises different ground disturbance scenarios and uses a finite-state machine to switch to the appropriate controller for each type of ground disturbance. The characterised ground disturbances are: step-up, step-down and tripping. Tripping can occur if the swing leg hits an upfront obstacle or it encounters an early ground impact event. The depth of a step-up or a step-down at ground impacts is detected by knowing the current joint angles and the

length of each leg. Tripping is detected by using contact switches located at robot’s shins and bottom of toes, and the knowledge of the current configuration of the robot. Video of MABEL going through a down-step of  $\approx 20$  cm is found at [31].

Recently, researchers have been concerned about building robots that mimic human gaits. Reference [32] presents the so-called **human-inspired control**, which is applied to a bipedal robot model of 5-degrees-of-freedom. The model consists of a stance leg, a stance thigh, a non-stance leg, a non-stance thigh and a torso link, see Figure 1.3a. The coordinates of the configuration space,  $\mathcal{Q}$ , are denoted by  $\theta := \text{col}(\theta_{sf}, \theta_{sk}, \theta_{sh}, \theta_{nsh}, \theta_{nsk})$ . Fundamentally, the author defines a set of human-inspired output functions that represent certain human walking behaviours. These behaviours are experimentally verified to have a form of either a linear function of time or a second-order system response as,

$$y(t) = vt \tag{1.13}$$

or,

$$y(t) = e^{-\zeta\omega_n t} (c_0 \cos(\omega_d t) + c_1 \sin(\omega_d t)) + g \tag{1.14}$$

The human behaviours studied in [32] are  $\delta p_{\text{hip}}(\theta)$ ,  $\delta m_{\text{nsl}}(\theta)$ ,  $\theta_{sk}$ ,  $\theta_{nsk}$  and  $\theta_{\text{tor}}(\theta)$ , see Figure 1.3b and Table 1.2. For mathematical expressions of these behaviours, the reader is referred to [32].

Table 1.2: The human-behaviours studied in [32].

<b>Behaviour</b>	<b>Description</b>
$\delta p_{\text{hip}}(\theta)$	Linearization of the $x$ -position of the hip.
$\delta m_{\text{nsl}}(\theta)$	Linearization of the line connecting the hip to the ankle of the non-stance leg.
$\theta_{\text{tor}}(\theta)$	The angle of the torso with reference taken to be the vertical line.

Based on experimental data, it turns out that  $\delta p_{\text{hip}}(\theta)$  is of form (1.13) and the rest of the behaviours are of form (1.14). Given certain human gait behaviour, the associated constants of (1.13) or (1.14) are evaluated by least square fit using data from a real human gait.

The above discussion motivates the following output functions  $y_1 : \mathcal{Q} \rightarrow \mathbb{R}$  and  $y_2 :$

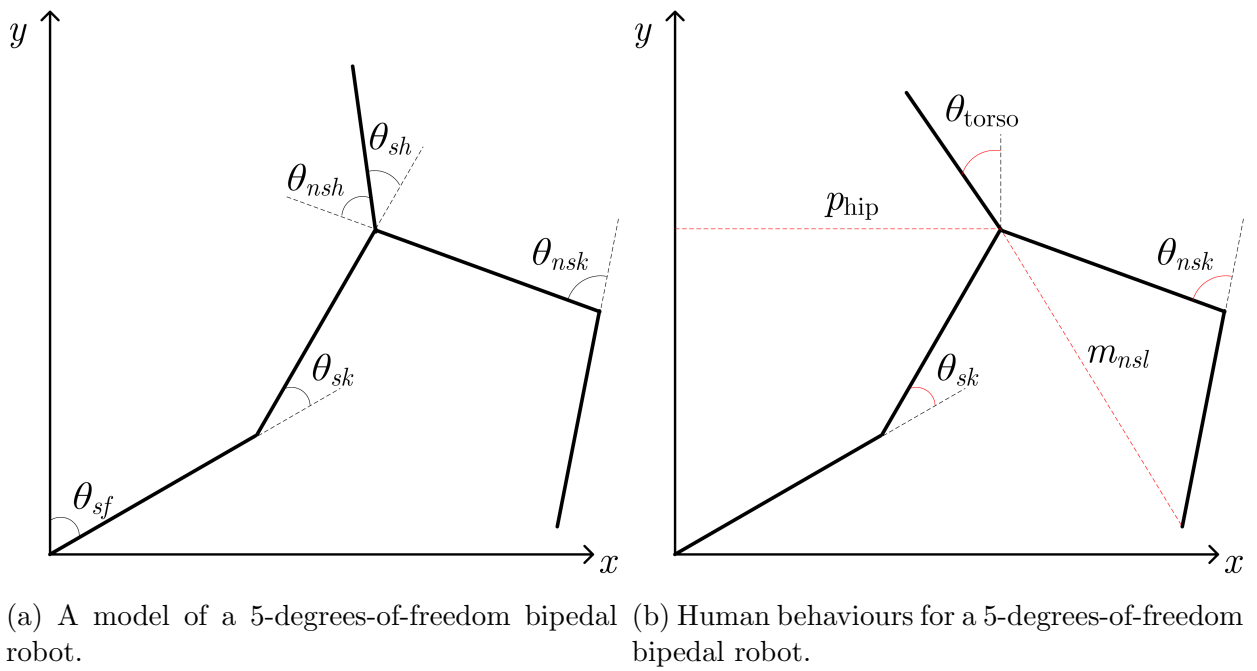


Figure 1.3: The 5-degrees-of-freedom bipedal robot studied in [32].

$\mathcal{Q} \rightarrow \mathbb{R}^4$  such that,

$$\begin{aligned} y_1(\theta) &= \delta p_{\text{hip}}(\theta) \\ y_2(\theta) &= \begin{bmatrix} \delta m_{nsl} \\ \theta_{sk} \\ \theta_{nsk} \\ \theta_{tor}(\theta) \end{bmatrix} \end{aligned} \tag{1.15}$$

The control objective becomes to derive the human behaviour functions (1.15) to zero and arrive at the hybrid zero dynamics of the system. However, reference [32] claims that it is difficult to maintain  $y_1(\theta) = 0$  under impact events. As a result, controllers are designed such that, under certain conditions,  $y_2(\theta) = 0$  is maintained invariant even under impact events. This gives rise to the term **partial hybrid zero dynamics**, which is introduced in [32].

In order to fulfil the control objective, feedback linearizing controllers were used resulting in two different closed-loop scenarios: full and under actuation. Those controllers were tested in simulation and on two physical robotic platforms, AMBER and NAO [32].

### 1.3 Organization and contributions

Chapter 2 introduces the model of the 2-DOF bipedal robot under study. A hybrid-system framework is followed. The continuous-time dynamics are modelled using an energy based approach, namely, Euler-Lagrange, whereas, under certain assumptions, the discrete-time dynamics are modelled by redefining coordinates at impact events and using the principle of conservation of angular momentum to model instantaneous change in velocities just after impact events.

Chapter 3 analyzes open-loop gaits, i.e. passive gaits, using the method of Poincaré sections. A numerical argument is made to show stability of the passive gait. Also, Chapter 3 views the passive gait as a functional relationship between stance and swing legs. This relation is approximated by a real-valued constant-coefficient polynomial.

Moving to controlled systems, Chapter 4 starts the discussion on VHC and extends it to hybrid VHC. Then, hybrid VHCs that define gait shapes are designed and used in closed-loop configurations. Chapter 4 presents two closed-loop configurations: fully actuated and underactuated configurations. Chapter 4 also discusses optimal control effort for the underactuated case.

The following are the main contributions of this work.

- Necessary and sufficient conditions for VHC that guarantee hybrid VHC, Section 4.3.
- As an extension to the result of Section 4.3, a design procedure is developed, which returns a feasible hybrid VHC.
- Section 4.5 presents sufficient conditions for dynamic stability of the fully actuated system in closed-loop configuration, which leads to the stability proof.
- Finally, Section 4.6 shows that if a hybrid VHC perfectly models the shape of a passive gait then, on the constraint manifold, the control torque can be designed such that it is identically zero.

# Chapter 2

## Modelling

The 2-DOF robot under study evolves according to both continuous-time and discrete-time dynamics. This means that the bipedal robot is an example of a hybrid system. In this chapter we review the hybrid systems formalism and show that the bipedal robot belongs to this class of systems.

### 2.1 Hybrid dynamical systems

A hybrid system (sometimes called a “hybrid automaton”) is a dynamical system with both continuous and discrete states. Many equivalent definitions of a hybrid automaton exist in systems and control literature. The interested reader is referred to [1], [33],[34] and [35]. In this thesis we adopt the definitions presented in [1].

The first order differential equation  $\dot{x} = f(x), x \in \mathbb{R}^n$  is common and widely used to model continuous-time dynamical systems. For hybrid systems, this model can further be expanded. First, the state vector  $x$  can be restricted to a subset  $C \subseteq \mathbb{R}^n$ . In a slider-crank mechanism, for example, this restriction might represent a slider moving along a line in space. Second, the function  $f(x)$  in the right-hand-side of the differential equation can be replaced by a general set that depends on the state vector  $x$ . This observation leads to a differential inclusion  $\dot{x} \in F(x)$ , where the map  $F(x)$  is set-valued. For more information on differential inclusions the reader is referred to [36]. We adopt the notation  $F : \mathbb{R}^m \rightrightarrows \mathbb{R}^n$  for a set-valued map from  $\mathbb{R}^m$  to  $\mathbb{R}^n$ . Combining these two generalizations leads to the constrained differential inclusion  $\dot{x} \in F(x), x \in C$ .

For discrete dynamical systems, the first order difference equation  $x^+ = g(x), x \in \mathbb{R}^n$  is a typical model. The notation  $x^+$  indicates that the next value of the state vector is given as a function of the current value  $x$  through the mapping  $g(x)$ . In hybrid dynamical systems we extend the first order difference equation to allow constrained difference equations and difference inclusions. This leads to the model  $x^+ \in G(x), x \in D$ , where  $G$  is a set-valued map and  $D \subseteq \mathbb{R}^n$ .

Using the above ideas, a general hybrid system is modelled with the following data

- The flow set  $C \subseteq \mathbb{R}^n$ .
- The set-valued flow map  $F : C \rightrightarrows \mathbb{R}^n$ .
- The jump set  $D \subseteq \mathbb{R}^n$ .
- The set-valued jump map  $G : D \rightrightarrows \mathbb{R}^n$ .

A shorthand notation for a hybrid system with this data is  $\mathcal{H} = (F, C, G, D)$ . Such systems can be written in the suggestive form

$$\mathcal{H} : \quad \begin{cases} \dot{x} \in F(x), & x \in C \\ x^+ \in G(x), & x \in D. \end{cases} \quad (2.1)$$

The model (2.1) captures a wide variety of dynamical behaviour. The generality afforded by (2.1) is often not needed. It is often the case that the set-valued maps and the corresponding inclusions can be replaced with equations.

The advantage of using the very general model (2.1) for a hybrid dynamical system is that it can be used to model hybrid automaton, switched systems, sampled-data control systems, and networked control systems. To make this advantage clear, we now introduce the notion of a hybrid automaton, based on the definition from [1], and then show how it can be modelled as a system of the form (2.1).

**Definition 2.1.1.** A hybrid automaton  $\mathcal{H}$  is a 6-tuple  $\mathcal{H} = (\mathcal{Q}, \text{Domain}, f, \text{Edges}, \text{Guard}, \text{Reset})$ , where

- $\mathcal{Q} = \{q_1, q_2, \dots\}$  is a set of modes which, in most situations, can be identified with a subset of the integers  $\mathbb{Z}$ .

- A **domain map**  $\text{Domain} : \mathcal{Q} \rightrightarrows \mathbb{R}^n$ , which gives, for each  $q \in \mathcal{Q}$ , the set  $\text{Domain}(q) \subseteq \mathbb{R}^n$  in which the continuous-time state  $\xi$  evolves.
- A **flow map**  $f : \mathcal{Q} \times \mathbb{R}^n \rightarrow \mathbb{R}^n$  which describes a differential equation that defines the continuous-time evolution of the continuous state variable  $\xi$ .
- A set of **edges**  $\text{Edges} \subset \mathcal{Q} \times \mathcal{Q}$  which identifies pairs  $(q, q')$  such that a transition from mode  $q$  to mode  $q'$  is possible.
- A **guard map**  $\text{Guard} : \text{Edges} \rightrightarrows \mathbb{R}^n$  which identifies, for each edge  $(q, q') \in \text{Edges}$ , the set  $\text{Guard}(q, q') \subset \mathbb{R}^n$  to which the continuous state  $\xi$  must belong so that a transition from  $q$  to  $q'$  can occur.
- A **reset map**  $\text{Reset} : \text{Edges} \times \mathbb{R}^n \rightarrow \mathbb{R}^n$  which describes, for each edge  $(q, q') \in \text{Edges}$ , the value to which the continuous state  $\xi \in \mathbb{R}^n$  is assigned during the transition from  $q$  to  $q'$ .

The pair  $(q, \xi) \in \mathcal{Q} \times \mathbb{R}^n$  is referred to as the **state** of  $\mathcal{H}$ .

The following example helps clarify the meaning of the objects in Definition 2.1.1.

---

**Example 2.1.1.** The bouncing ball system is a prototypical example of a hybrid system. The continuous-time dynamics of a bouncing ball can be written as

$$\begin{aligned}\dot{\xi}_1 &= \xi_2 \\ \dot{\xi}_2 &= -g\end{aligned}\tag{2.2}$$

where  $\xi_1$  represents the ball's height measured from the ground,  $\xi_2$  is ball's velocity and  $g$  is the gravitational acceleration constant. At the moment in time  $T \in \mathbb{R}$  when the ball hits the ground (i.e.  $\xi_1(T) = 0$ ,  $\xi_2(T) < 0$ ), the ball loses a fraction of its velocity and its new velocity, just after impact, equals  $-\epsilon\xi_2(T)$ ,  $\epsilon \in (0, 1)$  where  $\epsilon$  is constant and represents the coefficient of restitution. As a result, the ball starts moving upwards, evolving according to the differential Equation (2.2), with initial condition  $\xi_1(T^+) = 0$  and  $\xi_2(T^+) = -\epsilon\xi_2(T)$ .

In view of Definition 2.1.1, the bouncing ball system can be modelled as a hybrid automaton  $\mathcal{H} = (\mathcal{Q}, \text{Domain}, f, \text{Edges}, \text{Guard}, \text{Reset})$  where

- $\mathcal{Q} = \{q_1\}$ .

- The domain map is  $\text{Domain}(q_1) = \mathbb{R}^2$ .
- The flow map is  $f(q_1, \xi) = \text{col}(\xi_2, -g)$ .
- Edges =  $(q_1, q_1)$ .
- Guard  $(q_1, q_1) = \{\xi \in \mathbb{R}^2 : \xi_1 = 0, \xi_2 < 0\}$ .
- Reset  $(q_1, q_1, \xi) = \text{col}(\xi_1^+, \xi_2^+) = \text{col}(0, -\epsilon \xi_2)$ .

Figure 2.1 presents a common pictorial representation of the bouncing ball hybrid system.

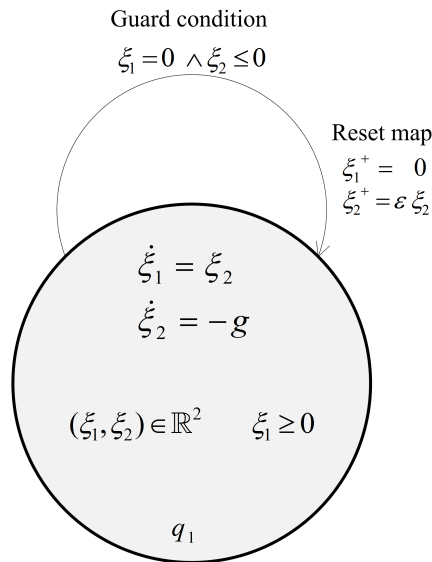


Figure 2.1: Graphical representation of the bouncing ball hybrid system.

△

---

The next example shows a hybrid system with two discrete states (modes).

---

**Example 2.1.2.** Consider Figure 2.2 which shows a bucket of water being cooled by a fan. The fan is operated by a relay-type controller. The objective is to keep the water temperature,  $\xi \in \mathbb{R}$ , below a given value  $T$ . The controller starts the fan when  $\xi \geq T + \epsilon$  and stops the fan when  $\xi \leq T - \epsilon$  where  $\epsilon > 0$  is a small positive constant.

Due to the switching in the controller, it is natural to model this system as a hybrid automaton as follows:

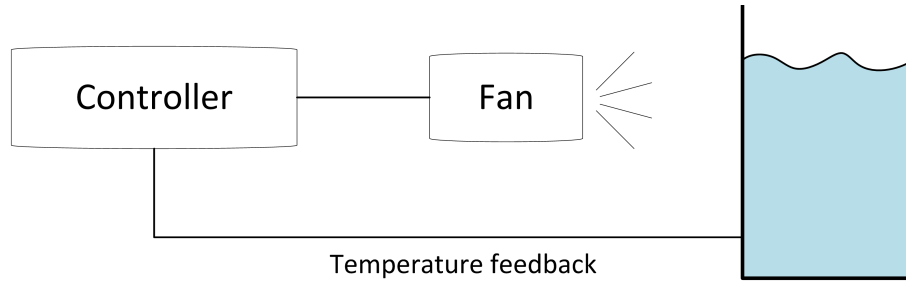


Figure 2.2: Water cooling system using a bang-bang controller.

- $\mathcal{Q} = \{q_1, q_2\}$  where  $q_1$  and  $q_2$  represent, respectively, the “ON” and “OFF” fan states.
- The associated domain map is

$$\text{Domain}(q_i) = \begin{cases} \{\xi \in \mathbb{R} : \xi \geq T - \epsilon\} & \text{if } i = 1, \\ \{\xi \in \mathbb{R} : \xi \leq T + \epsilon\} & \text{if } i = 2. \end{cases}$$

- Using Newton’s law of cooling, the flow map can be written as  $f(q_1, \xi) = -k_1(\xi - T_a)$  and  $f(q_2, \xi) = -k_2(\xi - T_a)$ , where  $T_a$  is the ambient temperature,  $k_1$  is the cooling constant and  $k_2$  is the heating constant. This tells us that if the fan is “ON” (i.e.  $q_1$  is active), the water temperature drops. And if the fan is “OFF” (i.e.  $q_2$  is active), the water temperature rises.
- Since the controller can switch from ON to OFF and from OFF to ON, the set of edges becomes  $\text{Edges} = \{(q_1, q_2), (q_2, q_1)\}$ .
- There are two guard conditions since there are two edges. The first guard condition  $\text{Guard}(q_1, q_2) = \{\xi \in \mathbb{R} : \xi < T - \epsilon\}$  has the following meaning. The system is at mode  $q_1$  is and, hence,  $\xi \geq T - \epsilon$ . To switch the system to mode  $q_2$ ,  $\xi$  must be less than  $T - \epsilon$ . Similarly, the second guard condition is  $\text{Guard}(q_2, q_1) = \{\xi \in \mathbb{R} : \xi > T + \epsilon\}$ , which has a similar interpretation.
- The reset map is simple in this case,  $\text{Reset}(q_1, q_2, \xi) = \text{Reset}(q_2, q_1, \xi) = \text{identity}$ .

Figure 2.3 shows a pictorial representation of the system.

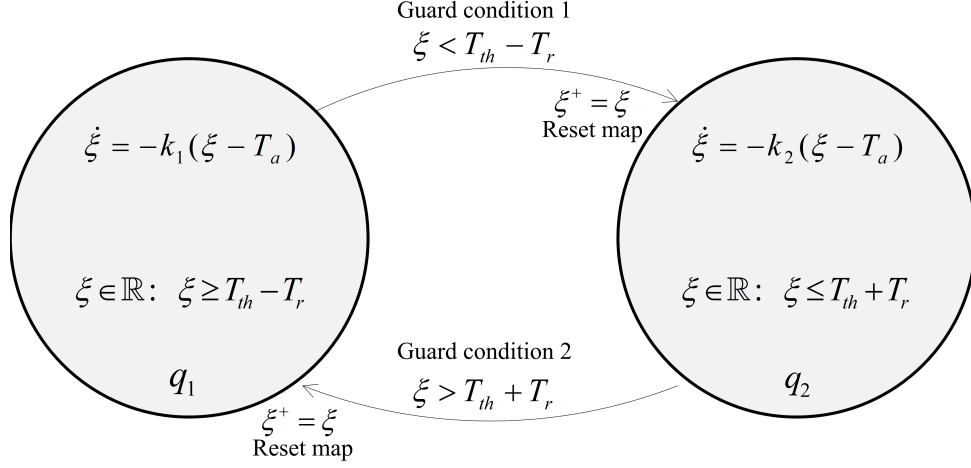


Figure 2.3: Graphical representation of water cooling hybrid system.

△

We now show how a hybrid automaton can be modelled as hybrid system of the form (2.1). For each  $q, q' \in \mathcal{Q}$  we let

$$\begin{aligned}
 C_q &:= \text{Domain}(q), & D_q &:= \bigcup_{(q,q') \in \text{Edges}} \text{Guard}(q, q') \\
 F_q(\xi) &:= f(q, \xi), \quad (\text{for all } \xi \in C_q), \\
 G_q(\xi) &:= \bigcup_{\{q': \xi \in \text{Guard}(q, q')\}} (\text{Reset}(q, q', \xi), q'), \quad (\text{for all } \xi \in D_q).
 \end{aligned}$$

When  $\xi$  is an element of two different guard sets  $\text{Guard}(q, q')$  and  $\text{Guard}(q, q'')$ ,  $G_q(\xi)$  is a set consisting of at least two points. Hence,  $G_q$  can be set-valued. With  $C_q$ ,  $F_q$ ,  $G_q$  and  $D_q$  defined as above, we consider the hybrid system with state  $(q, \xi) \in \mathcal{Q} \times \mathbb{R}^n$  and model

$$\mathcal{H} : \quad \begin{cases} \dot{\xi} \in F_q(\xi), & q \in \mathcal{Q}, \xi \in C_q \\ (\xi^+, x^+) \in G_q(x), & q \in \mathcal{Q}, \xi \in D_q. \end{cases} \quad (2.3)$$

## 2.2 Hybrid model of 2-D.O.F. bipedal robot

The model of the 2-DOF bipedal robot consists of two legs with identical mass and geometry connected by a revolute joint at the hip position. The hip is modelled as a point mass.

The following subsections present the continuous-time and discrete-time dynamics of the bipedal robot.

### 2.2.1 Continuous-time dynamics

In mechanics, one can obtain the equations of motion for a rigid multi-body system using the Newton-Euler balance laws. This approach requires the knowledge of reaction (or constraint) forces between bodies.

As another approach, one can think of the **generalized coordinates**<sup>1</sup> of a given mechanical multi-body system. Due to the presence of kinematic constraints, i.e. joints, the generalized coordinates can be categorized as constrained and unconstrained. The applied forces on the system associated along the direction of the unconstrained generalized coordinates are referred to as **generalized forces**. These generalized forces are directly responsible for the motion of the system and, therefore, it becomes natural to study the effect of the generalized forces on the motion of the system. The method of Euler-Lagrange presents another approach to write the equations of motion of a multi-body system. The Euler-Lagrange method forms one equation of motion per degree of freedom<sup>2</sup> resulting in as many equations as degrees of freedom. In addition, the Euler-Lagrange method can be formulated to avoid the computation of reaction forces of a multi-body system.

For a 2-DOF bipedal robot, two choices of unconstrained generalized coordinates are shown in Figure 2.5. The coordinates shown in Figures 2.5a are common in inverted double-pendulum control problems. In this thesis, we choose to use the model in Figure 2.5b because it is the most common in bipedal robot literature. In this model, the coordinates  $\theta_{st}$  and  $\theta_{sw}$  refer to the angular positions of the stance leg and swing leg, respectively, relative to the vertical line. Other two possible and common coordinates are presented in Appendix A.

The robot is actuated using an ankle torque,  $\tau_1$ , and a hip torque,  $\tau_2$ . Figure 2.4 pictures the actuation scenario. This model requires that the ZMP remains within the foot polygon (simply a line in our case) in order to maintain dynamic stability while walking. Assuming the foot has negligible mass and the origin of  $x'-y'$  system coincides with the ankle (Figure 2.4a), then in the  $x'-y'$  coordinates, the general equation of [14] that calculates the location of the ZMP reduces to

$$\text{ZMP} = \frac{\tau_1}{R_n} \tag{2.4}$$

---

<sup>1</sup>Generalized coordinates are any set of coordinates on the configuration space  $\mathcal{Q}$ .

<sup>2</sup>The number of degrees of freedom is equal to the minimum number of unconstrained generalized coordinates [37].

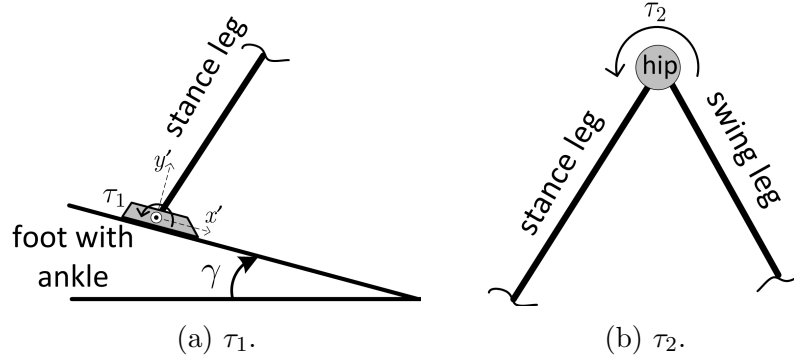


Figure 2.4: The actuation torques,  $\tau_1$  and  $\tau_2$ , of the 2-DOF bipedal robot. In Figure 2.4a, the  $x'$ -axis is parallel to the walking surface.

where  $R_n$  is the reaction force normal to the walking surface. This normal reaction is evaluated using static equilibrium for the foot along  $y'$ -axis as

$$R_n = ((m_1 + m_2 + m_H)g + m_1 a_{1y} + m_2 a_{2y} + m_H a_{Hy}) \cos(\gamma). \quad (2.5)$$

The terms  $a_{1y}$ ,  $a_{2y}$ ,  $a_{Hy}$  in the above equation are the  $y$ -components of the time derivatives of equations (2.11), (2.12) and (2.13), respectively. Throughout the thesis, it is assumed that the foot is large enough to accommodate the ZMP of the 2-DOF bipedal robot. It is shown through simulation in Chapter 4 that our proposed controllers fluctuate the ZMP within a reasonable range.

The continuous-time model of the 2-DOF bipedal robot is derived as follows. First, model (a) in Figure 2.5a is derived using an Euler-Lagrange formulation. Then, a simple coordinate change is applied in order to get model (b) in Figure 2.5b, which is the model used in this thesis.

Consider the schematic representation of the bipedal walker shown in Figure 2.5a. Throughout this thesis, the leg that touches the ground is referred to as the **stance leg** whereas the other leg is called the **swing leg**. The coordinate vector in Figure 2.5a is  $q = \text{col}(q_1, q_2) \in \mathbb{R} \times \mathbb{R}$ .

The total kinetic energy of the system is calculated as:

$$K(q, \dot{q}) = \underbrace{\frac{1}{2}m_1 v_1^2 + \frac{1}{2}m_2 v_2^2}_{\text{Trans. Term for legs}_{1,2}} + \underbrace{\frac{1}{2}I_1 \dot{q}_1^2 + \frac{1}{2}I_2 \dot{q}_2^2}_{\text{Rot. Term for legs}_{1,2}} + \underbrace{\frac{1}{2}m_H v_H^2}_{\text{Trans. K for Hip}} \quad (2.6)$$

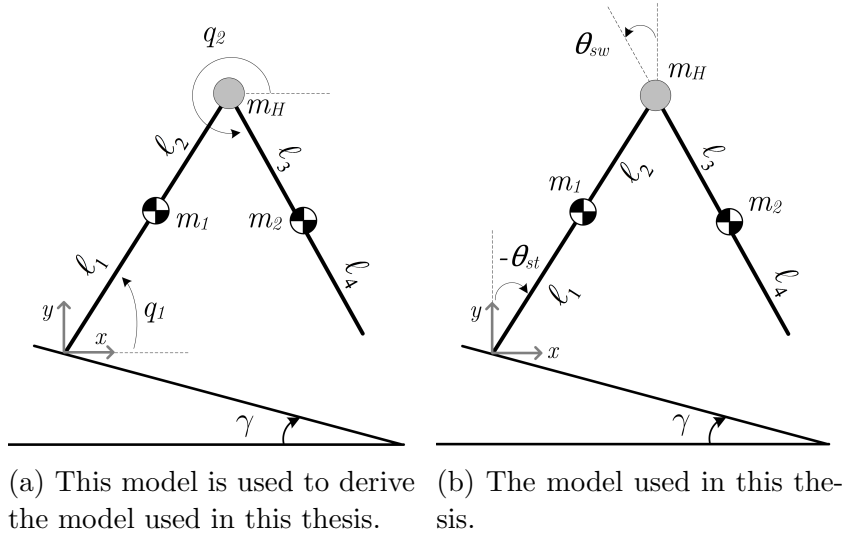


Figure 2.5: Two models for the continuous dynamics of the 2-DOF bipedal robot.

where  $I_1, I_2$  are moments of inertia about the center of mass for legs 1, 2. It is noted in Equation (2.6) that the hip mass is modelled as a point mass and, hence, has only translational kinetic energy. The mass distribution and geometry of legs 1,2 are captured by  $I_{1,2}$ . The potential energy is calculated as

$$P(q) = m_1 g l_1 \sin(q_1) + m_H g \ell \sin(q_1) + m_2 g (\ell \sin(q_1) + l_3 \sin(q_2)) \quad (2.7)$$

where  $\ell := l_1 + l_2 = l_3 + l_4$ . To evaluate the expression for  $K(q, \dot{q})$  in terms of the coordinates and their derivatives, we need to solve a forward kinematics problem.

- **Position level.** Let  $\vec{r}_1, \vec{r}_2$  and  $\vec{r}_H$  be the position vectors of the center of mass (CoM) of leg<sub>1</sub>, leg<sub>2</sub> and the hip, respectively. Then,

$$\vec{r}_1 = l_1 \cos(q_1) \hat{\mathbf{i}} + l_1 \sin(q_1) \hat{\mathbf{j}} \quad (2.8)$$

$$\vec{r}_2 = (\ell \cos(q_1) + l_3 \cos(q_2)) \hat{\mathbf{i}} + (\ell \sin(q_1) + l_3 \sin(q_2)) \hat{\mathbf{j}} \quad (2.9)$$

$$\vec{r}_H = \ell \cos(q_1) \hat{\mathbf{i}} + \ell \sin(q_1) \hat{\mathbf{j}} \quad (2.10)$$

where  $\hat{\mathbf{i}}$  and  $\hat{\mathbf{j}}$  are unit vectors along the  $x$ -axis and  $y$ -axis, respectively.

- **Velocity level.** Differentiating Equations (2.8)-(2.10) we arrive at velocity expres-

sions

$$\vec{v}_1 = -\ell_1 \sin(q_1) \dot{q}_1 \hat{\mathbf{i}} + \ell_1 \cos(q_1) \dot{q}_1 \hat{\mathbf{j}} \quad (2.11)$$

$$\vec{v}_2 = (-\ell \sin(q_1) \dot{q}_1 - \ell_3 \sin(q_2) \dot{q}_2) \hat{\mathbf{i}} + (\ell \cos(q_1) \dot{q}_1 + \ell_3 \cos(q_2) \dot{q}_2) \hat{\mathbf{j}} \quad (2.12)$$

$$\vec{v}_H = -\ell \sin(q_1) \dot{q}_1 \hat{\mathbf{i}} + \ell \cos(q_1) \dot{q}_1 \hat{\mathbf{j}} \quad (2.13)$$

Given the kinematic equations (2.8)-(2.13), the Lagrangian becomes:

$$\begin{aligned} L(q, \dot{q}) &= \frac{1}{2} m_1 \ell_1^2 \dot{q}_1^2 + \frac{1}{2} m_2 \ell^2 \dot{q}_1^2 + \frac{1}{2} m_2 \ell_3^2 \dot{q}_2^2 + m_2 \ell \ell_3 \cos(q_1 - q_2) \dot{q}_1 \dot{q}_2 \\ &+ \frac{1}{2} m_H \ell^2 \dot{q}_1^2 + \frac{1}{2} I_1 \dot{q}_1^2 + \frac{1}{2} I_2 \dot{q}_2^2 - m_1 g \ell_1 \sin(q_1) - m_H g \ell \sin(q_1) \\ &- m_2 g (\ell \sin(q_1) + \ell_3 \sin(q_2)) \end{aligned} \quad (2.14)$$

The generalized forces for each coordinate are evaluated as follows. The torque  $\tau_1$  does

Table 2.1: Input torque vector components.

	<b>Action</b>	<b>Reaction</b>
$\tau_1$	Stance leg	Ground
$\tau_2$	Swing leg	Stance leg

work on the coordinate  $q_1$  whereas the torque  $\tau_2$  does work on  $q_2 - q_1$  (Table 2.1). Therefore, the virtual work [37] of the system is

$$\begin{aligned} \delta W &= \tau_1 \delta q_1 + \tau_2 (\delta q_2 - \delta q_1) \\ &= (\tau_1 - \tau_2) \delta q_1 + \tau_2 \delta q_2 \end{aligned} \quad (2.15)$$

where  $\delta q_i$ ,  $i \in \{1, 2\}$ , are virtual displacements. As a result,

$$B(q)\tau = \begin{bmatrix} 1 & -1 \\ 0 & 1 \end{bmatrix} \begin{bmatrix} \tau_1 \\ \tau_2 \end{bmatrix}. \quad (2.16)$$

Now, let's substitute Equations (2.14) and (2.16) in (1.1). Then, we arrive at the

equations of motion and write it in matrix form as

$$\begin{aligned}
& \begin{bmatrix} m_1\ell_1^2 + m_2\ell^2 + m_H\ell^2 + I_1 & m_2\ell\ell_3 \cos(q_1 - q_2) \\ m_2\ell\ell_3 \cos(q_1 - q_2) & m_2\ell_3^2 + I_2 \end{bmatrix} \begin{bmatrix} \ddot{q}_1 \\ \ddot{q}_2 \end{bmatrix} \\
& + \begin{bmatrix} 0 & m_2\ell\ell_3 \sin(q_1 - q_2)\dot{q}_2 \\ -m_2\ell\ell_3 \sin(q_1 - q_2)\dot{q}_1 & 0 \end{bmatrix} \begin{bmatrix} \dot{q}_1 \\ \dot{q}_2 \end{bmatrix} \\
& + \begin{bmatrix} [m_1g\ell_1 + m_Hg\ell + m_2g\ell] \cos(q_1) \\ m_2g\ell_3 \cos(q_2) \end{bmatrix} = \begin{bmatrix} 1 & -1 \\ 0 & 1 \end{bmatrix} \begin{bmatrix} \tau_1 \\ \tau_2 \end{bmatrix}.
\end{aligned} \tag{2.17}$$

Model (b) (Figure 2.5b) is obtained from (2.17) via the global coordinate change

$$\begin{bmatrix} \theta_{st} \\ \theta_{sw} \end{bmatrix} = \begin{bmatrix} q_1 \\ q_2 \end{bmatrix} - \begin{bmatrix} \frac{\pi}{2} \\ \frac{3\pi}{2} \end{bmatrix}. \tag{2.18}$$

In  $(\theta_{st}, \theta_{sw})$ -coordinates, model (2.17) reads

$$\begin{aligned}
& \begin{bmatrix} m_1\ell_1^2 + m_2\ell^2 + m_H\ell^2 + I_1 & -m_2\ell\ell_3 \cos(\theta_{st} - \theta_{sw}) \\ -m_2\ell\ell_3 \cos(\theta_{st} - \theta_{sw}) & m_2\ell_3^2 + I_2 \end{bmatrix} \begin{bmatrix} \ddot{\theta}_{st} \\ \ddot{\theta}_{sw} \end{bmatrix} \\
& + \begin{bmatrix} 0 & -m_2\ell\ell_3 \sin(\theta_{st} - \theta_{sw})\dot{\theta}_{sw} \\ m_2\ell\ell_3 \sin(\theta_{st} - \theta_{sw})\dot{\theta}_{st} & 0 \end{bmatrix} \begin{bmatrix} \dot{\theta}_{st} \\ \dot{\theta}_{sw} \end{bmatrix} \\
& + \begin{bmatrix} -(m_1g\ell_1 + m_Hg\ell + m_2g\ell) \sin(\theta_{st}) \\ m_2g\ell_3 \sin(\theta_{sw}) \end{bmatrix} = \begin{bmatrix} 1 & -1 \\ 0 & 1 \end{bmatrix} \begin{bmatrix} \tau_1 \\ \tau_2 \end{bmatrix}.
\end{aligned} \tag{2.19}$$

In summary, the 2-DOF bipedal robot studied in this thesis has continuous-time dynamics modelled by (2.19). This is the model used throughout the rest of this thesis. The model (2.19) can be compactly written as

$$M(\theta)\ddot{\theta} + C(\theta, \dot{\theta})\dot{\theta} + G(\theta) = B\tau \tag{2.20}$$

where  $\theta := \text{col}(\theta_{st}, \theta_{sw}) \in \mathbb{R}^2$  and

$$M(\theta) := \begin{bmatrix} m_1 \ell_1^2 + m_2 \ell^2 + m_H \ell^2 + I_1 & -m_2 \ell \ell_3 \cos(\theta_{st} - \theta_{sw}) \\ -m_2 \ell \ell_3 \cos(\theta_{st} - \theta_{sw}) & m_2 \ell_3^2 + I_2 \end{bmatrix} \quad (2.21)$$

$$C(\theta, \dot{\theta}) := \begin{bmatrix} 0 & -m_2 \ell \ell_3 \sin(\theta_{st} - \theta_{sw}) \dot{\theta}_{sw} \\ m_2 \ell \ell_3 \sin(\theta_{st} - \theta_{sw}) \dot{\theta}_{st} & 0 \end{bmatrix} \quad (2.22)$$

$$G(\theta) := \begin{bmatrix} -(m_1 g \ell_1 + m_H g \ell + m_2 g \ell) \sin(\theta_{st}) \\ m_2 g \ell_3 \sin(\theta_{sw}) \end{bmatrix} \quad (2.23)$$

$$B := \begin{bmatrix} 1 & -1 \\ 0 & 1 \end{bmatrix}. \quad (2.24)$$

## 2.2.2 Discrete-time dynamics

The discrete-time dynamics consists of two entities:

- i. The guard condition, which in the case of the 2-DOF bipedal robot is the set where the swing foot reaches the ground surface from above followed by an impact event.
- ii. The reset map, which represents the instantaneous change in positions and velocities. The reset map is derived by swapping the role of the swing and stance legs and using the principle of conservation of angular momentum.

**Assumption 1.** The terrain on which the 2-DOF bipedal robot traverses is an inclined plane with angle of inclination  $\gamma \in (0, \pi/2)$ , see Figure 2.6.

To model impact with the ground surface, a local Cartesian coordinate system is introduced. The origin of this coordinate system is at the foot of the stance leg (Figure 2.6). In this local coordinate system, the ground can be expressed as a line,

$$\{(y_1, y_2) \in \mathbb{R}^2 : y_2 = \tan(-\gamma)y_1\}. \quad (2.25)$$

The vector  $\vec{r}$  (see Figure 2.6) and the vector  $\dot{\vec{r}}$  are given by

$$\begin{aligned} \vec{r} &= (-\ell \sin(\theta_{st}) + \ell \sin(\theta_{sw})) \hat{\mathbf{i}} + (\ell \cos(\theta_{st}) - \ell \cos(\theta_{sw})) \hat{\mathbf{j}} =: r_{y_1} \hat{\mathbf{i}} + r_{y_2} \hat{\mathbf{j}}, \text{ and} \\ \dot{\vec{r}} &= \left( -\ell \cos(\theta_{st}) \dot{\theta}_{st} + \ell \cos(\theta_{sw}) \dot{\theta}_{sw} \right) \hat{\mathbf{i}} + \left( -\ell \sin(\theta_{st}) \dot{\theta}_{st} + \ell \sin(\theta_{sw}) \dot{\theta}_{sw} \right) \hat{\mathbf{j}} =: \dot{r}_{y_1} \hat{\mathbf{i}} + \dot{r}_{y_2} \hat{\mathbf{j}}. \end{aligned}$$

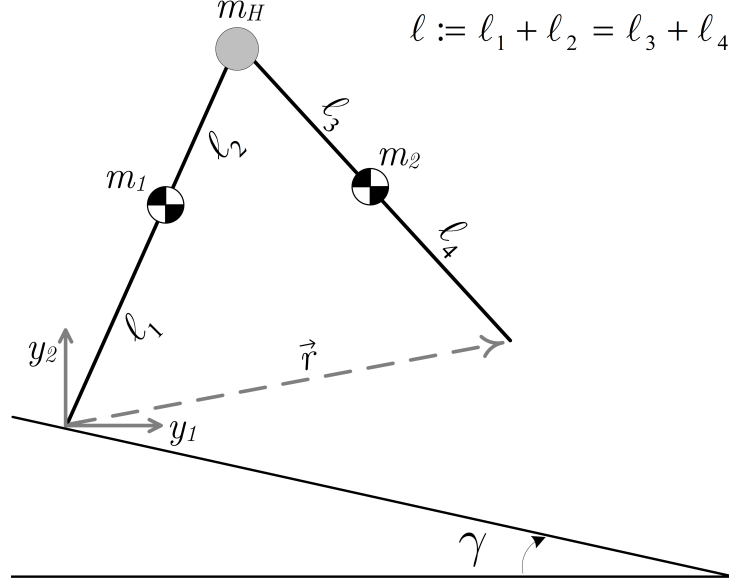


Figure 2.6: Ground modelled in local coordinate system.

The instant at which the swing foot hits the ground, we have that  $r_{y_2} = \tan(-\gamma)r_{y_1}$ . Define a height function  $H : \mathbb{R} \rightarrow \mathbb{R}$  as

$$H(\theta) := r_{y_2}(\theta) - \tan(-\gamma)r_{y_1}(\theta). \quad (2.26)$$

We have that

$$H(\theta) = 0 \iff \cos(\theta_{st} + \gamma) = \cos(\theta_{sw} + \gamma)$$

which implies that

$$\theta_{sw} = -\theta_{st} - 2\gamma \quad (2.27)$$

or

$$\theta_{st} = \theta_{sw}. \quad (2.28)$$

Physically, Equation (2.28) captures a mid-stance point where  $|\vec{r}^\dagger| = 0$ . The robot is assumed not to collide with ground at the mid-stance point. Equation (2.27) defines a jump line on which the swing leg is on the ground.

In order to capture the fact that the swing leg is approaching the ground from above, we use the time derivative of the height function

$$\frac{dH(\theta(t))}{dt} = dH_\theta \dot{\theta} = \dot{r}_{y_2}(\theta, \dot{\theta}) - \tan(-\gamma)\dot{r}_{y_1}(\theta, \dot{\theta}). \quad (2.29)$$

As the swing foot approaches the ground from above,  $H(\theta)$  is positive and decreases towards zero. Since  $H(\theta)$  is decreasing,  $dH_\theta\dot{\theta} < 0$  as the swing foot approaches the ground from above. This discussion motivates the following guard condition (impact surface) for the 2-DOF bipedal robot,

$$\mathcal{S} = \left\{ (\theta, \dot{\theta}) \in \mathbb{R}^4 : H(\theta) = 0 \wedge dH_\theta\dot{\theta} < 0 \right\} \setminus \left\{ (\theta, \dot{\theta}) \in \mathbb{R}^4 : \theta_{st} = \theta_{sw} \right\}. \quad (2.30)$$

In order to derive the reset map, we impose the following standing assumption.

**Assumption 2.** When the 2-DOF bipedal robot's swing leg collides with the ground, the collision is

- i. impulsive (i.e. all non-impulsive forces are negligible at collision),
- ii. inelastic,
- iii. instantaneous and only one leg touches the ground at every instant, and
- iv. does not cause slipping.

When the swing leg hits the impact surface, the roles of the configuration variables swap. Angular velocities are also instantaneously affected by collisions. Under Assumption 2, the angular velocities just after collision are evaluated using conservation of angular momentum at the impact instant. Consider Figure 2.7 which shows the robot just before and just after a collision event. Let the superscript “−” denote variables just before collision and the superscript “+” denote variables just before collision.

The configuration variables are redefined just after collision according to

$$\begin{aligned} \theta_{st}^+ &= \theta_{sw}^-, \text{ and} \\ \theta_{sw}^+ &= \theta_{st}^-. \end{aligned} \quad (2.31)$$

The angular momentum about a point on the robot is conserved during impact [38].

- i. Angular momentum about the contact point  $P$ , denoted  $L_P$ , is conserved and therefore

$$\dot{L}_P = 0 \Rightarrow L_P^- = L_P^+. \quad (2.32)$$

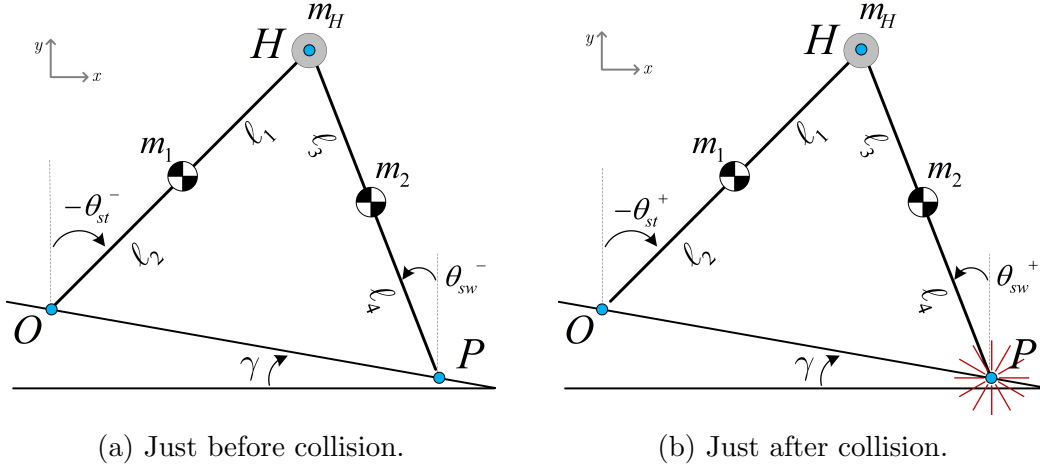


Figure 2.7: Collision event.

- ii. Angular momentum about the hip mass point  $H$ , denoted  $L_H$ , is conserved and therefore

$$\dot{L}_H = 0 \Rightarrow L_H^- = L_H^+. \quad (2.33)$$

Evaluating the expression of  $L_P^-$  for the whole mechanism yields [39]

$$L_P^- = I_1 \dot{\theta}_{st}^- + m_1 \vec{r}_1^- \times \vec{v}_1^- + I_2 \dot{\theta}_{sw}^- + m_2 \vec{r}_2^- \times \vec{v}_2^- + m_H \vec{r}_H^- \times \vec{v}_H^- \quad (2.34)$$

where,

$$\begin{aligned} \vec{r}_1^- &= (\ell_2 \sin(\theta_{st}^-) - \ell \sin(\theta_{sw}^-)) \hat{\mathbf{i}} + (-\ell_2 \cos(\theta_{st}^-) + \ell \cos(\theta_{sw}^-)) \hat{\mathbf{j}}, \\ \vec{v}_1^- &= \frac{d}{dt} \left( -\ell_1 \sin(\theta_{st}^-) \hat{\mathbf{i}} + \ell_1 \cos(\theta_{st}^-) \hat{\mathbf{j}} \right), \\ &= \left( -\ell_1 \cos(\theta_{st}^-) \dot{\theta}_{st}^- \right) \hat{\mathbf{i}} - \left( \ell_1 \sin(\theta_{st}^-) \dot{\theta}_{st}^- \right) \hat{\mathbf{j}}, \\ \vec{r}_2^- &= (-\ell_4 \sin(\theta_{sw}^-)) \hat{\mathbf{i}} + (\ell_4 \cos(\theta_{sw}^-)) \hat{\mathbf{j}}, \\ \vec{v}_2^- &= \frac{d}{dt} \left( (-\ell \sin(\theta_{st}^-) + \ell_3 \sin(\theta_{sw}^-)) \hat{\mathbf{i}} + (\ell \cos(\theta_{st}^-) - \ell_3 \cos(\theta_{sw}^-)) \hat{\mathbf{j}} \right) \\ &= \left( -\ell \cos(\theta_{st}^-) \dot{\theta}_{st}^- + \ell_3 \cos(\theta_{sw}^-) \dot{\theta}_{sw}^- \right) \hat{\mathbf{i}} + \left( -\ell \sin(\theta_{st}^-) \dot{\theta}_{st}^- + \ell_3 \sin(\theta_{sw}^-) \dot{\theta}_{sw}^- \right) \hat{\mathbf{j}}, \\ \vec{r}_H^- &= (-\ell \sin(\theta_{sw}^-)) \hat{\mathbf{i}} + (\ell \cos(\theta_{sw}^-)) \hat{\mathbf{j}}, \text{ and} \\ \vec{v}_H^- &= \left( -\ell \cos(\theta_{st}^-) \dot{\theta}_{st}^- \right) \hat{\mathbf{i}} - \left( \ell \sin(\theta_{st}^-) \dot{\theta}_{st}^- \right) \hat{\mathbf{j}}. \end{aligned}$$

Substituting the above expressions in (2.34) and simplifying, we arrive at

$$\begin{aligned} L_P^- &= I_1 \dot{\theta}_{st}^- + m_1 \left( \ell \ell_1 \cos(\theta_{st}^- - \theta_{sw}^-) \dot{\theta}_{st}^- - \ell_1 \ell_2 \dot{\theta}_{st}^- \right) \\ &+ I_2 \dot{\theta}_{sw}^- + m_2 \left( \ell \ell_4 \cos(\theta_{st}^- - \theta_{sw}^-) \dot{\theta}_{st}^- - \ell_3 \ell_4 \dot{\theta}_{st}^- \right) \\ &+ m_H \ell^2 \cos(\theta_{st}^- - \theta_{sw}^-) \dot{\theta}_{st}^-. \end{aligned} \quad (2.35)$$

$L_H^-$  is the momentum of the stance leg as it is about to leave the ground. Therefore, we evaluate it as

$$\begin{aligned} L_H^- &= I_1 \dot{\theta}_{st}^- + m_1 \left( \ell_2 \sin(\theta_{st}^-) \hat{\mathbf{i}} - \ell_2 \cos(\theta_{st}^-) \hat{\mathbf{j}} \right) \\ &\times \frac{d}{dt} \left( -\ell_1 \sin(\theta_{st}^-) \hat{\mathbf{i}} + \ell_1 \cos(\theta_{st}^-) \hat{\mathbf{j}} \right) \\ &= I_1 \dot{\theta}_{st}^- - m_1 \ell_1 \ell_2 \dot{\theta}_{st}^-. \end{aligned} \quad (2.36)$$

Now, we evaluate the angular momenta just after collision event

$$L_P^+ = I_1 \dot{\theta}_{sw}^+ + m_1 \vec{r}_1^+ \times \vec{v}_1^+ + I_2 \dot{\theta}_{st}^+ + m_2 \vec{r}_2^+ \times \vec{v}_2^+ + m_H \vec{r}_H^+ \times \vec{v}_H^+ \quad (2.37)$$

where,

$$\begin{aligned} \vec{r}_1^+ &= (-\ell \sin(\theta_{st}^+) + \ell_2 \sin(\theta_{sw}^+)) \hat{\mathbf{i}} + (\ell \cos(\theta_{st}^+) - \ell_2 \cos(\theta_{sw}^+)) \hat{\mathbf{j}}, \\ \vec{v}_1^+ &= \left( -\ell \cos(\theta_{st}^+) \dot{\theta}_{st}^+ + \ell_2 \cos(\theta_{sw}^+) \dot{\theta}_{sw}^+ \right) \hat{\mathbf{i}} + \left( -\ell \sin(\theta_{st}^+) \dot{\theta}_{st}^+ + \ell_2 \sin(\theta_{sw}^+) \dot{\theta}_{sw}^+ \right) \hat{\mathbf{j}}, \\ \vec{r}_2^+ &= (-\ell_4 \sin(\theta_{st}^+)) \hat{\mathbf{i}} + (\ell_4 \cos(\theta_{st}^+)) \hat{\mathbf{j}}, \text{ and} \\ \vec{v}_2^+ &= \left( \ell_4 \cos(\theta_{st}^+) \dot{\theta}_{st}^+ \right) \hat{\mathbf{i}} - \left( \ell_4 \sin(\theta_{st}^+) \dot{\theta}_{st}^+ \right) \hat{\mathbf{j}}. \end{aligned}$$

Substituting the above expressions in (2.37) and simplifying we obtain

$$\begin{aligned} L_P^+ &= I_1 \dot{\theta}_{sw}^+ + m_1 \left( \ell^2 \dot{\theta}_{st}^+ - \ell \ell_2 \cos(\theta_{st}^+ - \theta_{sw}^+) \dot{\theta}_{sw}^+ - \ell \ell_2 \cos(\theta_{st}^+ - \theta_{sw}^+) \dot{\theta}_{st}^+ + \ell_2^2 \dot{\theta}_{sw}^+ \right) \\ &+ I_2 \dot{\theta}_{st}^+ + m_2 \ell_4^2 \dot{\theta}_{st}^+ + m_H \ell^2 \dot{\theta}_{st}^+. \end{aligned} \quad (2.38)$$

Since  $L_H^+$  is the momentum about point  $H$  of the “new” swing leg as it just was standing, we evaluate it as

$$\begin{aligned} L_H^+ &= m_1 \left( \ell_2 \sin(\theta_{sw}^+) \hat{\mathbf{i}} - \ell_2 \cos(\theta_{sw}^+) \hat{\mathbf{j}} \right) \times \vec{v}_1^+ + I_1 \dot{\theta}_{sw}^+ \\ &= m_1 \left( -\ell \ell_2 \cos(\theta_{st}^+ - \theta_{sw}^+) \dot{\theta}_{st}^+ + \ell_2^2 \dot{\theta}_{sw}^+ \right) + I_1 \dot{\theta}_{sw}^+. \end{aligned} \quad (2.39)$$

Substituting Equations (2.35) and (2.38) into (2.32), and (2.36) and (2.39) into (2.33) the instantaneous change of velocities due to collision can be written in matrix form as

$$\underbrace{\begin{bmatrix} J_{11}^b & J_{12}^b \\ J_{21}^b & J_{22}^b \end{bmatrix}}_{:=J^b(\theta)} \begin{bmatrix} \dot{\theta}_{st}^+ \\ \dot{\theta}_{sw}^+ \end{bmatrix} = \underbrace{\begin{bmatrix} J_{11}^a & J_{12}^a \\ J_{21}^a & J_{22}^a \end{bmatrix}}_{:=J^a(\theta)} \begin{bmatrix} \dot{\theta}_{st}^- \\ \dot{\theta}_{sw}^- \end{bmatrix}. \quad (2.40)$$

where,

$$\begin{aligned}
J_{11}^a &:= I_1 - m_1 \ell_1 \ell_2 + (m_1 \ell \ell_1 + m_2 \ell \ell_4 + m_H \ell^2) \cos(2\alpha), \\
J_{12}^a &:= I_2 - m_2 \ell_3 \ell_4, \\
J_{21}^a &:= I_1 - m_1 \ell_1 \ell_2, \\
J_{22}^a &:= 0, \\
J_{11}^b &:= I_2 + m_1 \ell^2 + m_2 \ell_4^2 + m_H \ell^2 - m_1 \ell \ell_2 \cos(2\alpha), \\
J_{12}^b &:= I_1 + m_1 \ell_2^2 - m_1 \ell \ell_2 \cos(2\alpha), \\
J_{21}^b &:= -m_1 \ell \ell_2 \cos(2\alpha), \\
J_{22}^b &:= m_1 \ell_2^2 + I_1,
\end{aligned}$$

and

$$\alpha := \frac{\theta_{st}^- - \theta_{sw}^-}{2}.$$

The matrix  $J^b$  is invertible. Its determinant can be shown to be always positive as follows.

$$\begin{aligned}
\det(J^b) &= J_{11}^b J_{22}^b - J_{12}^b J_{21}^b \\
&= (I_2 + m_1 \ell^2 + m_2 \ell_4^2 + m_H \ell^2 - m_1 \ell \ell_2 \cos(2\alpha)) (m_1 \ell_2^2 + I_1) \\
&\quad + m_1 \ell \ell_2 \cos(2\alpha) (I_1 + m_1 \ell_2^2 - m_1 \ell \ell_2 \cos(2\alpha)) \\
&= m_1 \ell_2^2 I_2 + m_1^2 \ell_2^2 \ell^2 + m_2 m_1 \ell_2^2 \ell_4^2 + m_H m_1 \ell_2^2 \ell^2 \\
&\quad + I_1 I_2 + m_1 \ell^2 I_1 + m_2 \ell_4^2 I_1 + m_H \ell^2 I_1 - m_1^2 \ell^2 \ell_2^2 \cos^2(2\alpha).
\end{aligned}$$

All the terms in the above expression are positive except the last one. The extreme case of  $\cos^2(2\alpha) = 1$  makes the last term the most negative. In this case, we have

$$\begin{aligned}
\det(J^b) &= m_1 \ell_2^2 I_2 + m_2 m_1 \ell_2^2 \ell_4^2 + m_H m_1 \ell_2^2 \ell^2 \\
&\quad + I_1 I_2 + m_1 \ell^2 I_1 + m_2 \ell_4^2 I_1 + m_H \ell^2 I_1 \\
&> 0.
\end{aligned}$$

As a result, the expression of  $\det(J^b)$  remains positive at the extreme case and, therefore, is positive always. This result implies that  $J^b$  is invertible and Equation (2.40) can be compactly written as

$$\begin{bmatrix} \dot{\theta}_{st}^+ \\ \dot{\theta}_{sw}^+ \end{bmatrix} = (J^b)^{-1} J^a(\theta) \begin{bmatrix} \dot{\theta}_{st}^- \\ \dot{\theta}_{sw}^- \end{bmatrix} \quad (2.41)$$

Combining the effects of collision on angular positions and velocities and eliminating the “−” superscript, the reset map becomes

$$\begin{bmatrix} \theta_{st}^+ \\ \theta_{sw}^+ \\ \dot{\theta}_{st}^+ \\ \dot{\theta}_{sw}^+ \end{bmatrix} = J(\theta, \dot{\theta}) := \mathcal{J}(\theta) \begin{bmatrix} \theta_{st} \\ \theta_{sw} \\ \dot{\theta}_{st} \\ \dot{\theta}_{sw} \end{bmatrix} \quad (2.42)$$

where,

$$\mathcal{J}(\theta) := \begin{bmatrix} 0 & 1 & 0 & 0 \\ 1 & 0 & 0 & 0 \\ 0 & 0 & & \\ 0 & 0 & & j \end{bmatrix} \quad \text{and} \quad j := (J^b)^{-1} J^a(\theta). \quad (2.43)$$

### 2.2.3 The hybrid model

The aim of this subsection is to consolidate the ideas in this chapter and show that the 2-DOF bipedal robots can be modelled as a hybrid automaton  $\mathcal{H} = (\mathcal{Q}, \text{Domain}, F, \text{Edges}, \text{Guard}, \text{Reset})$  as in Definition 2.1.1.

- The 2-DOF only has one mode and therefore the set of discrete states,  $\mathcal{Q} = \{q_1\}$ , is a singleton.
- The domain map  $\text{Domain} : \mathcal{Q} \rightrightarrows \mathbb{R}^4$  is defined as  $\text{Domain}(q_1) = \mathbb{R}^4$ .
- The flow map  $F : \mathcal{Q} \times \mathbb{R}^4 \rightarrow \mathbb{R}^4$  describes a differential equation that defines the continuous-time evolution of the continuous state variable. Let  $x = \text{col}(x_1, x_2, x_3, x_4) := \text{col}(\theta_{st}, \theta_{sw}, \dot{\theta}_{st}, \dot{\theta}_{sw}) \in \mathbb{R}^4$  be continuous-time state vector of the robot. Then, Equation (2.19) can be written in state-space form as a control-affine system

$$\dot{x} = f(x) + g(x)\tau \quad (2.44)$$

where,  $f : \mathbb{R}^4 \rightarrow \mathbb{R}^4$  and  $g : \mathbb{R}^4 \rightarrow \mathbb{R}^4 \times \mathbb{R}^2$  are smooth and  $\tau \in \mathbb{R}^2$  is the input. Therefore, the flow map is defined as  $F(q_1, x) = f(x) + g(x)\tau$ .

- Since there is only one mode, there is only one edge and therefore  $\text{Edges} = \{(q_1, q_1)\}$ .
- The guard map  $\text{Guard} : \text{Edges} \rightrightarrows \mathbb{R}^4$  is defined as  $\text{Guard}(q_1, q_1) = \mathcal{S}$  where  $\mathcal{S}$  is given by (2.30).

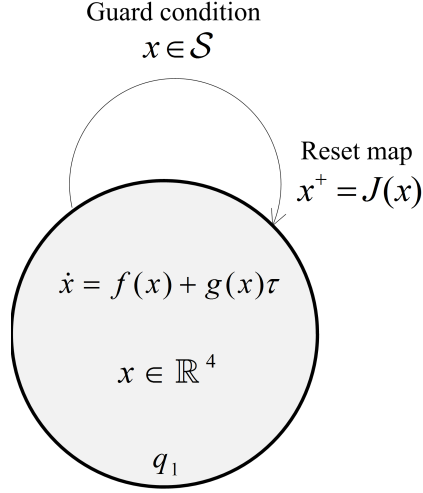


Figure 2.8: Graphical representation of the 2-DOF bipedal robot hybrid system.

- The reset map  $\text{Reset} : \text{Edges} \times \mathbb{R}^4 \rightarrow \mathbb{R}^4$  equals  $\text{Reset}(q_1, q_1, x) = J(x)$ .

Figure 2.8 represents the bipedal robot graphically.

Equivalently, in summary and with respect to the class of system (1.3), the 2-DOF bipedal robot model is given by

$$\text{EL}_{\mathcal{H}} : \begin{cases} M(\theta)\ddot{\theta} + C(\theta, \dot{\theta})\dot{\theta} + G(\theta) = B\tau, & (\theta, \dot{\theta}) \notin \mathcal{S} \\ (\theta^+, \dot{\theta}^+) = J(\theta, \dot{\theta}), & (\theta, \dot{\theta}) \in \mathcal{S}. \end{cases} \quad (2.45)$$

where the matrices  $M(\theta)$ ,  $C(\theta, \dot{\theta})$ ,  $G(\theta)$ ,  $B$  are given by (2.21), (2.22), (2.23), and (2.24) respectively. The set  $\mathcal{S}$  is given by (2.30) and map  $J(\theta)$  is given by (2.42) (2.43). In state-space, (2.45) has the form

$$\text{EL}_{\mathcal{H}} : \begin{cases} \dot{x} = f(x) + \sum_{i=1}^2 g_i(x)\tau_i, & x \notin \mathcal{S} \\ x = J(x), & x \in \mathcal{S}. \end{cases} \quad (2.46)$$

where,

$$f(x) = \begin{bmatrix} x_3 \\ x_4 \\ \frac{1}{\det(M)} (-C_{12}M_{22}x_4 - M_{22}G_1 + M_{12}C_{21}x_3 + M_{12}G_2) \\ \frac{1}{\det(M)} (C_{12}M_{21}x_4 + M_{21}G_1 - C_{21}M_{11}x_3 - M_{11}G_2) \end{bmatrix},$$

$$g_1(x) = \frac{1}{\det(M)} \begin{bmatrix} 0 \\ 0 \\ M_{22} \\ -M_{21} \end{bmatrix} \text{ and } g_2(x) = \frac{1}{\det(M)} \begin{bmatrix} 0 \\ 0 \\ -M_{12} - M_{22} \\ M_{11} + M_{21} \end{bmatrix}.$$

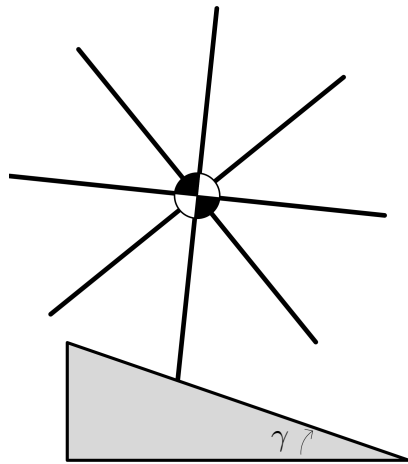
In summary, the 2-DOF bipedal robot under study belongs to the class of hybrid systems. The next chapter studies and analyzes the open-loop behaviour of the robot and motivates the concept of “hybrid virtual holonomic constraints” (hVHC). Chapter 4 formalizes hVHCs for systems of form (1.3) and utilizes this concept in order to facilitate closed-loop walking for the 2-DOF bipedal robot.

# Chapter 3

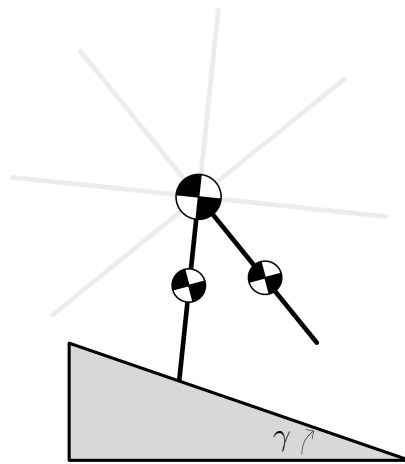
## Open-loop gaits

This chapter discusses the open-loop (or passive) behaviour of a 2-DOF bipedal robot. The idea of passive walking was motivated and studied by T. McGeer in the early 1990s [3], [8]. His idea was to convert the rolling of a rimless wheel along an inclined surface into walking by means of a clever mechanical design. A passive walker is an unactuated 2-DOF bipedal robot that can be viewed as a rimless wheel with only two spokes (Figure 3.1) with the massless spokes replaced by legs that possess mass and inertia. These two legs are connected by a revolute joint at the hip position making one leg standing on ground and the other leg swinging freely as a pendulum. In order for a 2-DOF bipedal robot to walk passively, the swing leg should land on the position where the next spoke in the rimless wheel is to land [3].

This chapter studies orbital stability of a 2-DOF passive bipedal robot. Due to the complexity of the analytical model, a numerical study is carried out based on the method of Poincaré sections. The stability problem of the hybrid gait is converted to stability of a non-linear discrete map. Stability is concluded by the calculation of the eigenvalues of the Jacobian of this non-linear discrete map. During a passive gait cycle, the functional relation between the configuration variables is viewed as a virtual constraint which motivates the idea of virtual constraints for hybrid systems. This idea is further developed in Chapter 4.



(a) Rimless wheel with massless spokes.



(b) Passive 2-DOF bipedal robot.

Figure 3.1: From rimless wheel to passive 2-DOF bipedal robot.

### 3.1 Orbital stability

This section reviews basic stability analysis for closed orbits in the state space of continuous-time systems. The following definition is due to Julés Henri Poincaré.

**Definition 3.1.1.** A limit cycle is a non-trivial, closed, isolated phase curve.

In Definition 3.1.1, non-trivial and closed means that the corresponding integral curve is non-constant and periodic. Isolated means that in a neighbourhood of the closed phase curve, there are no other closed phase curves. For general non-linear systems, there are no checkable conditions for there to exist a limit cycle. For systems on the plane there are results, including Bendixson's criterion, that can be used to find closed-orbits. For more about Bendixson's criterion, the reader is referred to [40].

Consider a continuous-time system

$$\dot{x} = f(x), \quad x \in \mathcal{X} \subseteq \mathbb{R}^n \tag{3.1}$$

where  $f$  is continuously differentiable and  $\mathcal{X}$  is a domain, i.e., an open and connected set. Given an initial condition  $x(0) = x_0 \in \mathcal{X}$ , let  $\phi(t, x_0)$  denote the corresponding solution

of (3.1). Suppose that (3.1) has a non-trivial closed phase curve  $\gamma$  passing through the point  $p \in \mathcal{X}$ . Let  $T > 0$  be the minimum period of  $\phi(t, p)$ . Then  $\phi(T, p) = p$  and  $\gamma = \phi([0, T], p)$ .

**Definition 3.1.2.** Given a set  $S \subseteq \mathbb{R}^n$  and a point  $x \in \mathbb{R}^n$ , the point-to-set distance is

$$\|x\|_S := \inf_{y \in S} \|x - y\|.$$

**Definition 3.1.3.** The closed orbit  $\gamma$  is orbitally asymptotically stable if

$$(\forall \epsilon > 0) (\exists \delta > 0) (\forall x_0 \in \mathcal{X}) \|x_0\|_\gamma < \delta \Rightarrow (\forall t \geq 0) \|\phi(t, x_0)\|_\gamma < \epsilon$$

and  $\|\phi(t, x_0)\|_\gamma \rightarrow 0$  as  $t \rightarrow \infty$ .

In other words, if the initial condition  $x_0$  is sufficiently close to  $\gamma$ , then the corresponding phase curve remains close to  $\gamma$  for all future time and approaches  $\gamma$  as  $t \rightarrow \infty$ .

In this section we present sufficient conditions for the asymptotic stability of  $\gamma$ . Unfortunately, the conditions are difficult to check in practice because they rely on the knowledge of the solution to (3.1). However, they can be checked approximately using numerical methods. Most importantly, they are very important in understanding the nature of the stability problem.

Poincaré's idea for studying orbital stability is illustrated in Figure 3.2. Let  $S$  be an open subset of an  $(n - 1)$ -dimensional hyperplane<sup>1</sup> passing through  $p$  and transverse to  $f$ . That is, for each  $x \in S$ , the vector  $f(x)$  is not tangent to  $S$  and is not zero either. Such a hyperplane is called a local section of  $\gamma$ . Picking an initial condition  $x_0$  in  $S$  sufficiently close to  $p$ , the phase curve through  $x_0$  intersects  $S$  again at another point  $x_1$ . If  $x_1$  is sufficiently close to  $p$ , then the same phase curve will intersect  $S$  at another point  $x_2$ . If the sequence of points obtained  $x_i$  converges to  $p$ , it is clear that the phase curve through  $x_0$  approaches the closed orbit  $\gamma$ . If the same is true for any initial  $x_0$  in a small neighbourhood of  $p$ , then  $\gamma$  is orbitally asymptotically stable. In this way, the stability problem is reduced to the study of the properties of a discrete-time system  $x_{k+1} = g(x_k)$ .

More precisely, for any  $x_0$  in a sufficiently small neighbourhood  $W$  of  $p$ , there is a time  $\tau(x_0) > 0$  such that the phase curve intersects  $S$ , i.e.,  $\phi(\tau(x_0), x_0) \in S$ . In fact [41],

<sup>1</sup>By an open subset of a hyperplane is meant the intersection of the hyperplane with an open subset of  $\mathbb{R}^n$ .

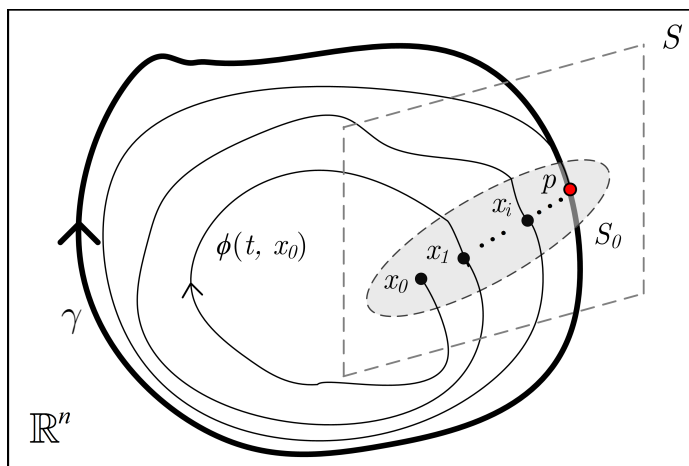


Figure 3.2: An illustration of Poincaré's method for determining orbital stability of a closed-orbit  $\gamma$ .

there exists a unique continuously differential map  $x_0 \mapsto \tau(x_0)$  such that  $\tau(p) = T$ . Let  $S_0 = S \cap W$  and define  $g : S_0 \rightarrow S$  as

$$g(x) := \phi(\tau(x), x). \quad (3.2)$$

Given  $x \in S_0$ ,  $g(x)$  represents the next intersection of the phase curve through  $x$  with the section  $S$ . The function  $g$  is called a **Poincaré map**. The map  $g$  is  $C^1$  because  $\tau$  and  $\phi$  are  $C^1$ . Now consider the non-linear discrete-time system

$$x_{k+1} = g(x_k), \quad x_k \in S_0, \quad k \in \mathbb{Z}_+ \quad (3.3)$$

with initial condition  $x_0$ . The state-space of the system is  $S_0$  which is an open subset of an  $(n - 1)$ -dimensional vector space. Note that

$$g(p) = \phi(\tau(p), p) = \phi(T, p) = p.$$

Therefore  $p$  is an equilibrium of (3.3).

**Definition 3.1.4.** The equilibrium  $p$  of (3.3) is asymptotically stable if

$$(\forall \epsilon > 0) (\exists \delta > 0) (\forall x_0 \in S_0) \|x_0 - p\| < \delta \Rightarrow (\forall k \in \mathbb{Z}_+) \|x_k - p\| < \epsilon$$

and  $x_k \rightarrow p$  as  $k \rightarrow \infty$ .

The next theorem reduces the stability study of the limit cycle,  $\gamma$ , to the study of the equilibrium point of (3.2).

**Theorem 3.1.5** ([40]). *The closed-orbit,  $\gamma$ , is orbitally asymptotically stable if and only if the equilibrium point of (3.3) is asymptotically stable.*

Based on Theorem 3.1.5, if all eigenvalues of  $dg_p$  are inside the unit disk, then the closed-orbit  $\gamma$  of (3.1) is orbitally asymptotically stable.

## 3.2 Passive 2-D.O.F. bipedal robot

Consider the 2-DOF bipedal robot model (2.45) with  $\tau = 0$ . When the system is properly initialized, the robot performs a successful gait using only the force of gravity to provide energy [3]. The corresponding gait is called passive because there is no active control of the motion. Without loss of generality, assign numbers to each of the legs on the robot. Let the angular position of leg 1 be  $\theta_1 \in \mathbb{R}$  and the angular position of leg 2 be  $\theta_2 \in \mathbb{R}$ . The coordinates  $\text{col}(\theta_1, \theta_2)$  are referred to as **leg coordinates**. During a successful gait, leg 1 plays the role of the stance leg for some time (i.e.  $\theta_1 = \theta_{st}$ ) and, when the states of (2.45) hit the guard condition, leg 1 becomes the swing leg (i.e.  $\theta_1 = \theta_{sw}$ ). The sequence of leg 1 acting as the stance leg followed leg 1 acting as the swing leg continues indefinitely during a successful gait. This “periodic” motion can be visualized by graphing the phase curves on the  $(\theta_1, \dot{\theta}_1)$  and  $(\theta_2, \dot{\theta}_2)$  planes. The periodicity of this motion is captured by the closed orbits in the  $(\theta_1, \dot{\theta}_1)$ ,  $(\theta_2, \dot{\theta}_2)$  planes. Figure 3.3 shows a typical closed orbit corresponding to leg 2 undergoing a passive gait. In addition, Table 3.1 summarizes the parameters used in our simulations.

Table 3.1: Parameters used in simulations.

$m_1$	$m_2$	$m_H$	$I_1$	$I_2$	$\ell_1$	$\ell_2$	$\ell_3$	$\ell_4$	$\gamma$
5 kg	5 kg	10 kg	0.333 kg·m <sup>2</sup>	0.333 kg·m <sup>2</sup>	0.5 m	0.5 m	0.5 m	0.5 m	2.5°

The closed-orbit is divided into four stages and described as follows. Stage 1 is where the leg undergoes swinging and is called the swing leg, i.e.,  $\theta_2 = \theta_{sw}$ . Stage 2 indicates that the leg hits the ground and is ready to transfer its role from being swinging and become pinned to ground, i.e., standing. Also, as discussed in the previous chapter, leg 2 loses a fraction of its angular velocity as a result of impact. Once the leg enters stage 3, it becomes the stance leg, i.e.,  $\theta_2 = \theta_{st}$ . At the end of stage 3, the leg gains velocity as compared to

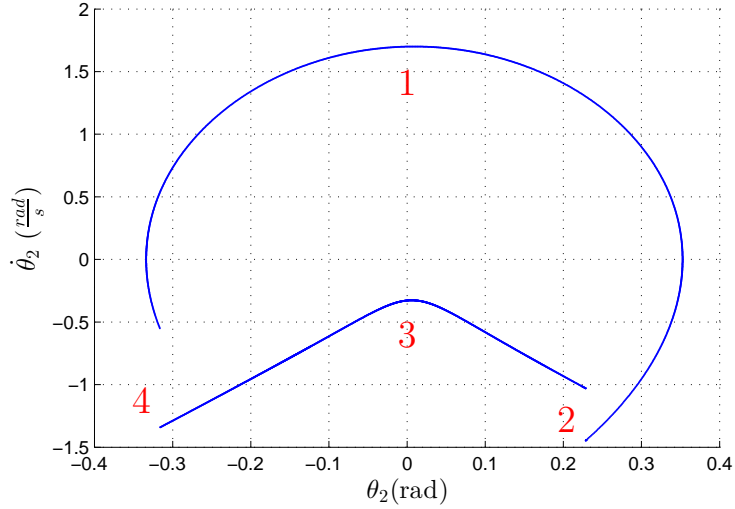
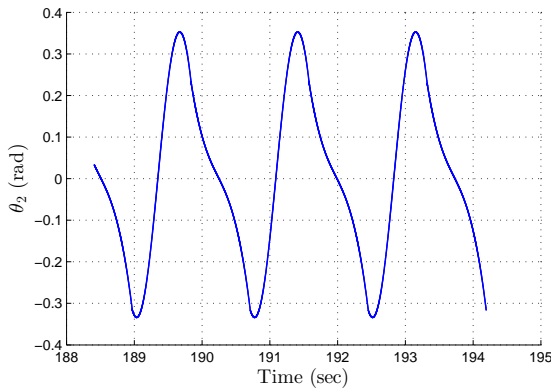
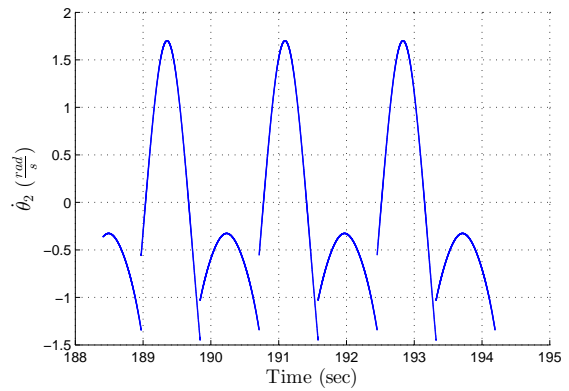


Figure 3.3: A typical closed-orbit for the the 2-DOF bipedal robot.

the start of stage 3. Then, at stage 4, leg 2 returns to being the swing leg, where impact causes the leg to lose some of its gained velocity in such a way that makes its lost velocity equal to the velocity at the beginning of stage 1. Since this closed-orbit is found to be isolated, it is referred to as hybrid limit cycle (HLC).



(a) Angular position versus time.

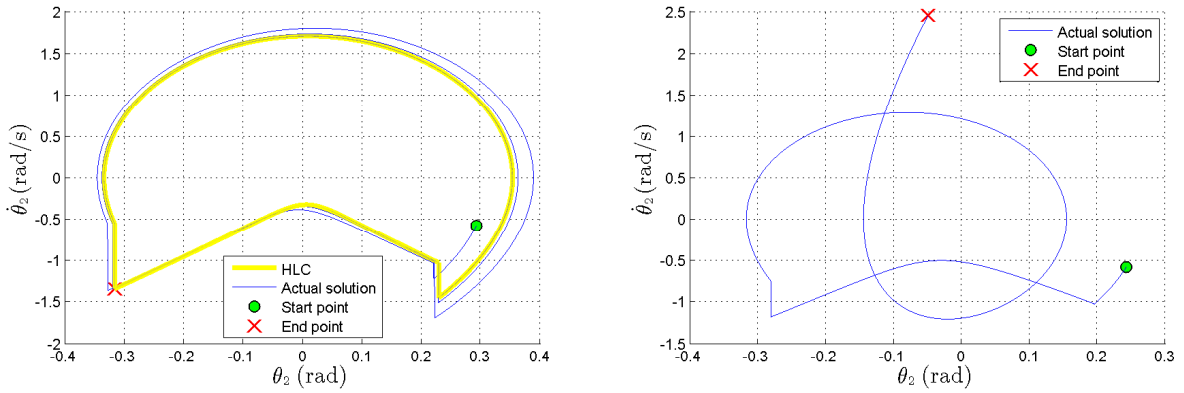


(b) Angular velocity versus time.

Figure 3.4: Angular position and angular velocity of leg 2 as functions of time.

Figure 3.4 shows the angular quantities of leg 2 undergoing a passive gait in steady-state as functions of time. Note the instantaneous jumps in angular velocity values at impact points.

One drawback of a passive gait is its sensitivity to system parameters and initial conditions. Figure 3.5 shows a set of initial conditions that converge to the closed orbit. A small perturbation to the initial conditions results in divergence from the closed orbit (Figure 3.5b).



(a) Set of initial conditions that converge to the HLC.

(b) Set of initial conditions that diverge from the HLC.

Figure 3.5: The passive gait is sensitive to initial conditions.

### 3.2.1 Numerical stability test using Poincaré's method

The stability of the passive gait is studied numerically (through the method of Poincaré) since the analytical model of continuous-time dynamics of the 2-DOF bipedal robot are complex. The detailed unforced continuous-time dynamics in state-space form are

$$\begin{aligned}
 \dot{x}_1 &= x_3 \\
 \dot{x}_2 &= x_4 \\
 \dot{x}_3 &= \frac{1}{\det(M)} (-C_{12}M_{22}x_4 - M_{22}G_1 + M_{12}C_{21}x_3 + M_{12}G_2) \\
 \dot{x}_4 &= \frac{1}{\det(M)} (C_{12}M_{21}x_4 + M_{21}G_1 - C_{21}M_{11}x_3 - M_{11}G_2)
 \end{aligned} \tag{3.4}$$

The quantities  $M_{ij}$ ,  $C_{ij}$  and  $G_i$  are the  $(i, j)^{\text{th}}$  entries of, respectively, the mass matrix (2.21), centripetal force matrix (2.22) and gravity vector (2.23) in (2.20).

**Proposition 3.2.1.** For all  $x \in \mathbb{R}^4$ ,  $\det(M) \neq 0$ .

*Proof.* The expression for  $\det(M)$  is

$$\det(M) := M_{11}M_{22} - M_{12}(x)M_{21}(x).$$

Suppose that  $\det(M) = 0$ . Then,

$$\begin{aligned} \det(M) = 0 &\Leftrightarrow M_{11}M_{22} = M_{12}(x)M_{21}(x) \\ &\Leftrightarrow \frac{M_{11}M_{22}}{(m_2\ell\ell_3)^2} = \cos^2(x_1 - x_2). \end{aligned}$$

Since  $\cos^2(x_1 - x_2) \leq 1$ , we necessarily have that

$$\frac{M_{11}M_{22}}{(m_2\ell\ell_3)^2} \leq 1.$$

But,

$$M_{11}M_{22} = (m_2\ell\ell_3)^2 + \underbrace{m_1m_2(\ell_1\ell_3)^2 + m_Hm_2(\ell\ell_3)^2 + I_1m_2\ell_3^2 + I_2(m_1\ell_1^2 + m_2\ell^2 + m_H\ell^2 + I_1)}_{:=w}.$$

with all terms being positive. Therefore,

$$\frac{M_{11}M_{22}}{(m_2\ell\ell_3)^2} = 1 + \frac{w}{(m_2\ell\ell_3)^2} > 1.$$

This shows that  $M$  is non-singular. □

We will implement a naïve numerical method to compute the Jacobian of the Poincaré map for the 2-DOF bipedal robot. We will apply this numerical procedure on one leg, say, leg 2. The obtained results also apply to the other leg due to mechanical symmetry of the system. Define a subspace in  $\mathbb{R}^4$

$$\mathcal{R} := \text{span} \left\{ \begin{bmatrix} 0 \\ 1 \\ 0 \\ 0 \end{bmatrix}, \begin{bmatrix} 0 \\ 0 \\ 0 \\ 1 \end{bmatrix} \right\}. \quad (3.5)$$

From Figure 3.3 we suspect that the projection of the solution of (3.4) onto  $\mathcal{R}$  generates closed orbits. Let  $\pi : \mathbb{R}^4 \rightarrow \mathcal{R}$  denote the natural projection. Then, a Poincaré section,  $S$ , to the two-dimensional projected vector field,  $\pi \circ f(x)$ , is a one-dimensional affine subspace, i.e. a line.

Our numerical procedure proceeds as follows.

- (a) Pick an initial condition  $x(0) = x_0 \in \mathbb{R}^4$ . Simulate the unforced system (3.4) for a sufficiently long time so that the solution  $x(t)$  at the end of the simulation is approximately on the hybrid limit cycles. Let  $x_f$  denote the final state of this simulation.
- (b) Project  $x_f$  on  $\mathcal{R}$  as  $\pi(x_f)$ . Then, project the vector field of (3.4) on  $\mathcal{R}$  and evaluate it at  $\pi(x_f)$ . This results in a vector  $\pi \circ f(x)$  that is tangent to the hybrid limit cycle at  $\pi(x_f)$ . Rotate this vector by  $90^\circ$  in order to generate a transverse set,  $S$ .
- (c) Solve the differential Equation (3.4) with initial condition  $x_f$  until  $\pi(x(t))$  crosses  $S$  for the first time. The crossing point, being on  $S$  and also approximately on the hybrid limit cycle, can be considered the equilibrium  $p$  of the Poincaré map.
- (d) We now write a function that approximately implements the Poincaré maps  $g : S \rightarrow S$ .
- (e) Using the functions from part (d), we use finite difference approximation of the derivative to compute  $dg$  near  $p$ . We numerically verify that  $|dg| < 1$ .

The above numerical procedure was carried out as follows.

- (a) A vector of initial states  $x_0$  that converged to the hybrid limit cycle was found to be  $x_0 = \text{col}(-0.226, 0.272, -1.01, -0.732)$ . This vector is a result of many simulation iterations. The solution was carried out for a sufficiently large time until it approached a hybrid limit cycle. At the end of the simulation, the final point was reported to be  $x_f = \text{col}(-0.142, 0.353, -0.759, -1.55 \times 10^{-11})$ .
- (b) The projection of  $x_f$  onto  $\mathcal{R}$  becomes  $\pi(x_f) = \text{col}(0, 0.353, 0, -1.55 \times 10^{-11})$ . Then,  $\pi \circ f(x_f) = \text{col}(0, -1.55 \times 10^{-11}, 0, -8.53)$ , which is tangent to the hybrid limit cycle at  $\pi(x_f)$ . On  $\mathcal{R}$ , rotating this vector by  $\approx 90^\circ$  results in the line  $x_4 = 0$ . Therefore, the section

$$S := \{x \in \mathcal{R} : x_4 = 0\} \tag{3.6}$$

is transverse to the hybrid limit cycle.

- (c) The differential equations (3.4) were solved with initial condition  $x_f$  until  $\pi(x(t))$  crossed  $S$  for the first time resulting in an equilibrium point  $p = \text{col}(-0.142, 0.353, -0.759, 0)$ . Then, the point  $\pi(p)$  becomes  $\pi(p) = \text{col}(0, 0.353, 0, 0) \in S$ .
- (d) The discrete map  $g : S \rightarrow S$  was generated as follows. The system was initialized such that  $\pi(x(0)) \in S$ . Then, solution was carried out until the event  $\pi(x) \in S$  occurred, at which the simulation was halted. The event corresponds to the projected states

belonging to  $S$ . Then, the point  $x(t)|_S$  was recorded. The system was re-initialized at  $x_0 = x(t)|_S$  and solved until the event  $\pi(x) \in S$  occurred again. This process was repeated until  $\pi \circ x(t)|_S$  converged to  $p$  resulting in a non-linear discrete maps  $g$ . This map is shown in Figure 3.6 near its equilibrium,  $p$ .

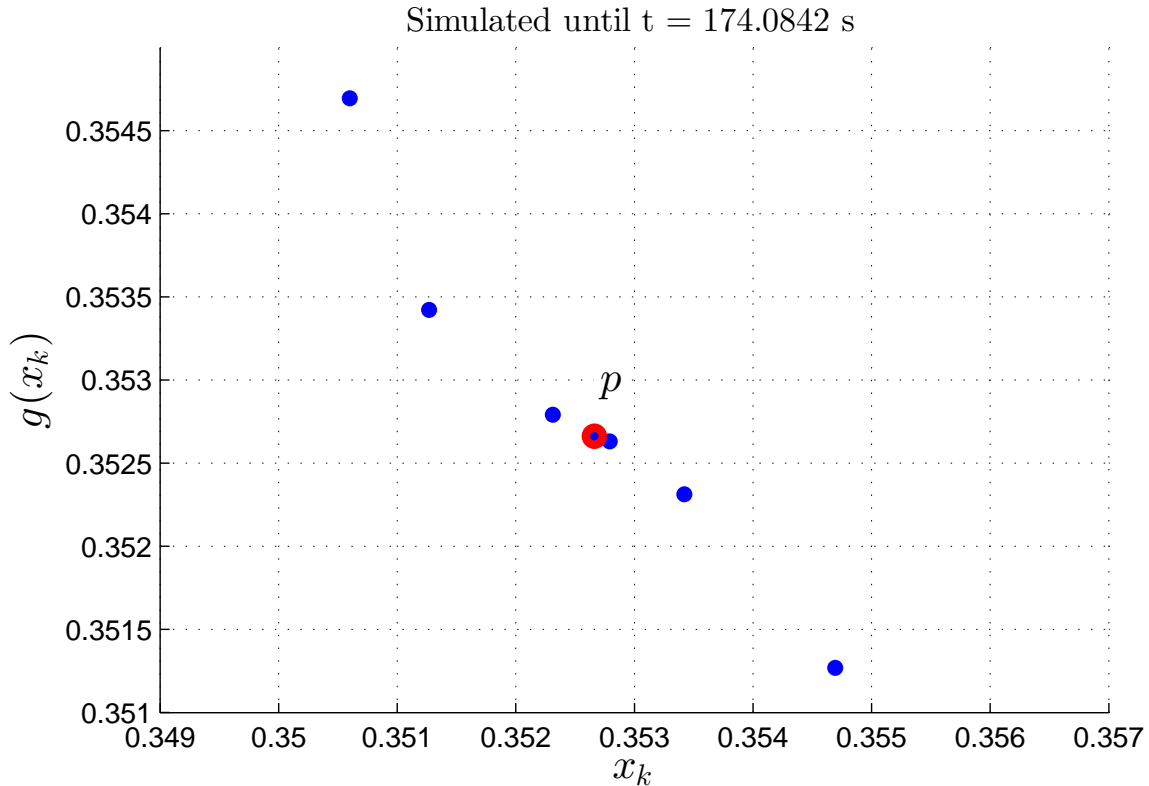


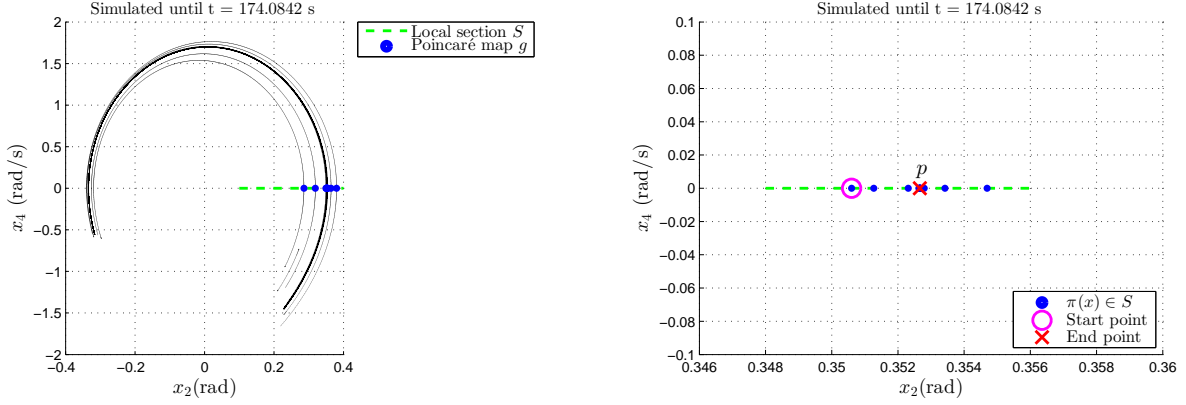
Figure 3.6: Poincaré map of the passive 2-DOF bipedal robot (leg 2).

- (e) The derivative  $dg$  near the equilibrium  $p$  is found using finite difference approximation as  $dg = -0.902$ , showing that  $p$  is a stable equilibrium for  $g$ .

It is left to note that all numerical solutions above were performed in MATLAB<sup>TM</sup> using the built-in solver `ode23`.

Figures 3.7 illustrates the above discussion.

**Proposition 3.2.2.** *The set  $S$  (3.6) is a local section of the projection of the vector field (3.4) onto  $\mathcal{R}$ .*



(a) The local section  $S$  with solutions projected onto  $\mathcal{R}$ . (b) Enlarged view of the local section  $S$  with projected solutions onto  $\mathcal{R}$  evaluated  $S$ .

Figure 3.7: Poincaré sections.

*Proof.* To show that  $S$  is local section to  $\pi \circ f(x)$ , i.e. not tangent to  $\pi \circ f(x)|_S$ , we will show that  $\pi \circ f(x)|_S$  is not normal to the Jacobian of the equation defining  $S$ . The projection of the vector field of (3.4) on  $\mathcal{R}$  is

$$\pi \circ f(x) = \begin{bmatrix} 0 \\ x_4 \\ 0 \\ \frac{1}{\det(M)} (C_{12}M_{21}x_4 + M_{21}G_1 - C_{21}M_{11}x_3 - M_{11}G_2) \end{bmatrix}.$$

Then, when  $\pi \circ f(x)$  is evaluated at  $S$  we have

$$\pi \circ f(x)|_S = \begin{bmatrix} 0 \\ 0 \\ 0 \\ \frac{1}{\det(M)|_S} (-M_{11}G_2) \end{bmatrix}.$$

The Jacobian of the equation defining  $S$  is  $n := [0 \ 0 \ 0 \ 1]$ . Then, we have

$$\begin{aligned} n \cdot \pi \circ f(x)|_S &= [0 \ 0 \ 0 \ 1] \begin{bmatrix} 0 \\ 0 \\ 0 \\ \frac{1}{\det(M)|_S} (-M_{11}G_2) \end{bmatrix} \\ &= \frac{1}{\det(M)|_S} (-M_{11}G_2) \\ &= -\frac{1}{\det(M)|_S} (m_1\ell_1^2 + m_2\ell^2 + m_H\ell^2 + I_1) m_2g\ell_3 \sin(x_2) \end{aligned}$$

As a result,  $n$  is not tangent to  $\pi \circ f(x)|_S$  as long as  $x_2 \neq 0$ . Therefore,  $S$  is a local section to  $\pi \circ f(x)$  by definition.  $\square$

### 3.2.2 Modelling passive gaits as hybrid virtual holonomic constraints

We conclude this chapter by making an observation that will lead us to the control design studied in the subsequent chapter. The stable gait for the unforced system we identified in Section 3.2.1 can be viewed as a holonomic constraint between the stance and the swing legs. More precisely, the holonomic constraint defines the “shape” of the gait. Figure 3.8 plots the functional relation between the swing and the stance leg over a gait cycle. The

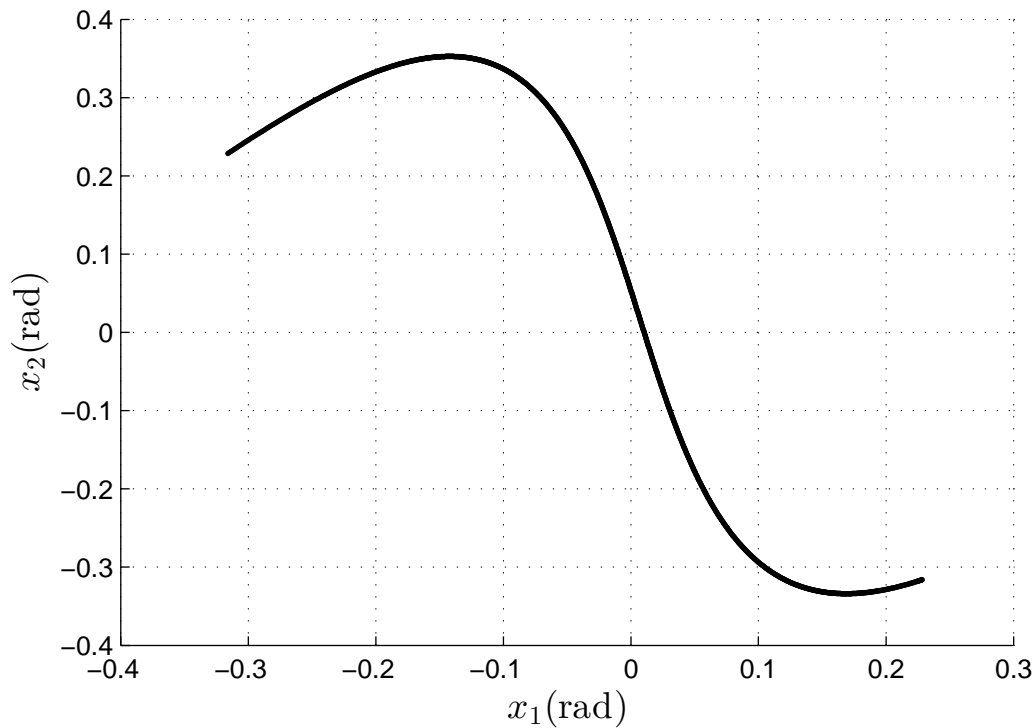


Figure 3.8: Functional relation between the swing and stance legs over a gait cycle.

constraint depicted in Figure 3.8 can be viewed as a function  $h : \mathbb{R}^4 \rightarrow \mathbb{R}$ ,  $(x_1, x_2) \mapsto h(x_1, x_2)$ . This constraint defines the shape of the gait in the sense that the functional

relationship does not provide any information about the time parameterization of the motion along the gait. It is clear that the set

$$\Gamma := \{x \in \mathbb{R}^4 : h(x_1, x_2) = dh_{x_1, x_2} \text{col}(x_3, x_3) = 0\}$$

is attractive and invariant for the unforced system. Our objectives in the next chapter are to, through feedback control, enlarge the region of attraction of  $\Gamma$  and to design other stable gaits that do not necessarily have the shape of the passive gait depicted in Figure 3.8.

# Chapter 4

## Hybrid virtual holonomic constraints

In this chapter, the idea of virtual holonomic constraints (VHC) is extended to hybrid VHC of a hybrid Euler-Lagrange system of the form (1.3). The concept of hybrid VHC is utilized to design two distinct feedback-linearizing control laws for a 2-DOF bipedal robot. The first control law (Section 4.5) yields a fully actuated closed-loop system whereas the second control law (Section 4.6) generates an under-actuated closed-loop system.

### 4.1 Virtual holonomic constraints

As its name suggests, a virtual holonomic constraint (VHC) is a non-physical constraint that depends on configuration variables (i.e. positions). For a continuous-time Euler-Lagrange control system, the control input must enforce invariance of the constraint manifold in the sense of Definition 1.1.1.

---

**Example 4.1.1.** Consider a particle of mass  $m$  falling under the effect of gravity with a horizontal force applied on it. Let the gravitational constant be  $g_r$ . The particle can be restricted to a vertical plane while falling by means of the applied horizontal force. On the other hand, the same applied horizontal force can not restrict the particle to a horizontal plane due to the presence of the gravity force. Figure 4.1 illustrates this concept. The vertical plane of Figure 4.1a is a feasible VHC and the horizontal plane of Figure 4.1b is not a feasible VHC.

---

△

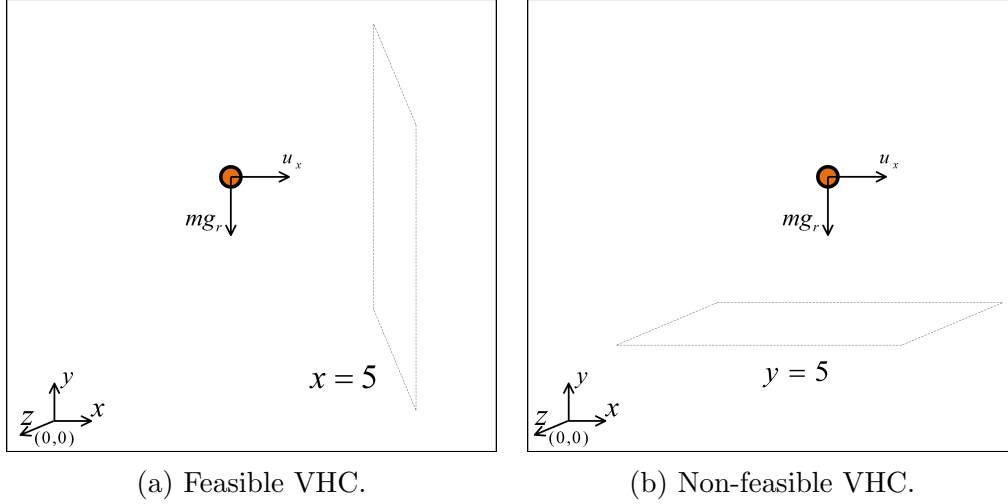


Figure 4.1: Feasible versus non-feasible VHCs.

In the control systems literature, a formal definition of continuous-time VHC exploiting feasibility was given in [2], see also Definition 1.1.1. The next definition characterizes those virtual holonomic constraints for which invariance of the set constraint manifold  $\Gamma$  can be achieved through partial state feedback linearization.

**Definition 4.1.1** (Regular VHC). A virtual holonomic constraint (VHC) of order  $k$  for System (1.2) is called a **regular VHC** if the function  $y = h(q)$  yields a well-defined relative degree of  $\{2, \dots, 2\}$  everywhere on the set  $\Gamma$ .

---

**Example 4.1.2.** Let the state vector of the particle in Example 4.1.1 be  $\xi := \text{col}(x, y, z, \dot{x}, \dot{y}, \dot{z}) \in \mathbb{R}^6$ . Then, the particle's evolution is described by a system of the form

$$\dot{\xi} = f(\xi) + g(\xi)u \quad (4.1)$$

where  $f(\xi) = \text{col}(\xi_4, \xi_5, \xi_6, 0, -g_r, 0)$ ,  $g(\xi) = \text{col}(0, 0, 0, \frac{1}{m}, 0, 0)$  and  $u = u_x$ .

Define a candidate virtual holonomic constraint

$$\begin{aligned} h : \mathbb{R}^6 &\rightarrow \mathbb{R} \\ \xi &\mapsto \xi_1 - 5. \end{aligned} \quad (4.2)$$

In this case, the constraint manifold is

$$\Gamma = \{\xi \in \mathbb{R}^6 : \xi_1 - 5 = \xi_4 = 0\}. \quad (4.3)$$

Equations (4.1) and (4.2) can be viewed as a single-input single-output system. The relative degree of the system is computed by differentiating (4.2) with respect to time as

$$\begin{aligned} \dot{h}(t) &= dh_\xi \dot{\xi} = \xi_4 \\ \ddot{h}(t) &= d \left( dh_\xi \dot{\xi} \right)_\xi \dot{\xi} = \frac{u_x}{m}. \end{aligned}$$

Therefore, for all  $m \in \mathbb{R}$ , system (4.1) with output (4.2) has a relative degree of 2 at every  $\xi \in \mathbb{R}^6$  and, in particular, on the constraint manifold  $\Gamma$ . Therefore, the relation (4.2) is a regular VHC.

Now, consider the following candidate virtual holonomic constraint

$$h(\xi) = \xi_2 - 5. \quad (4.4)$$

Then,

$$\begin{aligned} \dot{h}(t) &= dh_\xi \dot{\xi} = \dot{\xi}_2 \\ \ddot{h}(t) &= d \left( dh_\xi \dot{\xi} \right)_\xi \dot{\xi} = -g_r \\ h^{(3)}(t) &= 0. \end{aligned}$$

Therefore, system (4.1) with output (4.4) does not have a well defined relative degree and, thus, relation (4.4) is not a regular VHC.

△

## 4.2 Hybrid virtual holonomic constraints

In the previous section, we reviewed the notion of regular VHC for continuous-time Euler-Lagrange systems. In this section, we extend the notion of regularity of VHCs to hybrid systems of the form (1.3) and introduce hybrid regular VHC. We begin with the following definitions.

**Definition 4.2.1** (Hybrid VHC of order  $k$ ). A hybrid virtual holonomic constraint of order  $k$  (hVHC) for system (1.3) is a continuous-time VHC of order  $k$  such that the constraint manifold is invariant under the discrete-time dynamics

$$J(\mathcal{S} \cap \Gamma) \subseteq \Gamma.$$

Based on Definition 4.2.1, a hVHC can be satisfied even if the states “jump” instantaneously due to discrete-time dynamics. This feature is not captured in Definition 1.1.1.

**Definition 4.2.2** (Regular Hybrid VHC). A hVHC of order  $k$  for system (1.3) is called a regular hybrid virtual holonomic constraint if the output function  $y = h(q)$  yields a well-defined vector relative degree  $\{2, \dots, 2\}$  everywhere on the constraint manifold  $\Gamma$ .

In Section 3.2, we showed that the passive gait of the 2-DOF bipedal robot can be modelled as a functional relationship between the swing and stance legs (i.e. configuration variables). This functional relationship can be viewed as a hVHC of degree 1 to be enforced. This motivates us to study the following class of constraint functions.

**Assumption 3.** The VHCs for system (1.3) considered in this Chapter have order  $N - 1$  and the form

$$h(x_1, \dots, x_N) = \text{col}(x_2 - p_1(x_1), \dots, x_N - p_{N-1}(x_1)) \quad (4.5)$$

where  $p_i : \mathbb{R} \mapsto \mathbb{R}$  are  $C^1$ ,  $i \in \{1, 2, \dots, N - 1\}$ .

The next result gives conditions on a VHC under Assumption 3 resulting in a hVHC of order  $N - 1$  for the entire hybrid system (1.3).

**Proposition 4.2.3.** *Let  $h : \mathbb{R}^N \rightarrow \mathbb{R}^{N-1}$  be a VHC of the form (4.5) for the continuous dynamics of the hybrid Euler-Lagrange system (1.3). Then,  $h$  is hVHC for (1.3) if and only if, for all  $x \in \mathcal{S} \cap \Gamma$ ,*

$$p_1(J_1(x)) = J_2(x), \quad \dots, \quad p_{N-1}(J_{N-1}(x)) = J_N(x) \quad (4.6)$$

and,

$$\left. \frac{\partial p_1}{\partial x_1} \right|_{x_1^+} = \frac{J_{N+2}(x)}{J_{N+1}(x)}, \quad \dots, \quad \left. \frac{\partial p_{N-1}}{\partial x_1} \right|_{x_1^+} = \frac{J_{2N}(x)}{J_{N+1}(x)} \quad (4.7)$$

where  $J_i$  is the  $i^{\text{th}}$  row of the function  $J$  in (1.3).

*Proof.* We will show that conditions (4.6) and (4.7) are necessary and sufficient for a VHC,  $h$ , of the form (4.5) to be a hVHC in the sense of Definition 4.2.1. Since  $h$  is assumed to be a VHC, then if the system is initialized on the constraint manifold, it remains on it until the system reaches  $x \in \mathcal{S} \cap \Gamma$ . Throughout this proof and the rest of the thesis, let the “-” superscript denotes variables when the state vector belongs to the guard condition.

**Necessity.** We will show that if  $h$  is hVHC in the sense of Definition 4.2.1, then the function  $p$  must satisfy the conditions (4.6) and (4.7). In other words, we will show that if the constraint manifold is invariant under discrete dynamics, then the function  $p$  must satisfy the conditions (4.6) and (4.7). Suppose  $x \in \mathcal{S} \cap \Gamma$ , then

$$\begin{aligned} h_1(x^-) &= x_2^- - p_1(x_1^-) \\ &= 0 \end{aligned}$$

But since  $h$  is a hVHC in the sense of Definition 4.2.1 (by hypothesis), we have

$$\begin{aligned} h_1(x^+) &= x_2^+ - p_1(x_1^+) \\ &= 0 \\ \Rightarrow J_2(x^-) - p_1(J_1(x^-)) &= 0 && \text{(By definition of } J) \\ \Rightarrow p_1(J_1(x^-)) &= J_2(x^-) \end{aligned}$$

Similarly,

$$p_2(J_2(x^-)) = J_3(x^-), \dots, p_{N-1}(J_{N-1}(x^-)) = J_N(x^-)$$

where,  $x^- = \text{col}(x_1^-, p_1(x_1^-), \dots, p_{N-1}(x_1^-))$  since  $x \in \mathcal{S} \cap \Gamma$  implies  $h_1(x^-) = h_2(x^-) = \dots = h_{N-1}(x^-) = 0$ .

Now for  $x \in \mathcal{S} \cap \Gamma$  we have,

$$\begin{aligned} \dot{h}_1(x^-) &= x_{N+2}^- - \left. \frac{\partial p_1}{\partial x_1} \right|_{x_1^-} (x_{N+1}^-) \\ &= 0. \end{aligned}$$

But,

$$\begin{aligned}
\dot{h}_1(x^+) &= x_{N+2}^+ - \left. \frac{\partial p_1}{\partial x_1} \right|_{x_1^+} (x_{N+1}^+) \\
&= 0 && \text{(By hypothesis and Definition 4.2.1)} \\
\Rightarrow \left. \frac{\partial p_1}{\partial x_1} \right|_{x_1^+} &= \frac{x_{N+2}^+}{x_{N+1}^+} \\
\Rightarrow \left. \frac{\partial p_1}{\partial x_1} \right|_{x_1^+} &= \frac{J_{N+2}(x^-)}{J_{N+1}(x^-)} && \text{(By definition of } J)
\end{aligned}$$

Similarly,

$$\left. \frac{\partial p_2}{\partial x_1} \right|_{x_1^+} = \frac{J_{N+3}(x^-)}{J_{N+1}(x^-)}, \dots, \left. \frac{\partial p_{N-1}}{\partial x_1} \right|_{x_1^+} = \frac{J_{2N}(x^-)}{J_{N+1}(x^-)}$$

where

$$x^- = \text{col} (x_1^-, p_1(x_1^-), \dots, p_{N-1}(x_1^-)).$$

**Sufficiency.** Here we will show that if  $h$  satisfies (4.6) and (4.7), then  $h$  is a hVHC in the sense of Definition (4.2.1). Suppose  $x \in \mathcal{S} \cap \Gamma$ , then

$$\begin{aligned}
h_1(x^-) &= x_2^- - p_1(x_1^-) \\
&= 0.
\end{aligned}$$

Since  $h$  satisfies (4.6), we have

$$\begin{aligned}
p_1(J_1(x^-)) &= J_2(x^-) \\
\Rightarrow J_2(x^-) - p_1(J_1(x^-)) &= 0 \\
\Rightarrow x_2^+ - p_1(x_1^+) &= 0 && \text{(by definition of } J) \\
\Rightarrow h_1(x^+) &= 0
\end{aligned}$$

Similarly,

$$h_2(x^+) = h_3(x^+) = \dots = h_{N-1}(x^+) = 0.$$

Now for  $x \in \mathcal{S} \cap \Gamma$  we have,

$$\begin{aligned}
\dot{h}_1(x^-) &= x_{N+1}^- - \left. \frac{\partial p_1}{\partial x_1} \right|_{x_1^-} x_{N+1}^- \\
&= 0.
\end{aligned}$$

Since  $h$  satisfies (4.7), we have

$$\begin{aligned}
& \frac{\partial p_1}{\partial x_1} \Big|_{x_1^+} = \frac{J_{N+2}(x^-)}{J_{N+1}(x^-)} \\
\Rightarrow J_{N+2}(x^-) - \frac{\partial p_1}{\partial x_1} \Big|_{x_1^+} J_{N+1}(x^-) &= 0 \\
\Rightarrow x_{N+2}^+ - \frac{\partial p_1}{\partial x_1} \Big|_{x_1^+} x_{N+1}^+ &= 0 \quad (\text{by definition of } J) \\
\Rightarrow \dot{h}_1(x^+) &= 0
\end{aligned}$$

Similarly,

$$\dot{h}_2(x^+) = \dot{h}_3(x^+) = \dots = \dot{h}_{N-1}(x^+) = 0.$$

This completes the proof.  $\square$

The above result allows us to design hVHCs for Euler-Lagrange systems with impacts (1.3). We will use this result in the next section in order to design a hVHC for the 2-DOF bipedal robot.

### 4.3 Virtual holonomic constraints applied to the 2-D.O.F bipedal robot

Consider the 2-DOF bipedal robot whose model was derived in Chapter 2 and can be compactly written in state-space form as

$$\text{EL}_{\mathcal{H}} : \begin{cases} \dot{x} = f(x) + \sum_{i=1}^2 g_i(x)\tau_i, & x \notin \mathcal{S} \\ x = J(x), & x \in \mathcal{S}. \end{cases} \quad (4.8)$$

Let the desired motion of the robot be defined such that the swing leg is expressed as a function of the stance leg (i.e.  $x_2 = p(x_1)$ ). Then, the objective is to enforce the following virtual holonomic constraint,

$$h(x) = x_2 - p(x_1), \quad (4.9)$$

which satisfies Assumption 3. Now, Equations (4.8) with output function (4.9) constitute a multi-input single-output system. For (4.9) to be a regular VHC of (4.8), the relative degree must be 2 on the constraint manifold.

**Proposition 4.3.1.** *Any VHC that satisfies Assumption 3 is a regular VHC for the continuous dynamics of (4.8).*

*Proof.* Define the output  $y = h(x)$  for the continuous-time dynamics of (4.8). The system has 2 inputs and 1 output. Then,

$$\begin{aligned} L_{g_1}h(x) &= 0 \\ L_{g_1}L_fh(x) &= -\frac{1}{\det(M)} \left( \frac{\partial p}{\partial x_1} M_{22} + M_{21}(x) \right) \end{aligned}$$

and,

$$\begin{aligned} L_{g_2}h(x) &= 0 \\ L_{g_2}L_fh(x) &= \frac{1}{\det(M)} \left( \frac{\partial p}{\partial x_1} (M_{12}(x) + M_{22}) + M_{11} + M_{21}(x) \right) \end{aligned}$$

where  $M_{ij}$ ,  $i, j = 1, 2$  are the entries of the mass matrix  $M(x)$  in (2.19) and  $\det(M) \neq 0$  for all  $x \in \mathbb{R}^4$  (see Proposition 3.2.1).

Now, define

$$A_1(x) = [L_{g_1}L_fh(x) \quad L_{g_2}L_fh(x)] \quad (4.10)$$

Assume there exists  $x \in \mathbb{R}^4$  such that  $A_1(x)$  is not full rank. This implies that,

$$\begin{aligned} -\frac{\partial p}{\partial x_1} M_{22} - M_{21}(x) &= 0, \\ \left( \frac{\partial p}{\partial x_1} (M_{12}(x) + M_{22}) + M_{11} + M_{21}(x) \right) &= 0. \end{aligned}$$

Noting that  $M_{12}(x) \equiv M_{21}(x)$ , the above two equations lead to,

$$\frac{\partial p}{\partial x_1} = -\frac{M_{21}(x)}{M_{22}}$$

and,

$$\frac{\partial p}{\partial x_1} = \frac{-M_{11} - M_{21}(x)}{M_{21}(x) + M_{22}}$$

For the above two equations to hold simultaneously,

$$\begin{aligned}
-\frac{M_{21}(x)}{M_{22}} &= -\frac{M_{11} + M_{21}(x)}{M_{21}(x) + M_{22}}, \\
\Rightarrow M_{21}^2(x) + M_{21}(x)M_{22} &= M_{11}M_{22} + M_{21}(x)M_{22}, \\
\Rightarrow M_{21}^2(x) &= M_{11}M_{22}, \\
\Rightarrow (m_2\ell\ell_3)^2 \cos^2(x_1 - x_2) &= M_{11}M_{22}, \\
\Rightarrow \cos^2(x_1 - x_2) &= \frac{M_{11}M_{22}}{(m_2\ell\ell_3)^2}.
\end{aligned}$$

But from the proof of Proposition 3.2.1 we have,

$$\frac{M_{11}M_{22}}{(m_2\ell\ell_3)^2} > 1 \quad \forall x \in \mathbb{R}^4$$

Therefore, there does not exist  $x \in \mathbb{R}^4$  such that  $A_1(x)$  is not full rank which implies that, for all  $x \in \mathbb{R}^4$ ,  $A_1(x)$  is full rank. As a result, the continuous dynamics of (4.8) with output function  $y = h(x)$  have a relative degree of  $r = 2$  for all  $x \in \mathbb{R}^4$ , and hence, have a relative degree of 2 on the constraint manifold. This implies that  $h(x)$  is a regular VHC by definition.  $\square$

So far we have shown that (4.9) is a regular VHC, and hence, a feasible VHC for the continuous-time dynamics of the 2-DOF bipedal robot. Next we extend the VHC (4.9) to hVHC to the whole hybrid system (4.8).

**Proposition 4.3.2.** *Let  $h : \mathbb{R}^N \rightarrow \mathbb{R}^{N-1}$  be a VHC of the form (4.5) for the continuous dynamics of the 2-DOF bipedal robot (4.8). Then,  $h$  is hVHC for (4.8) if and only if, for all  $x \in \mathcal{S} \cap \Gamma$ ,*

$$\begin{aligned}
i) \quad & p \circ p(x_1) = x_1, \\
ii) \quad & \frac{\partial p}{\partial x_1} \Big|_{x_1^+} = \frac{\left( j_{11} + j_{12} \frac{\partial p}{\partial x_1} \right) \Big|_x x_3}{\left( j_{21} + j_{22} \frac{\partial p}{\partial x_1} \right) \Big|_x x_3}.
\end{aligned} \tag{4.11}$$

*Proof.* This proof utilizes the result of Proposition 4.2.3. Simply, the conditions (4.6) and (4.7) are applied to the 2-DOF bipedal robot model (4.8) and written as in (4.11).

For a 2 DOF-bipedal robot, condition (4.6) reads

$$p(J_1(x^-)) = J_2(x^-).$$

Using the definition of the reset map,  $J$ , of the 2-DOF bipedal robot, the above equation becomes

$$\begin{aligned} p(x_2^-) &= x_1^- \\ \Rightarrow p(p(x_1^-)) &= x_1^- \quad (\text{since } h \text{ is enforced by assumption}) \end{aligned}$$

In other words, for a 2-DOF bipedal robot with  $x \in \mathcal{S} \cap \Gamma$ , condition (4.6) reduces to

$$p \circ p(x_1) = x_1.$$

Similarly, condition (4.7) reads

$$\left. \frac{\partial p}{\partial x_1} \right|_{x_1^+} = \frac{J_4(x^-)}{J_3(x^-)}.$$

Using the definition of the reset map,  $J$ , of the 2-DOF bipedal robot, the above equation becomes

$$\begin{aligned} \left. \frac{\partial p}{\partial x_1} \right|_{x_1^+} &= \frac{j_{21}x_3^- + j_{22}x_4^-}{j_{11}x_3^- + j_{12}x_4^-} \\ &= \frac{j_{21}x_3^- + j_{22} \left. \frac{\partial p}{\partial x_1} \right|_{x_1^-} x_3^-}{j_{11}x_3^- + j_{12} \left. \frac{\partial p}{\partial x_1} \right|_{x_1^-} x_3^-} \quad (\text{since } h \text{ is enforced by assumption}) \end{aligned}$$

In other words, for a 2-DOF bipedal robot with  $x \in \mathcal{S} \cap \Gamma$ , condition (4.7) reduces to

$$\left. \frac{\partial p}{\partial x_1} \right|_{x_1^+} = \frac{\left( j_{11} + j_{12} \frac{\partial p}{\partial x_1} \right) \Big|_x x_3}{\left( j_{21} + j_{22} \frac{\partial p}{\partial x_1} \right) \Big|_x x_3}.$$

□

**Proposition 4.3.3.** *Any hVHC that satisfies Assumption 3 is regular hVHC for system (4.8).*

*Proof.* Any hVHC is, by definition, also a VHC. Also, any VHC under Assumption 3 is a regular VHC, by Proposition 4.3.1. In addition, for  $x \notin \mathcal{S}$ , any regular VHC of (4.8) implies that the relative degree on the constraint manifold is  $\{2, \dots, 2\}$ , by definition. As a result, any hVHC for (4.8) under Assumption 3 has a relative degree  $\{2, \dots, 2\}$  on the constraint manifold for  $x \notin \mathcal{S}$ . Therefore, any hVHC under Assumption 3 is regular hVHC for system (4.8), by definition. □

A convenient choice for the function  $p$  in (4.9) is polynomials. The next subsection proposes a design procedure that generates a polynomial  $p$  satisfying (4.11).

### 4.3.1 Polynomial design generating a hybrid V.H.C.

This section introduces a design procedure that returns a “shape” polynomial  $p$  in (4.9) satisfying conditions in (4.11). Let the polynomial be written as

$$p(x_1) = \alpha_m x_1^m + \alpha_{m-1} x_1^{m-1} + \cdots + \alpha_0$$

where  $m \geq 3$ .

- 1) Given a slope  $\gamma$ , pick a value for the angle of the stance leg just before impact, i.e.  $x_1^-$ . Since the impact results in a new stance angle,  $x_1^+$ , we need to set  $x_1^+$  accordingly. Then,  $x_2^- = x_1^+$  (by definition of  $J$  (2.42)) and  $x_2^- = -x_1^- - 2\gamma$  (by definition of the impact surface  $\mathcal{S}$  (2.30)). Therefore, set  $x_1^+ = -x_1^- - 2\gamma$ .
- 2) We need  $x \in \mathcal{S} \cap \Gamma$  just before an impact event. This means that

$$\begin{aligned} h(x^-) &= 0 \\ \Rightarrow x_2^- - p(x_1^-) &= 0 \\ \Rightarrow p(x_1^-) &= x_2^- \\ \Rightarrow p(x_1^-) &= x_1^+ \quad (\text{by definition of } J) \end{aligned}$$

Therefore, set  $p(x_1^-) = x_1^+$ . This implies

$$\alpha_m (x_1^-)^m + \alpha_{m-1} (x_1^-)^{m-1} + \cdots + \alpha_0 = x_1^+. \quad (4.12)$$

Steps (1) and (2) imply condition (i) in (4.11) since  $p(x_1^+) = p(p(x_1^-)) = x_1^- \Rightarrow p \circ p(x_1^-) = x_1^-$ .

- 3) We also need that the states remain in  $\Gamma$  just after impact, i.e.  $x^+ \in \Gamma$ . This means that

$$\begin{aligned} h(x^+) &= 0 \\ \Rightarrow x_2^+ - p(x_1^+) &= 0 \\ \Rightarrow p(x_1^+) &= x_2^+ \\ \Rightarrow p(x_1^+) &= x_1^- \quad (\text{by definition of } J) \end{aligned}$$

Therefore, set  $p(x_1^+) = x_1^-$ . This implies

$$\alpha_m (x_1^+)^m + \alpha_{m-1} (x_1^+)^{m-1} + \cdots + \alpha_0 = x_1^-. \quad (4.13)$$

- 4) Set  $\left. \frac{\partial p}{\partial x_1} \right|_{x_1^-} = k_1$ , where  $k_1$  is a design parameter that determines the change in  $x_1$  relative to  $x_2$  just before the impact point. This implies

$$\alpha_m (x_1^-)^{m-1} + \cdots + \alpha_1 = k_1. \quad (4.14)$$

The condition  $k_1 > k_2$ , where  $k_2$  is defined in Step 6, turns out to be a sufficient condition for stability of the origin of the  $\xi$ -subsystem presented in Sections 4.5 and 4.6. In order to fulfil  $k_1 > k_2$ , the following must hold true assuming the two legs are rigid rods with identical geometry and inertial properties with  $\ell_1 = \ell_2 = \ell_3 = \ell_4$  (see Appendix B)

$$\frac{b - c + \sqrt{(c - b)^2 + 4ad}}{2d} < k_1 < \frac{b - c - \sqrt{(c - b)^2 + 4ad}}{2d} \quad (4.15)$$

where the constants  $a$ ,  $b$ ,  $c$  and  $d$  are defined in Appendix B.

- 5) Using the result from Step 5, condition (ii) in (4.11) implies that

$$\left. \frac{\partial p}{\partial x_1} \right|_{x_1^+} = \frac{j_{21} + j_{22}k_1}{j_{11} + j_{12}k_1} =: k_2 \text{ where } j \text{ defined in (2.43).}$$

Therefore, we have

$$m\alpha_m (x_1^+)^{m-1} + \cdots + \alpha_1 = k_2. \quad (4.16)$$

- 6) Solve

$$X \begin{bmatrix} \alpha_m \\ \alpha_{m-1} \\ \vdots \\ \alpha_0 \end{bmatrix} = \begin{bmatrix} x_1^+ \\ x_1^- \\ k_1 \\ k_2 \end{bmatrix} \quad (4.17)$$

for  $\alpha_m, \dots, \alpha_0$ , where,

$$X := \begin{bmatrix} x_1^{-m} & x_1^{-m-1} & \cdots & x_1^- & 1 \\ x_1^{+m} & x_1^{+m-1} & \cdots & x_1^+ & 1 \\ mx_1^{-m-1} & (m-1)x_1^{-m-2} & \cdots & 1 & 0 \\ mx_1^{+m-1} & (m-1)x_1^{+m-2} & \cdots & 1 & 0 \end{bmatrix} \in \mathbb{R}^{4 \times (m+1)}$$

It is noted that the above design procedure is valid for polynomials of degree  $m \geq 3$ .

**Proposition 4.3.4.** *When  $m \geq 3$ , system (4.17) is solvable if and only if  $X$  is full row rank.*

*Proof.* **Case**  $m = 3$ . In this case, the  $X$  matrix is square and written as,

$$X := \begin{bmatrix} x_1^{-3} & x_1^{-2} & x_1^- & 1 \\ x_1^{+3} & x_1^{+2} & x_1^+ & 1 \\ 3x_1^{-2} & 2x_1^- & 1 & 0 \\ 3x_1^{+2} & 2x_1^+ & 1 & 0 \end{bmatrix}. \quad (4.18)$$

The determinant of  $X$  is  $\det(X) = -(x_1^- - x_1^+)^4$  and, clearly,  $X$  is non-singular if and only if  $x_1^- \neq x_1^+$ . Therefore, system (4.17) is solvable if and only if  $x_1^- \neq x_1^+$ .

**Case**  $m > 3$ . Based on the above argument, if  $x_1^- \neq x_1^+$ , then  $X$  is full row-rank and a right-inverse exists for  $X$ . As a result, system (4.17) is solvable if and only if  $x_1^- \neq x_1^+$ .  $\square$

It is noted that for  $m > 3$  there exist infinitely many polynomials  $p$  that satisfy conditions (4.11) since right inverse of  $X$  is not unique. Next, we discuss more cases where the proposed design procedure is not applicable.

**Case**  $m = 2$ . In this case, the above design procedure is not applicable since there are 3 unknowns and 4 equations. Therefore, the designer cannot choose  $k_1$ . Instead, Equations (4.14) and (4.16) combine into one non-linear equation in the parameters, which needs to be solved simultaneously with (4.12) and (4.13).

**Case**  $m = 1$ . Finally, the conditions (4.11) cannot be fulfilled since  $m = 1$  would imply that  $k_1 = k_2 = \alpha_1$ , which conflicts the reset map,  $J$ , of the system.

---

**Example 4.3.1.** This example uses the above design procedure in order to come up with a polynomial of degree 3,  $p(x_1) = \alpha_3 x_1^3 + \alpha_2 x_1^2 + \alpha_1 x_1 + \alpha_0$ , that satisfies (4.11). The goal is to find the correct coefficients  $\alpha_3, \dots, \alpha_0$ . The slope of the ground is taken to be  $2.5^\circ$ .

- 1) Pick  $x_1^- = -0.400$  rad, which represents the angular position of the stance leg at which the stance leg hits the ground. Then,  $x_2^- = 0.400 - (2)(2.5)(\pi/180) = 0.313$  rad. Now, using the definition of the reset map  $J$ , we have  $x_1^+ = x_2^- = 0.313$  rad.
- 2) We now form Equation (4.12):  $(-0.400)^3 \alpha_3 + (-0.400)^2 \alpha_2 - 0.400 \alpha_1 + \alpha_0 = 0.313$
- 3) We now form Equation (4.13):  $0.313^3 \alpha_3 + 0.313^2 \alpha_2 + 0.313 \alpha_1 + \alpha_0 = -0.400$

4) Choose  $k_1 = 1$ . The constants  $a = 5.22, b = -1.86, c = 16.0$  and  $d = -1.56$  imply that

$$\frac{b - c + \sqrt{(c - b)^2 + 4ad}}{2d} = 0.300$$

$$\frac{b - c - \sqrt{(c - b)^2 + 4ad}}{2d} = 11.2$$

and, therefore  $\frac{b-c+\sqrt{(c-b)^2+4ad}}{2d} < k_1 < \frac{b-c-\sqrt{(c-b)^2+4ad}}{2d}$ . As a result, we form Equation (4.14) as  $(3)(-0.400)^2\alpha_3 + (2)(-0.400)\alpha_2 + \alpha_1 = 1$ .

5) Given the values of  $x_1^-$  and  $x_2^-$ , calculation the entries of the  $j$  matrix results in  $j_{11} = 0.715, j_{12} = -0.0694, j_{21} = 0.233$  and  $j_{22} = -0.0829$ . Then,  $k_2 = 0.232$  resulting in Equation (4.16)  $(3)(0.313)^2\alpha_3 + (2)(0.313)\alpha_2 + \alpha_1 = 0.232$

6) The coefficients  $\alpha_3, \dots, \alpha_0$  are computed using

$$\begin{bmatrix} (-0.400)^3 & (-0.400)^2 & -0.400 & 1 \\ 0.313^3 & 0.313^2 & 0.313 & 1 \\ (3)(-0.400)^2 & (2)(-0.400) & 1 & 0 \\ (3)(0.313)^2 & (2)(0.313) & 1 & 0 \end{bmatrix} \begin{bmatrix} \alpha_3 \\ \alpha_2 \\ \alpha_1 \\ \alpha_0 \end{bmatrix} = \begin{bmatrix} 0.313 \\ -0.400 \\ 1 \\ 0.232 \end{bmatrix}.$$

Also,  $\det(X) = -0.258$  implies that  $X$  is invertible. Solving the above expression for the parameters, we get

$$\begin{bmatrix} \alpha_3 \\ \alpha_2 \\ \alpha_1 \\ \alpha_0 \end{bmatrix} = \begin{bmatrix} 6.36 \\ 0.294 \\ -1.82 \\ -0.0546 \end{bmatrix}.$$

Finally, the polynomial becomes

$$p(x_1) = 6.36x_1^3 + 0.294x_1^2 - 1.82x_1 - 0.0546,$$

which satisfies (4.11).

△

## 4.4 State transformation

So far we have developed the notion of hybrid VHCs. The ultimate goal is to enforce a given hVHC. For the 2-DOF bipedal robot, we introduce a new set of states that when

nulled, enforce a given hVHC. We arrive at these new states by applying an appropriate state transformation map,  $T : \mathbb{R}^4 \rightarrow \mathbb{R}^4$ , as follows.

Consider the following output functions to the continuous dynamics of (4.8)  $h_1 : \mathbb{R}^4 \rightarrow \mathbb{R}$  and  $h_2 : \mathbb{R}^4 \rightarrow \mathbb{R}$  such that,

$$\begin{aligned} h_1(x) &:= x_2 - p(x_1) \\ h_2(x) &:= x_1 \end{aligned} \tag{4.19}$$

where  $h_1$  is hVHC.

**Proposition 4.4.1.** *The continuous-time dynamics of the 2-DOF bipedal robot (4.8) with output (4.19) yields a well-defined vector relative degree of  $\{2, 2\}$  for all  $x \in \mathbb{R}^4$ .*

*Proof.* The system has 2 inputs and 2 outputs. Simple calculations reveal

$$\begin{aligned} L_{g_1} h_1(x) &= \frac{\partial h_1}{\partial x} g_1 \\ &= 0 \\ L_{g_1} L_f h_1(x) &= -\frac{1}{\det(M)} \left( \frac{\partial p}{\partial x_1} M_{22} + M_{21}(x) \right) \end{aligned}$$

and,

$$\begin{aligned} L_{g_2} h_1(x) &= \frac{\partial h_1}{\partial x} g_2 \\ &= 0 \\ L_{g_2} L_f h_1(x) &= \frac{1}{\det(M)} \left( \frac{\partial p}{\partial x_1} (M_{12}(x) + M_{22}) + M_{11} + M_{21}(x) \right) \end{aligned}$$

Similarly for  $h_2(x)$ ,

$$\begin{aligned} L_{g_1} h_2(x) &= 0 \\ L_{g_1} L_f h_2(x) &= \frac{1}{\det(M)} M_{22} \end{aligned}$$

and,

$$\begin{aligned} L_{g_2} h_2(x) &= 0 \\ L_{g_2} L_f h_2(x) &= -\frac{1}{\det(M)} (M_{12}(x) + M_{22}) \end{aligned}$$

Now, define

$$A_2(x) := \begin{bmatrix} L_{g_1} L_f h_1(x) & L_{g_2} L_f h_1(x) \\ L_{g_1} L_f h_2(x) & L_{g_2} L_f h_2(x) \end{bmatrix} \in \mathbb{R}^{2 \times 2} \quad (4.20)$$

The determinant of  $A_2(x)$  is evaluated as,  $\det(A_2) := M_{12}^2(x) - M_{11}M_{22}$ . To show that  $A_2(x)$  is non-singular, its determinant is shown not to equal zero for all  $x \in \mathbb{R}^4$ . Assume there exists  $x \in \mathbb{R}^4$  such that  $\det(A_2) = 0$ . This implies that,

$$\begin{aligned} M_{12}^2(x) &= M_{11}M_{22} \quad (\text{by setting } \det(A_2) = 0 \text{ and simplifying}) \\ \Rightarrow \cos^2(x_2 - x_1) &= \frac{M_{11}M_{22}}{(m_2 \ell \ell_3)^2}. \end{aligned}$$

From the proof of Propositions 3.2.1 and 4.3.1 we have,

$$\frac{M_{11}M_{22}}{(m_2 \ell \ell_3)^2} > 1 \quad \forall x \in \mathbb{R}^4.$$

Therefore,

$$\det(A_2) \neq 0 \quad \forall x \in \mathbb{R}^4$$

This implies that, for all  $x \in \mathbb{R}^4$ ,  $A_2(x)$  is full rank. Therefore, the relative degree of the systems is  $\{r_1, r_2\} = \{2, 2\}$ .  $\square$

Since the continuous dynamics of (4.8) with output functions (4.19) have a vector relative degree such that  $r_1 + r_2 = 4$ , then for every  $x_0 \in \mathbb{R}^4$  the transformation (4.21) is a diffeomorphism of a neighbourhood of  $x_0$  onto its image.

$$T(x) = \begin{bmatrix} h_1(x) \\ L_f h_1(x) \\ h_2(x) \\ L_f h_2(x) \end{bmatrix} = \begin{bmatrix} x_2 - p(x_1) \\ x_4 - \frac{\partial p(x_1)}{\partial x_1} x_3 \\ x_1 \\ x_3 \end{bmatrix} \quad (4.21)$$

The next theorem imposes necessary and sufficient conditions that result in a transformation  $T(x)$  to be a global diffeomorphism. The proof of the theorem is given in [42] and [43].

**Theorem 4.4.2** ([40]). *A transformation  $T(x)$  is a global diffeomorphism if and only if*

- (i)  $\frac{\partial T}{\partial x}$  is non-singular for all  $x \in \mathbb{R}^n$ , and

$$(ii) \lim_{\|x\| \rightarrow \infty} \|T(x)\| = \infty.$$

**Proposition 4.4.3.** *Given relations (4.19), transformation (4.21) is a global diffeomorphism.*

*Proof.* We show that (4.21) satisfies the conditions in Theorem 4.4.2.

$$\frac{\partial T}{\partial x} = \begin{bmatrix} -\frac{\partial p}{\partial x_1} & 1 & 0 & 0 \\ -\frac{\partial^2}{\partial x_1^2} p(x_1) x_3 & 0 & -\frac{\partial p}{\partial x_1} & 1 \\ 1 & 0 & 0 & 0 \\ 0 & 0 & 1 & 0 \end{bmatrix} \text{ and } \det \left( \frac{\partial T}{\partial x} \right) = -1.$$

Therefore,  $\frac{\partial T}{\partial x}$  is non-singular for all  $x \in \mathbb{R}^4$ . Also the 2-norm of  $T(x)$  is,

$$\|T(x)\|_2 = \sqrt{x_1^2 + x_3^2 + (x_2 - p(x_1))^2 + \left(x_4 - \frac{\partial p}{\partial x_1} x_3\right)^2}.$$

Since  $p$  is a polynomial, then  $|x_1| < \infty$  implies  $|p(x_1)| < \infty$  and  $dp(x_1) < \infty$ . Then, we necessarily have,

$$\lim_{\|x\|_2 \rightarrow \infty} \|T(x)\|_2 = \lim_{\|x\|_2 \rightarrow \infty} \sqrt{\left(x_1^2 + x_3^2 + (x_2 - p(x_1))^2 + \left(x_4 - \frac{\partial p}{\partial x_1} x_3\right)^2\right)} = \infty$$

As a result, the conditions of Theorem 4.4.2 are met and, hence, relation (4.21) is a global diffeomorphism.  $\square$

In order to come up with the new states, let

$$(\xi, \eta) := T(x) = \begin{bmatrix} x_2 - p(x_1) \\ x_4 - \frac{\partial p(x_1)}{x_1} x_3 \\ x_1 \\ x_3 \end{bmatrix} \quad (4.22)$$

where  $(\xi, \eta) = \text{col}(\xi_1, \xi_2, \eta_1, \eta_2) \in \mathbb{R}^4$  is the new state vector. Throughout the thesis, the term “ $\xi$ -dynamics” refers to the dynamics of  $\xi_1$  and  $\xi_2$ , and the term “ $\eta$ -dynamics” refers

to the dynamics of  $\eta_1$  and  $\eta_2$ . In addition, the inverse mapping of (4.22) is given by

$$x = T^{-1}(\xi, \eta) = \begin{bmatrix} \eta_1 \\ \xi_1 + p(\eta_1) \\ \eta_2 \\ \xi_2 + \frac{\partial p(\eta_1)}{\partial \eta_1} \eta_2 \end{bmatrix} \quad (4.23)$$

In the  $(\xi, \eta)$ -coordinates, the 2-DOF robot reads

$$\text{EL}_{\mathcal{H}} : \begin{cases} (\dot{\xi}, \dot{\eta}) = \hat{f}(\xi, \eta) + \hat{g}(\xi, \eta)\tau & \text{if } (\xi, \eta) \notin \hat{\mathcal{S}} \\ (\xi^+, \eta^+) = \hat{J}(\xi, \eta) & \text{if } (\xi, \eta) \in \hat{\mathcal{S}} \end{cases} \quad (4.24)$$

where,

- $\hat{f} : \mathbb{R}^4 \rightarrow \mathbb{R}^4$  such that  $\hat{f} = \frac{\partial T}{\partial x} f(x) \Big|_{x=T^{-1}(\xi, \eta)}$ ,
- $\hat{g} : \mathbb{R}^4 \rightarrow \mathbb{R}^{4 \times 2}$  such that  $\hat{g} = [\hat{g}_1, \hat{g}_2]$  with  $\hat{g}_1 = \frac{\partial T}{\partial x} g_1(x) \Big|_{x=T^{-1}(\xi, \eta)}$  and  $\hat{g}_2 = \frac{\partial T}{\partial x} g_2(x) \Big|_{x=T^{-1}(\xi, \eta)}$ ,
- $\hat{J}(\xi, \eta) := T(J(x)) \Big|_{x=T^{-1}(\xi, \eta)}$ , and
- $\hat{\mathcal{S}} = T(\mathcal{S}) \Big|_{x=T^{-1}(\xi, \eta)} = \{(\xi, \eta) \in \mathbb{R}^4 : \xi_1 = -p(\eta_1) - \eta_1 - 2\gamma\}$

Note that

$$\hat{J}(\xi, \eta) = \begin{bmatrix} \eta_1 - p(\xi_1 + p(\eta_1)) \\ \eta_2 \hat{j}_{21} + \left( \xi_2 + \frac{\partial p(\eta_1)}{\partial \eta_1} \eta_2 \right) \hat{j}_{22} - \frac{\partial p(\eta_1)}{\partial \eta_1} \left( \eta_2 \hat{j}_{11} + \left( \xi_2 + \frac{\partial p(\eta_1)}{\partial \eta_1} \eta_2 \right) \hat{j}_{12} \right) \\ \xi_1 + p(\eta_1) \\ \eta_2 \hat{j}_{11} + \left( \xi_2 + \frac{\partial p(\eta_1)}{\partial \eta_1} \eta_2 \right) \hat{j}_{12} \end{bmatrix} \quad (4.25)$$

where  $\hat{j}_{ij} = j_{ij} \Big|_{(\xi, \eta)=T^{-1}(x)}$ ,  $i, j \in \{1, 2\}$  with  $j_{ij}$  are entries of  $j$  defined in (2.43).

In these new coordinates, the hVHC  $h_1$  is enforced by nulling  $\xi_1$  and  $\xi_2$ , which serves as the main control objective. In other words, the hVHC to be enforced in the  $(\xi, \eta)$ -coordinates reads,

$$\hat{h} = \xi_1 \quad (4.26)$$

Then, the constrain manifold in  $(\xi, \eta)$ -coordinates become,

$$\hat{\Gamma} := \{(\xi, \eta) \in \mathbb{R}^4 : \xi_1 = 0 \text{ and } \xi_2 = 0\} \quad (4.27)$$

The next objective is to enforce (4.27) through feedback linearization (Sections 4.5 and 4.6).

## 4.5 Feedback linearization yielding a fully actuated closed-loop configuration

In this section, the 2-DOF bipedal robot is feedback linearized resulting in fully actuated closed-loop configuration where the continuous dynamics of system (4.8) are decoupled. This generates two decoupled linear double-integrators each with an auxiliary control input. The resulting  $\xi$ -dynamics are regulated by an auxiliary linear control law. For the  $\eta$ -dynamics, the auxiliary control input is used to let  $\eta_1(t)$  track a desired trajectory  $\eta_1^{\text{ref}}(t)$ . In other words, by regulating the  $\xi$ -dynamics we enforce the hVHC  $h_1$ , and by letting  $\eta_1(t)$  track a reference trajectory we essentially let  $\theta_{st}$  to track a desired trajectory. The discrete dynamics of (4.29) remain coupled. Finally, sufficient conditions are proposed that guarantee stability for the hybrid  $\xi$ -dynamics. In this context, it is worth pointing that some attempts have been made to linearize the discrete-time dynamics of a walking robot using feedback [24].

Consider the following feedback linearizing control input

$$\tau = A_2^{-1}(x)|_{x=T^{-1}(\xi,\eta)} \begin{bmatrix} -L_f^2 h_1(x)|_{x=T^{-1}(\xi,\eta)} + v_1 \\ -L_f^2 h_2(x)|_{x=T^{-1}(\xi,\eta)} + v_2 \end{bmatrix} \quad (4.28)$$

where  $v_{1,2} \in \mathbb{R}$  are the two auxiliary inputs. With (4.28), system (4.24) becomes

$$(\dot{\xi}, \dot{\eta}) = \begin{bmatrix} \xi_1 \\ v_1 \\ \eta_1 \\ v_2 \end{bmatrix} \quad \text{if } (\xi, \eta) \notin \hat{\mathcal{S}}, \quad (4.29)$$

$$(\xi^+, \eta^+) = \hat{J}(\xi, \eta) \quad \text{if } (\xi, \eta) \in \hat{\mathcal{S}}.$$

It is noted that there always exists a  $\tau$  that satisfies (4.28) since output functions (4.19) yield vector relative degree of  $\text{col}(2, 2)$  (see Proposition 4.4.1), which implies that  $A_2(x)$  is always invertible by definition.

### 4.5.1 Simulation results

The controller (4.28) was tested through numerical simulation on the system (4.8) with  $v_{1,2}$  being two auxiliary controllers of the form,

$$\begin{aligned} v_1 &= -K_{D_1} \xi_1 - K_{P_1} \xi_2 \\ v_2 &= -K_{D_2} e_\eta - K_{P_2} \dot{e}_\eta + \ddot{\eta}_1^d \end{aligned} \quad (4.30)$$

where  $e_\eta(t) := \eta_1(t) - \eta_1^{\text{ref}}(t)$ . The desired trajectory,  $\eta_1^{\text{ref}}(t)$ , is selected to be the trajectory of the stance leg performing a passive gait.

The gains  $K_{P_1}$  and  $K_{D_1}$  are designed to generate an over-damped subsystem (damping ratio = 1.11) with a relatively fast settling time ( $\approx 0.25$  sec) for the  $\xi$ -dynamics. In addition,  $K_{P_2}$  and  $K_{D_2}$  are designed such that the  $\eta_1$  quickly tracks  $\eta_1^{\text{ref}}$ . Table 4.1 shows the values of the gains used in simulations.

Table 4.1: Values of gains in Equation (4.30).

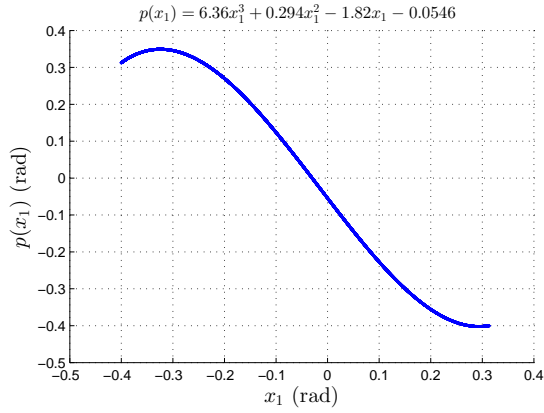
$K_{P_1}$	$K_{D_1}$	$K_{P_2}$	$K_{D_2}$
200	31.3	30	9

VHC and hVHC were generated separately and used in simulations. Figures 4.2, 4.3 and 4.5 illustrate the results. Figure 4.2a shows a degree-3 polynomial that satisfies (4.11). This polynomial was carefully designed using the procedure of Section 4.3.1. The gait generated using this polynomial is shown in leg coordinates (Figure 4.2b).

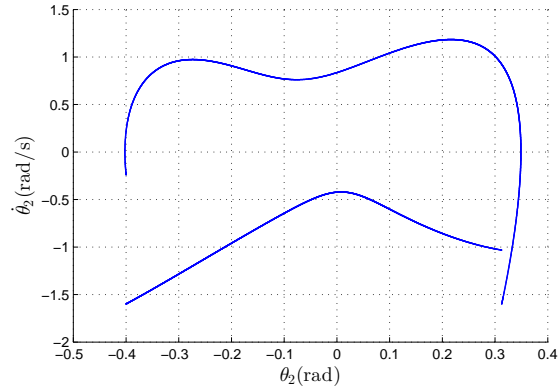
Figure 4.3 shows the regulation of the  $\xi$ -dynamics based on three distinct controllers. Figure 4.3a shows the regulation result based on a controller that utilizes a VHC. At impact events, the controller is not able to maintain invariance of the constraint manifold. In Figure 4.3b,  $\xi_1$  is regulated during the continuous phase but gently jumps off-zero at ground collision points. In this case,  $p$  was generated by *approximating* a passive gait shape and, hence, generating a VHC; not a hVHC. A virtual constraint that perfectly models the shape of a passive gait is a hVHC since passive gaits are naturally invariant. Finally, Figure 4.3c shows that these jumps in  $\xi_1$  at ground collisions are vanished. In this case, a hVHC is carefully designed by using the polynomial of Figure 4.2a.

It is noted that a hVHC defined in the sense of Definition 4.2.1 under Assumption 3 with  $p$  satisfying (4.11) does not necessarily imply closed-loop invariance under the  $\eta$ -dynamics. Figure 4.5 illustrates this fact. Figure 4.5 shows the tracking of  $\eta_1$  with a VHC-based (approximating a passive gait shape) controller and a hVHC-based controller. This figure reveals the fact that  $\eta_1$  is almost able to track  $\eta_1^{\text{ref}}$  in the case of a controller utilizing a polynomial  $p$  that approximates the passive gait. Tracking is slightly lost at impact events. On the other hand, tracking is lost at impact points when using polynomial  $p$  that satisfies (4.11). The invariance of the  $\eta$ -dynamics under hVHC-based controllers presented in this thesis still remain an open question and needs further investigation.

Since the 2-DOF bipedal robot under study has feet, its important to ensure the ZMP

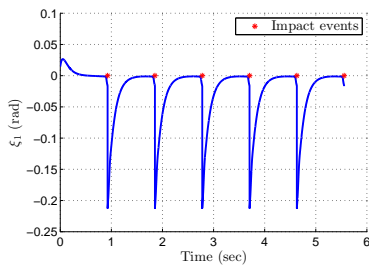


(a) Polynomial  $p$  satisfying (4.11).

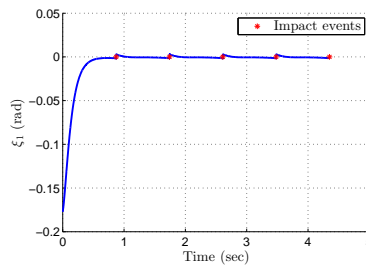


(b) The resulting HLC in leg coordinates.

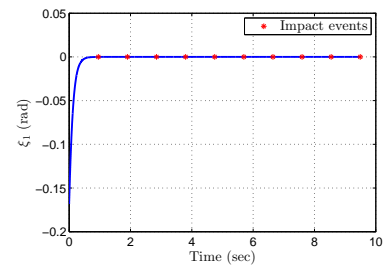
Figure 4.2: A  $p$  polynomial satisfying (4.11) results in a gait pattern not necessarily the same as the passive gait pattern.



(a) Regulation of  $\xi_1$  using a VHC (not satisfying the conditions in (4.11)).



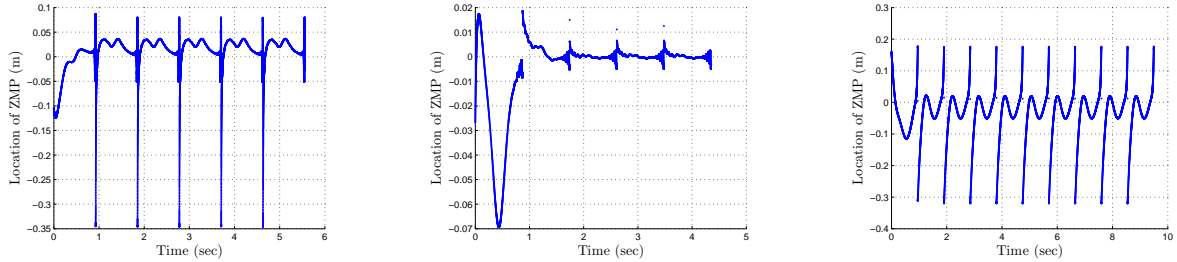
(b) Regulation of  $\xi_1$  using a VHC that approximates a passive gait.



(c) Regulation of  $\xi_1$  using a hVHC (satisfying the conditions in (4.11)).

Figure 4.3: The regulation of  $\xi_1$  using a VHC based controller, VHC approximating passive-gait based controller and a hVHC based controller.

to stay within the area of the foot in contact with ground. Figure 4.4 shows the location of the ZMP for different closed-loop configurations.



(a) The ZMP of the simulation of Figure 4.3a. (b) The ZMP of the simulation of Figure 4.3b. (c) The ZMP of the simulation of Figure 4.3c.

Figure 4.4: Location of the ZMP for the fully actuated closed-loop configuration utilizing different constraints.

Finally, the increased region of attraction (of the passive gait) due to control effort can be seen in Figure 4.6. In this simulation,  $p$  approximates a passive gait shape.

## 4.5.2 Stability analysis

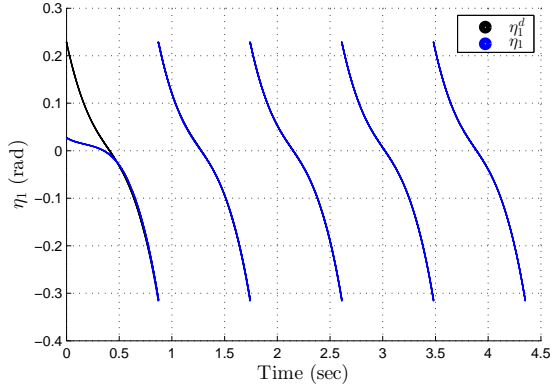
Consider the following definition.

**Definition 4.5.1** (Open ball in  $\mathbb{R}^n$ ). Let  $\tilde{x}$  be a point that belongs to  $\mathbb{R}^n$ . Then, the set  $B_r(\tilde{x}) := \{x \in \mathbb{R}^n : \|x - \tilde{x}\| < r\}$  is called an **open ball** of radius  $r$  centred at  $\tilde{x}$ .

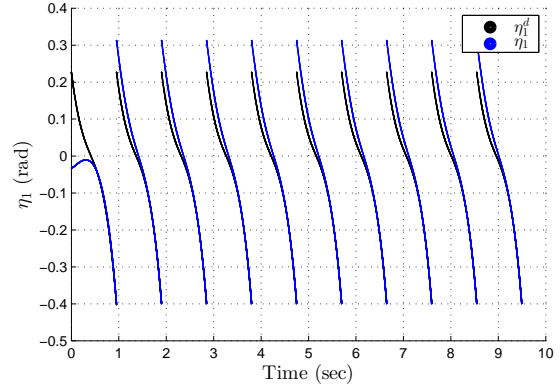
The stability of the  $\xi$ -dynamics for system (4.29) under the control law (4.28) is studied through the following proposition.

**Proposition 4.5.2.** Consider system (4.29). Define the point  $(\xi_\star^-, \eta_\star^-) \in \mathbb{R}^4$  such that  $(\xi_\star^-, \eta_\star^-) \in \hat{\mathcal{S}}$  and  $(\xi_\star^-, \eta_\star^-) \in \hat{\Gamma}$ . Assume that the polynomial  $p$  satisfy (4.11). Assume the auxiliary control input  $v_1$  in (4.29) yields an exponentially stable linear second order closed-loop system for the continuous  $\xi$ -dynamics with damping ratio  $> 1$ . Then, system (4.29) is asymptotically stable if

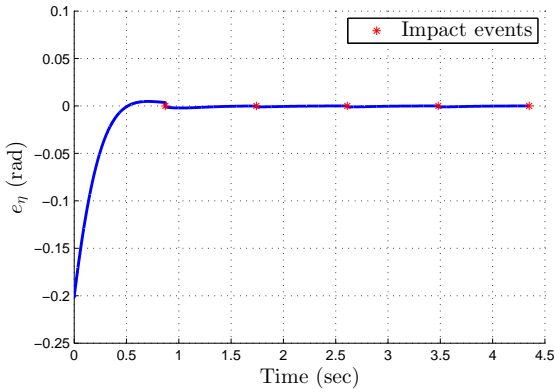
$$\left. \frac{\partial p(\eta_1)}{\partial \eta_1} \right|_{\eta_{1\star}^-} > \left. \frac{\partial p(\eta_1)}{\partial \eta_1} \right|_{\eta_{1\star}^+} \quad (4.31)$$



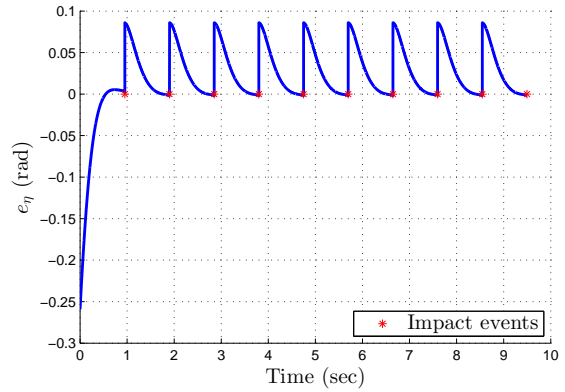
(a) Tracking results for  $\eta_1$  with  $p$  approximating a passive gait.



(b) Tracking results for  $\eta_1$  with a  $p$  satisfies (4.11), which is shown in Figure 4.2a.

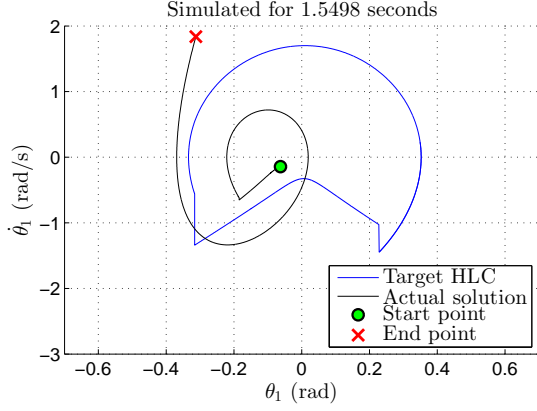


(c) Tracking error using a polynomial  $p$  that approximates a passive gait.

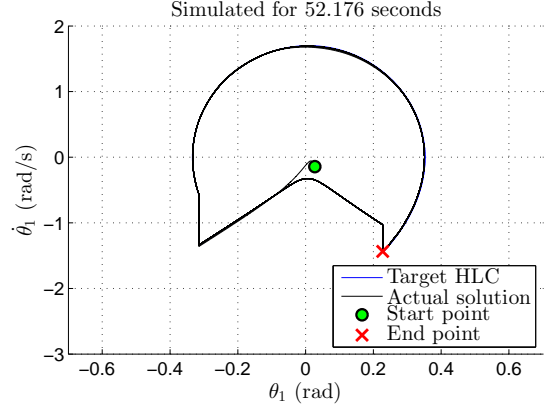


(d) Tracking error using a polynomial  $p$  satisfying (4.11), which is shown in Figure 4.2a.

Figure 4.5: This figure shows the tracking of  $\eta_1$  to  $\eta_1^{\text{ref}}$ , which *approximates* a passive gait.



(a) Without control effort.



(b) Full actuation control effort.

Figure 4.6: The controller increases the region of attraction of the passive HLC.

*Proof.* The discrete map  $\hat{J}$  is continuous since  $p$  is continuous. The continuity of  $\hat{J}$  implies that for all  $\epsilon > 0$ , there exists  $\delta > 0$ , for all  $(\tilde{\xi}, \tilde{\eta}) \in \mathbb{R}^4$  such that  $(\xi, \eta) \in B_\delta(\tilde{\xi}, \tilde{\eta}) \Rightarrow J(\xi, \eta) \in B_\epsilon(\tilde{\xi}, \tilde{\eta})$ . Then, we can write

$$\begin{aligned} \eta_1^- \in B_\delta(\eta_{1\star}^-) &\Rightarrow \hat{J}(\eta_1^-) \in B_\epsilon(\hat{J}(\eta_{1\star}^-)) \quad (\text{by continuity of } \hat{J}) \\ &\Rightarrow \eta_1^+ \in B_\epsilon(\eta_{1\star}^+) \quad (\text{by definition of } \hat{J}) \end{aligned} \quad (4.32)$$

where  $\epsilon$  is an arbitrarily small quantity. Similarly,

$$\xi_1^- \in B_\delta(0) \Rightarrow \xi_1^+ \in B_\epsilon(0).$$

Now,

$$\xi_1^- = -\eta_1^- - p(\eta_1^-) - 2\gamma \quad (\text{since } (\xi^-, \eta^-) \in \hat{\mathcal{S}}).$$

Since  $\eta_1^- \in B_\delta(\eta_{1\star}^-)$  with  $\delta$  arbitrarily small, we can linearize  $p(\eta_1^-)$  about  $\eta_{1\star}^-$  as  $p(\eta_1^-) \approx p(\eta_{1\star}^-) + \frac{\partial p(\eta_1)}{\partial \eta_1} \Big|_{\eta_{1\star}^-} (\eta_1^- - \eta_{1\star}^-)$ . This implies,

$$\xi_1^- \approx -\eta_1^- \left( 1 + \frac{\partial p(\eta_1)}{\partial \eta_1} \Big|_{\eta_{1\star}^-} \right) - p(\eta_{1\star}^-) + \frac{\partial p(\eta_1)}{\partial \eta_1} \Big|_{\eta_{1\star}^-} \eta_{1\star}^- - 2\gamma.$$

But,

$$p(\eta_{1\star}^-) = -\eta_{1\star}^- - 2\gamma \quad (\text{since } (\xi_{1\star}^-, \eta_{1\star}^-) \in \hat{\mathcal{S}} \text{ and } (\xi_{1\star}^-, \eta_{1\star}^-) \in \hat{\Gamma}).$$

Therefore,

$$\xi_1^- \approx -\eta_1^- \left( 1 + \frac{\partial p(\eta_1)}{\partial \eta_1} \Big|_{\eta_{1\star}^-} \right) + \eta_{1\star}^- \left( 1 + \frac{\partial p(\eta_1)}{\partial \eta_1} \Big|_{\eta_{1\star}^-} \right) \quad (I)$$

Now we have,

$$\begin{aligned} \xi_1^+ &= \eta_1^- - p(\xi_1^- + p(\eta_1^-)) && \text{(by definition of } \hat{J}) \\ &= \eta_1^- - p(\eta_1^+) && \text{(by definition of } \hat{J}) \\ &= -p(\eta_1^-) - \xi_1^- - 2\gamma - p(\eta_1^+) && \text{(since } (\xi^-, \eta^-) \in \hat{\mathcal{S}}) \\ &= -\eta_1^+ - 2\gamma - p(\eta_1^+) && \text{(by definition of } \hat{J}) \\ \therefore \xi_1^+ &= -\eta_1^+ - p(\eta_1^+) - 2\gamma && \text{(i)} \end{aligned}$$

Since continuity implies  $\eta_1^+ \in B_\epsilon(\eta_{1\star}^+)$ , we can similarly linearize  $p(\eta_1^+)$  about  $\eta_{1\star}^+$  and write

$$\xi_1^+ \approx -\eta_1^+ \left( 1 + \frac{\partial p(\eta_1)}{\partial \eta_1} \Big|_{\eta_{1\star}^+} \right) - p(\eta_{1\star}^+) + \frac{\partial p(\eta_1)}{\partial \eta_1} \Big|_{\eta_{1\star}^+} \eta_{1\star}^+ - 2\gamma \quad \text{(ii)}$$

Noting that since  $p$  satisfies (4.11) and  $(\xi_\star^-, \eta_\star^-) \in \hat{\Gamma}$  by assumption, then

$$\begin{aligned} \xi_{1\star}^+ &= \eta_{1\star}^- - p(\xi_{1\star}^- + p(\eta_{1\star}^-)) && \text{(by definition of } \hat{J}) \\ &= \eta_{1\star}^- - p(p(\eta_{1\star}^-)) && \text{(since } (\xi_\star^-, \eta_\star^-) \in \hat{\Gamma}) \\ &= \eta_{1\star}^- - \eta_{1\star}^- && \text{(since } p \text{ satisfies (4.11) by assumption)} \\ &\equiv 0 \end{aligned}$$

Then, Equation (i) implies

$$p(\eta_{1\star}^+) = -\eta_{1\star}^+ - 2\gamma \quad \text{(iii)}$$

Substituting Equation (iii) into (ii), we arrive at

$$\xi_1^+ \approx -\eta_1^+ \left( 1 + \frac{\partial p(\eta_1)}{\partial \eta_1} \Big|_{\eta_{1\star}^+} \right) + \eta_{1\star}^+ \left( 1 + \frac{\partial p(\eta_1)}{\partial \eta_1} \Big|_{\eta_{1\star}^+} \right)$$

But,

$$\begin{aligned} \eta_{1\star}^+ &= p(\eta_{2\star}^-) && \text{(by definition of } \hat{J} \text{ with } (\xi_\star^-, \eta_\star^-) \in \hat{\Gamma}) \\ &= -\eta_{1\star}^- - 2\gamma && \text{(by definition of } \hat{\mathcal{S}}) \end{aligned}$$

and,

$$\begin{aligned}
\eta_1^+ &= -\xi_1^+ - p(\eta_1^+) - 2\gamma && \text{(by Equation (i))} \\
&= -\eta_1^- + p(\xi_1^- + p(\eta_1^-)) - p(\eta_1^+) - 2\gamma && \text{(by definition of } \hat{J} \text{)} \\
&= -\eta_1^- + p(\eta_1^+) - p(\eta_1^+) - 2\gamma && \text{(by definition of } \hat{J} \text{)} \\
&= -\eta_1^- - 2\gamma
\end{aligned}$$

Therefore,

$$\xi_1^+ \approx - \left( -\eta_1^- \left( 1 + \frac{\partial p(\eta_1)}{\partial \eta_1} \Big|_{\eta_{1\star}^-} \right) + \eta_{1\star}^- \left( 1 + \frac{\partial p(\eta_1)}{\partial \eta_1} \Big|_{\eta_{1\star}^+} \right) \right) \quad (II)$$

Since  $\frac{\partial p(\eta_1)}{\partial \eta_1} \Big|_{\eta_{1\star}^-} > \frac{\partial p(\eta_1)}{\partial \eta_1} \Big|_{\eta_{1\star}^+}$  by hypothesis, then (I) and (II) imply

$$|\xi_1^+| < |\xi_1^-| \quad (III)$$

Inequality (III) with the assumption made on  $v_1$  imply asymptotic stability of (4.29)  $\square$

## 4.6 Feedback linearization yielding an under-actuated closed-loop configuration

This section discusses under-actuation of the 2-DOF bipedal robot represented by the  $(\xi, \eta)$ -coordinates. Consider the feedback-linearizing input

$$\tau = [A_1^+(x) (v - L_f^2 h_1(x))]_{x=T^{-1}(\xi, \eta)} \quad (4.33)$$

where  $v$  is the auxiliary control input and  $A_1^+$  is a pseudo-inverse of  $A_1$ . Then, system (4.8) becomes

$$(\dot{\xi}, \dot{\eta}) = \begin{bmatrix} \xi_1 \\ v \\ \eta_1 \\ \nu(\xi, \eta) \end{bmatrix} \quad \text{if } (\xi, \eta) \notin \hat{\mathcal{S}}, \quad (4.34)$$

$$(\xi^+, \eta^+) = \hat{J}(\xi, \eta) \quad \text{if } (\xi, \eta) \in \hat{\mathcal{S}}$$

where  $\nu(\xi, \eta) = L_f^2 h_2(x)_{x=T^{-1}(\xi, \eta)} + [L_{g_1} L_f h_2(x), L_{g_2} L_f h_2(x)] (A_1^+(v - L_f^2 h_1(x))) \Big|_{x=T^{-1}(\xi, \eta)}$ . Clearly, the  $\xi$ -dynamics can be regulated by a PD auxiliary controller,

$$v = -K_D \xi_1 - K_P \xi_2 \quad (4.35)$$

The settling time is chosen to be  $\approx 0.400$  (sec) and the damping ratio is chosen to be  $\approx 0.707$  yielding an under-damped system. Those requirements need the gains to have values shown in Table 4.2.

Table 4.2: Values of gains in Equation (4.35).

$K_P$	$K_D$
200	20

Once  $\xi$ -dynamics are regulated,  $\eta$ -dynamics are left uncontrolled. It is noted that there always exists a  $\tau$  that satisfies (4.33) since the VHC (4.9) is shown to be regular everywhere and, hence, the matrix  $A_1^+$  is always full rank (see Proposition 4.3.1).

This controller was tested numerically using VHCs and hVHCs separately. Figure 4.8 illustrates regulation of the state  $\xi_1$  using a hVHC (i.e. polynomial  $p$  satisfying (4.11)) and a VHC (i.e. polynomial  $p$  not satisfying (4.11)). Figure 4.7 shows a polynomial of degree 6 generated by the design procedure of Section 4.3.1.

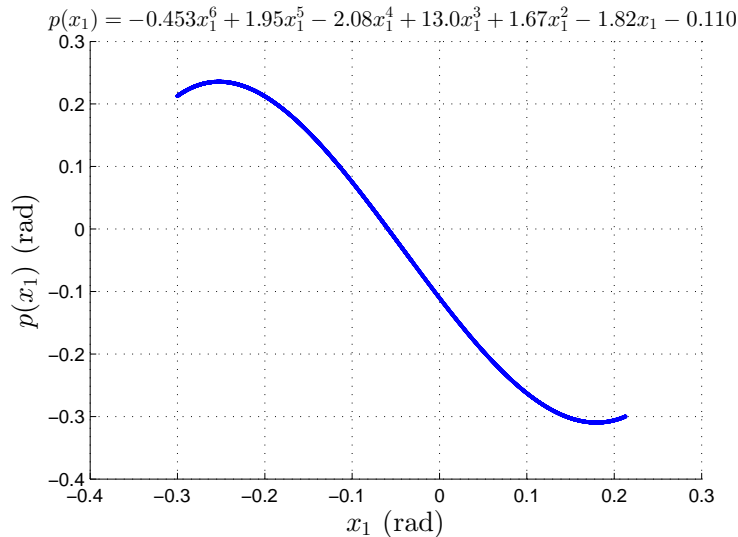


Figure 4.7: The polynomial  $p$  satisfying (4.11).

It is clear from Figure 4.8 that the control input (4.33) enforces the hVHC whereas the same input (4.33) is unable to enforce the VHC at impact events. Although the  $\xi$ -dynamics

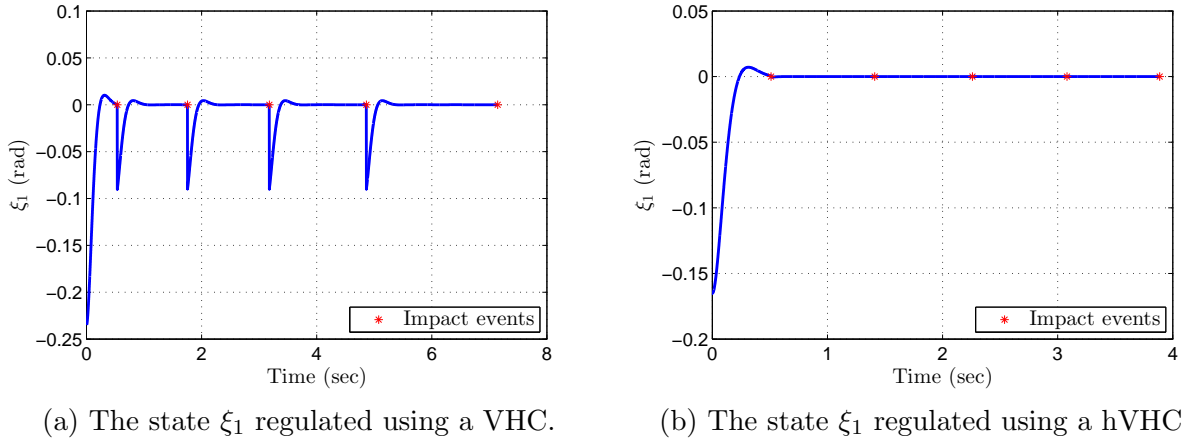


Figure 4.8: The regulation of  $\xi_1$  using a VHC-based controller and a hVHC-based controller.

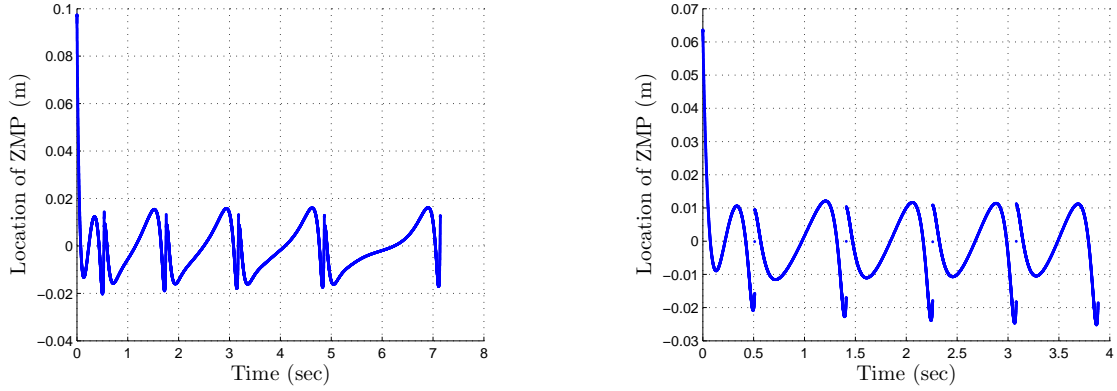
are regulated, the 2-DOF bipedal robot might not perform a gait since the  $\eta$ -dynamics are left uncontrolled. This motivates the study of stability properties of the  $\eta$ -dynamics on the set  $\hat{\Gamma}$  (4.27), which is the subject of the next subsection. Finally, Figure 4.9 shows the corresponding location of the ZMP of the simulations depicted in Figure 4.8.

### 4.6.1 Stability study

This subsection presents a numerical argument to study stability properties on the set  $\hat{\Gamma}$ . Once  $(\xi, \eta) \in \hat{\Gamma}$ , i.e.  $\xi$ -dynamics are regulated, the following hold true.

1.  $(\xi, \eta) \in \hat{\Gamma} (\equiv x \in \Gamma)$ ,
2.  $v = 0$ , and
3. the 1-DOF  $\eta$ -dynamics are left uncontrolled.

Given an initial condition  $(\xi_0, \eta_0) \in \mathbb{R}^4$  which does not belong to  $\hat{\Gamma}$ , Figure 4.10 shows all possible behaviours of the  $\eta$ -dynamics once solutions approach  $\hat{\Gamma}$ . The phase portrait of the zero dynamics on  $\hat{\Gamma}$  is divided into three regions. Region 1 is where the robot starts by walking downhill with relatively high negative velocity. The robot keeps losing fraction of its velocity after every impact until the solution approaches the stable hybrid limit cycle (shown in thick black curve). Region 2 is where the robot starts with a relatively low speed



(a) The ZMP of the simulation of Figure 4.8a. (b) The ZMP of the simulation of Figure 4.8b.

Figure 4.9: The regulation of  $\xi_1$  using a VHC-based controller and a hVHC-based controller.

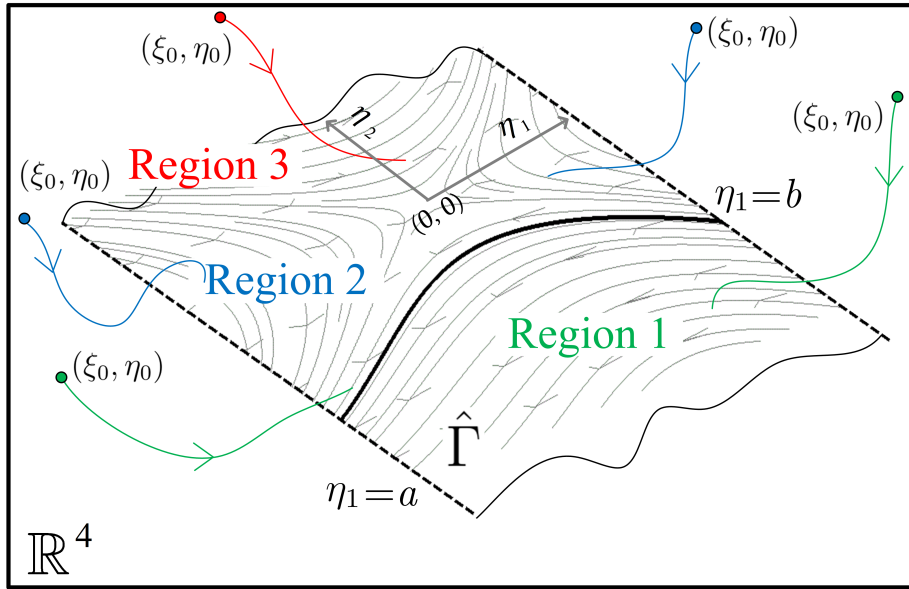


Figure 4.10: The dynamics on  $\hat{\Gamma}$  are divided into three regions. Region 1 yield stable solutions whereas Region 2 yields marginally stable solutions. Region 3 could lead to stable or marginally stable solutions.

and keeps going back and forth until it loses all its energy due to impacts and eventually stops still. Region 3 is where the robot starts with a relatively high positive velocity causing it to go in reverse direction. Solutions in Region 3 have two possible behaviours. Energy losses due to impacts may derive a solution to the hybrid limit cycle (Region 3(a)). Else, impacts may cause a solution to approach the same fixed point of Region 2 (Region 3(b)). Figures 4.11 and 4.12 illustrate all possible behaviours given a solution that belongs to  $\hat{\Gamma}$ .

To study stability of the  $\eta$ -dynamics on  $\hat{\Gamma}$ , we follow the context of Section 3.2.1. Let the gait be designed such that the points  $\eta_1 = a$  and  $\eta_1 = b$ , with  $b > a$ , be the two points where ground impact event occurs (Figure 4.10). Then, consider the following section,

$$\hat{S} = \{(\xi, \eta) \in \hat{\Gamma} : \eta_1 - b = 0\} \quad (4.36)$$

**Proposition 4.6.1.** *The section (4.36) is a local section for the vector field of (4.34) restricted to  $\hat{\Gamma}$ .*

*Proof.* The vector field of (4.34) restricted to  $\hat{\Gamma}$  is

$$f_{\hat{\Gamma}} := \text{col}(0, 0, \eta_1, \nu(\xi, \eta))$$

Also, the Jacobian of the equation defining (4.36) is

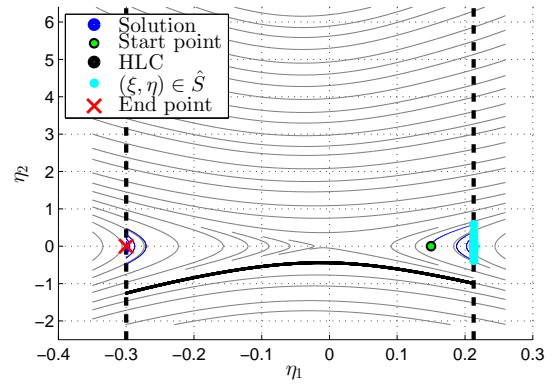
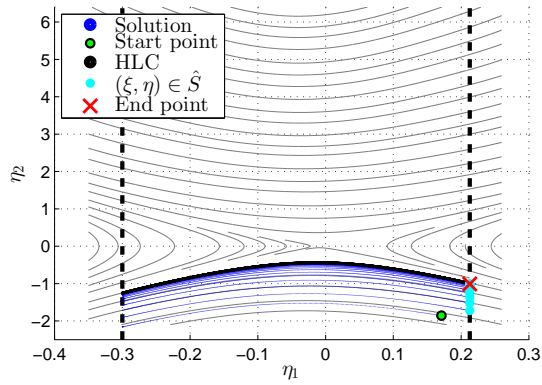
$$\hat{n} := [0, 0, 1, 0]$$

Therefore,

$$\hat{n} \cdot f_{\hat{\Gamma}} = \eta_1$$

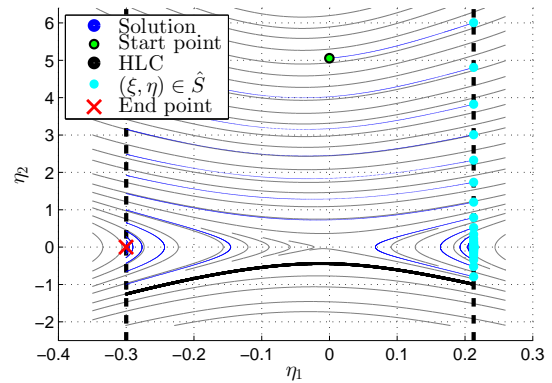
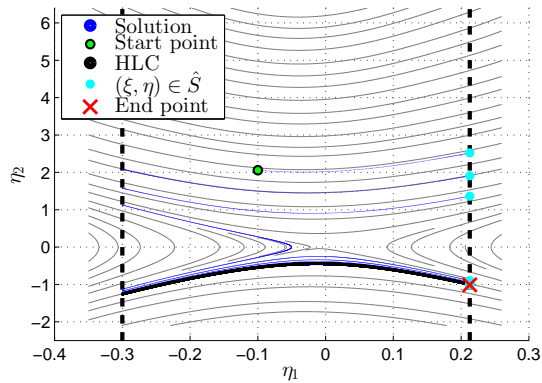
As a result, the section  $\hat{S}$  is not tangent to the vector field  $f_{\hat{\Gamma}}$  as long as  $\eta_1 \neq 0$ . Then,  $\hat{S}$  is a local section by definition.  $\square$

The Poincaré map on  $\hat{S}$ , denoted  $\mathbf{g} : \hat{S} \rightarrow \hat{S}$ , is found numerically for solutions belonging to regions 1, 2 and 3 separately. Figure 4.13 shows  $\mathbf{g}$  and its fixed point  $\hat{p}$  for all regions. It is noted that the fixed-point of  $\mathbf{g}$  in region 1 corresponds to a hybrid limit cycle. Similarly, the fixed-point of  $\mathbf{g}$  in region 3(a) correspond to a stable gait. In region 2, the origin of  $\mathbf{g}$  is a marginally stable fixed-point. The same is true for  $\mathbf{g}$  of region 3(b). Table 4.3 shows the fixed points, their corresponding eigenvalue and their physical significance.



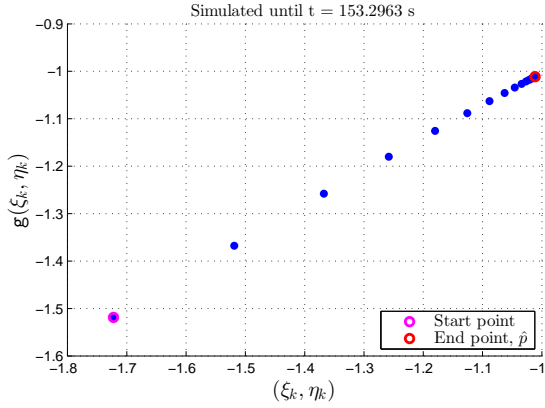
(a) Region 1: convergence to a stable hybrid limit cycle. (b) Region 2: convergence to a marginally stable still stance.

Figure 4.11: Regions 1 and 2 on  $\hat{\Gamma}$ .

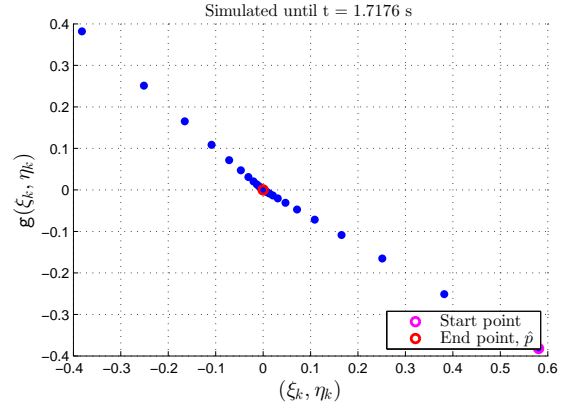


(a) Region 3(a): convergence to a stable hybrid limit cycle. (b) Region 3(b): convergence to a marginally stable still stance.

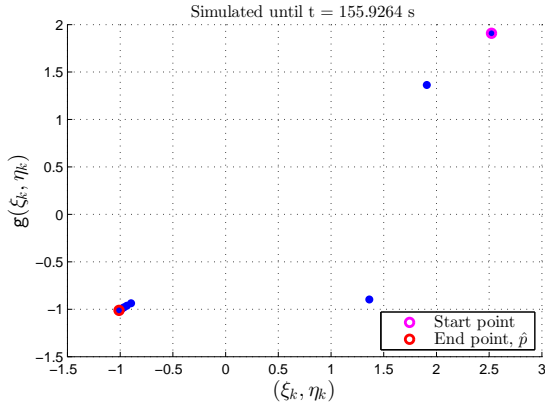
Figure 4.12: Region 3 on  $\hat{\Gamma}$ .



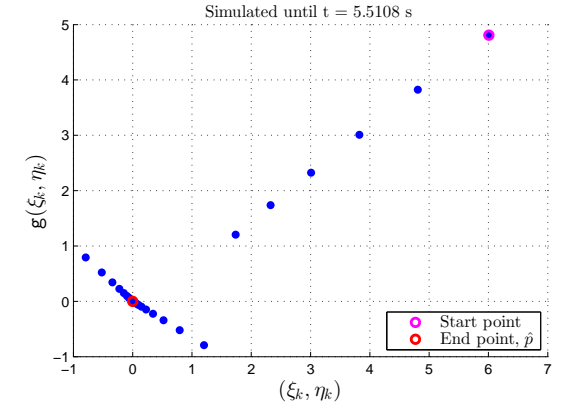
(a)  $g$  for region 1.



(b)  $g$  for region 2.



(c)  $g$  for region 3(a).



(d)  $g$  for region 3(b).

Figure 4.13: Poincaré map  $g$  restricted to  $\hat{\Gamma}$  for all three regions.

Table 4.3: Eigenvalues of the linearized Poincaré map near fixed points.

	Region 1	Region 2	Region 3(a)	Region 3(b)
<b>Reported fixed-point</b>	-1.01	$-3.78 \times 10^{-7}$	-1.01	$-3.79 \times 10^{-7}$
<b>Reported eigenvalue</b>	0.663	-1.00	0.661	-1.00
<b>Physical significance</b>	HLC	stand still	HLC	stand still

## Analogy to the rimless wheel

It is of interest to note that the phase-portrait of dynamics of the 2-DOF bipedal robot restricted to  $\hat{\Gamma}$  is qualitatively similar to the phase-portrait of the rimless wheel (Figure 4.14). For a rimless wheel, an analytical expression for the Poincaré map can be found in robotics literature [44] and [45].

However, it is difficult to evaluate an analytic expression for the Poincaré map of dynamics on  $\hat{\Gamma}$  of a 2-DOF bipedal robot with controller (4.33) since the continuous flow is relatively complicated. This similarity may potentially lead to an analytic stability study for the dynamics on  $\hat{\Gamma}$  of a 2-DOF bipedal robot with controller (4.33).

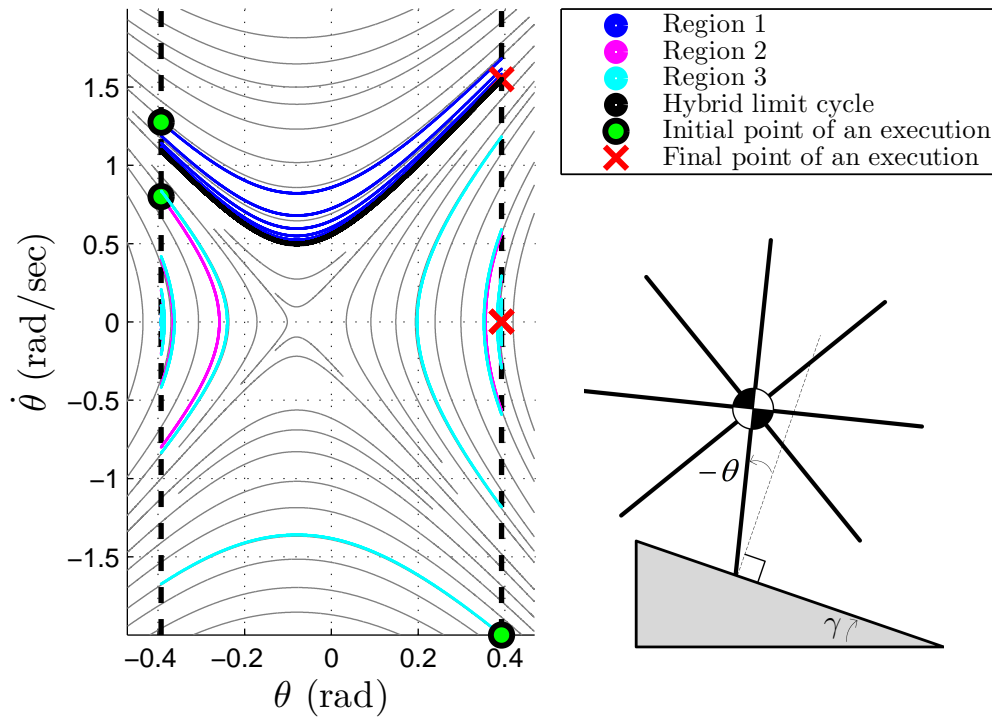


Figure 4.14: Phase-portrait of rimless wheel with solutions.

## 4.6.2 Optimal control effort

Equation (4.33) suggests that there exist infinitely many  $\tau$ 's that result in (4.34) due to the fact that  $A_1^+ \in \mathbb{R}^{2 \times 1}$  is a right inverse of  $A_1 := [A_{1_1}, A_{1_2}]$ . Dropping arguments, define  $A_1^+ := \frac{1}{A_{1_1}^2 + A_{1_2}^2} \text{col}(A_{1_1}, A_{1_2})$  to be a right inverse of  $A_1$ . Then, a general torque that results in system (4.34) is written as

$$\tau = (A_1^+ + \hat{N})(v - L_f^2 h_1) \quad (4.37)$$

where  $\hat{N} \in \ker(A_1)$ . This subsection is purposed to obtain an expression for the optimal  $\tau$ .

In this context, the method of Lagrange multipliers is used [46]. Let  $B := v - L_f^2 h_1$  and consider the minimization problem

$$\min_{\tau, A_1 \tau = B} \tau^\top P \tau \quad \text{with } P \in \mathbb{R}^{2 \times 2} \quad (4.38)$$

The Lagrangian is formed as

$$L(\tau, \lambda) = \tau^\top P \tau + \lambda^\top (A_1 \tau - B) \quad (4.39)$$

where  $\lambda$  is the Lagrange multiplier. Necessary conditions for optimality are

$$\begin{aligned} \frac{\partial L}{\partial \tau} &= 0 \\ \frac{\partial L}{\partial \lambda} &= 0 \end{aligned} \quad (4.40)$$

This leads to,

$$\begin{aligned} 2\tau^\top P + \lambda^\top A_1 &= 0 \\ A_1 \tau - B &= 0 \\ \Rightarrow \begin{bmatrix} 2P & A_1^\top \\ A_1 & 0 \end{bmatrix} \begin{bmatrix} \tau \\ \lambda \end{bmatrix} &= \begin{bmatrix} 0_{2 \times 1} \\ B \end{bmatrix} \end{aligned}$$

Solving for  $\tau$ , we get

$$\tau = A_1^+ B \quad (4.41)$$

Therefore, regardless of the weighting matrix  $P$ , the optimal torque is

$$\boxed{\tau = A_1^+ (v - L_f^2 h_1)} \quad (4.42)$$

## Hybrid VHC mimicking a passive gait

This section shows the fact that if the polynomial  $p$  is designed such that it perfectly models a passive gait, the input  $\tau$  (4.33) becomes identically zero once the dynamics belong to the passive constraint manifold. Let  $p = p^*$  be a perfect model of a passive gait. Then, the continuous dynamics of the robot undergoing a passive gait in  $(\xi, \eta)$  coordinates become

$$\begin{aligned}\dot{\xi}_1 &= \xi_2 \\ \dot{\xi}_2 &= L_f^2 h_1^* \\ \dot{\eta}_1 &= \eta_2 \\ \dot{\eta}_2 &= L_f^2 h_2\end{aligned}\tag{4.43}$$

where  $h_1^* = x_2 - p^*(x_1)$ . When the robot performs a passive gait, we have

$$\xi_2 = L_f^2 h_1^* = 0\tag{4.44}$$

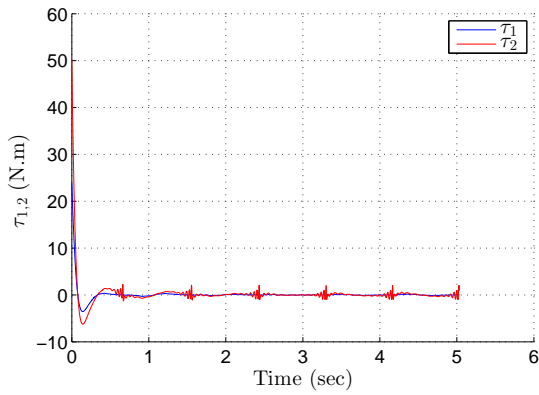
since passive gaits are invariant.

Now, consider the optimal control law  $\tau = A_1^+(v - L_f^2 h_1^*)$ . If the robot configuration variables,  $(x_1, x_2)$ , belong to the set

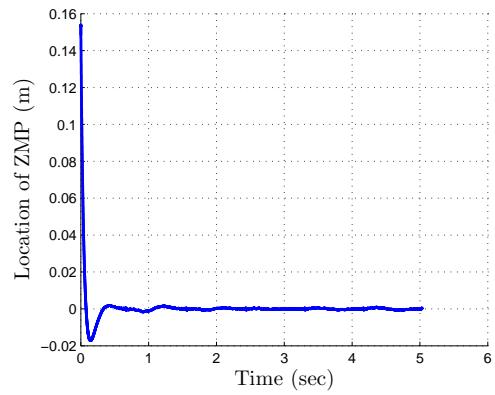
$$\Gamma^* := \{x \in \mathbb{R}^4 : h_1^*(x_1, x_2) = 0 \text{ and } dh_{1_{x_1, x_2}}^* \text{col}(x_3, x_4) = 0\}\tag{4.45}$$

then  $v = 0$ . Also,  $L_f^2 h_1^* = 0$  (Equation (4.44)). Therefore,  $\tau \equiv 0$ . In other words, as long as the hVHC mimicking a passive gait is satisfied, the controller (4.33) consumes no energy.

However, in this work, the shape of the passive gait of the 2-DOF bipedal robot was approximated numerically. Figure 4.15 shows numerical results of the input torque controller  $\tau = A_1^+(v - L_f^2 h_1^*)$ . It is noted that the input torque is initially relatively high because the point-to-set distance of  $x(0)$  from  $\Gamma^*$  is relatively high. Once the states approach  $\Gamma^*$ , then  $\tau$  drops significantly and gently fluctuates around zero.



(a) Optimal torque.



(b) The corresponding location of ZMP.

Figure 4.15: Optimal controller utilizing an approximation of the passive gait shape.

# Chapter 5

## Conclusions and future work

This thesis extended the notion of VHC to hybrid VHC of an Euler-Lagrange system with impacts. Hybrid VHC can be made invariant through feedback control. This work also presented a design procedure that returns a feasible hybrid VHC.

The ideas presented were applied to a 2-DOF bipedal robot, which was modelled as a hybrid system. The robot undergoes a continuous flow governed by a set of differential equations followed by an instantaneous change in states due to ground impact events. This instantaneous change and the ground surface constitutes the discrete dynamics of the robot, which are governed by a set of non-linear algebraic equations. The goal was to, through feedback, increase the region of attraction of a passive gait and to achieve a large family of gait shapes not necessarily mimicking a passive gait.

In the context of VHCs, the main control objective is to enforce a given hybrid VHC. To help achieving this objective, the state vector of the 2-DOF bipedal robot was transformed into a new state vector. The new state vector had the property that when two of its states are nulled, the given hybrid VHC becomes enforced.

To null those states, two feedback-linearizing closed-loop configurations were explored. The first closed-loop configuration resulted in a fully actuated system. Stability analysis was carried out which led to sufficient conditions that guarantee stability for the hybrid dynamics on the constraint manifold. The second closed-loop configuration yielded an under-actuated system. Stability analysis were carried out numerically using the method of Poincaré maps. The numerical calculation of Poicaré maps revealed two possible behaviours of the dynamics on the constraint manifold. The first behaviour resulted in convergence to a stable gait. The other behaviour showed that the robot might eventually stand still due to lose of energy caused by impact events. Finally, it was shown that if the robot states

stay in the passive constraint manifold,  $\Gamma^*$ , then the controller consumes no energy. Once the robot deviates from  $\Gamma^*$ , the controller consumes energy to “correct” it back to  $\Gamma^*$ .

### Future work

The notion of hybrid regular VHC should be extended to the most general hybrid automaton with arbitrary number of modes, guard conditions and reset maps.

The presented hybrid VHC were unable to make the  $\eta$ -dynamics invariant of the fully actuated closed-loop configuration. In fact, the author believes that the desired trajectory,  $\eta_1^{\text{ref}}$ , should satisfy certain conditions in order to guarantee invariance under controller (4.28).

Also, it is worth to extend the stability analysis for the under-actuated closed loop system (4.34) beyond numerical analysis. In the view of [19] and [2], the integral of motion for the zero dynamics of (4.34) could potentially be solved for the state  $\eta_2$ . This could lead to an expression of  $\eta_2$  in terms of  $\eta_1^-$  and  $\eta_2^-$ . Together with the discrete dynamics constrained to  $\hat{\Gamma}$ , the expression of  $\eta_2^+$  on  $\hat{\Gamma}$  could be utilized to show that  $|\eta_{2_{k+1}}^+| < |\eta_{2_k}^+|, k \in \mathbb{Z}_+$ , which could potentially lead to a stability proof. In addition, the analogy of the phase-portrait of the rimless wheel and the constraint manifold of the under-actuated closed-loop configuration of the 2-DOF bipedal robot can also be potentially utilized to analytically study stability of (4.34) on the constraint manifold  $\hat{\Gamma}$ .

The proposed controllers do not influence the ZMP. The author believes that these controllers should be modified so that they also force the ZMP to remain within a desired range.

Another aspect to extend this work is to remove the ankle torque from the robot resulting in an under-actuated model with only hip torque. In this case, there becomes no need to keep track of the ZMP.

Robustness and disturbance rejection of the proposed controller are worth investigation. Finally, experimental validation of this work should be conducted.

# APPENDICES

# Appendix A

## Other continuous-time models found in robotics literature

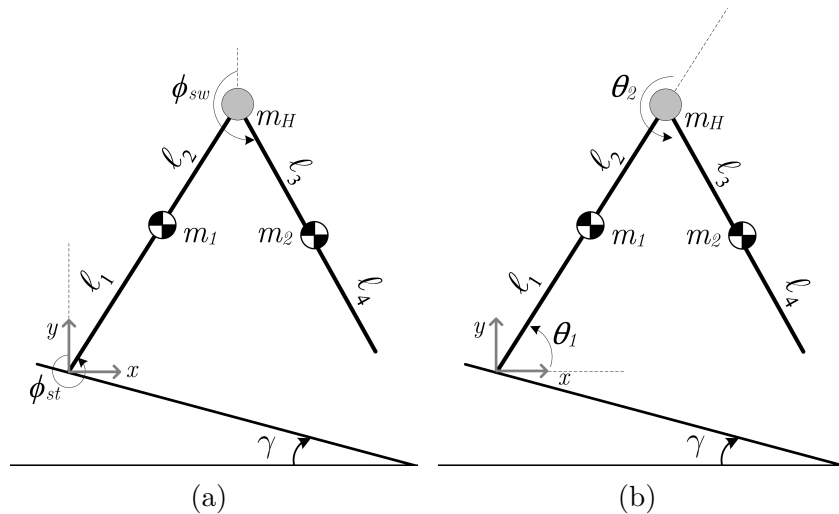


Figure A.1: Alternative models found in literature.

Figure A.1 shows a pair of models that are also commonly found in the literature. For the sake of completeness, we now show how these models are derived in relation to model (2.17).

- $(\phi_{st}, \phi_{sw})$ -coordinates (Figure A.1a)

The model in Figure A.1a can be obtained directly from (2.17) using the following

global coordinate change

$$\begin{bmatrix} \phi_{st} \\ \phi_{sw} \end{bmatrix} = \begin{bmatrix} q_1 \\ q_2 \end{bmatrix} - \begin{bmatrix} \frac{\pi}{2} \\ \frac{\pi}{2} \end{bmatrix}. \quad (\text{A.1})$$

Expressing (2.17) in  $(\phi_{st}, \phi_{sw})$ -coordinates we obtain

$$\begin{aligned} & \begin{bmatrix} m_1 \ell_1^2 + m_2 \ell^2 + m_H \ell^2 + I_1 & m_2 \ell \ell_3 \cos(\phi_{st} - \phi_{sw}) \\ m_2 \ell \ell_3 \cos(\phi_{st} - \phi_{sw}) & m_2 \ell_3^2 + I_2 \end{bmatrix} \begin{bmatrix} \ddot{\phi}_{st} \\ \ddot{\phi}_{sw} \end{bmatrix} \\ & + \begin{bmatrix} 0 & m_2 \ell \ell_3 \sin(\phi_{st} - \phi_{sw}) \dot{\phi}_{sw} \\ -m_2 \ell \ell_3 \sin(\phi_{st} - \phi_{sw}) \dot{\phi}_{st} & 0 \end{bmatrix} \begin{bmatrix} \dot{\phi}_{st} \\ \dot{\phi}_{sw} \end{bmatrix} \\ & + \begin{bmatrix} -[m_1 g \ell_1 + m_H g \ell + m_2 g \ell] \sin(\phi_{st}) \\ -m_2 g \ell_3 \sin(\phi_{sw}) \end{bmatrix} = \begin{bmatrix} 1 & -1 \\ 0 & 1 \end{bmatrix} \begin{bmatrix} \tau_1 \\ \tau_2 \end{bmatrix} \end{aligned} \quad (\text{A.2})$$

- **$(\theta_1, \theta_2)$ -coordinates (Figure A.1b)**

Finally, this model is derived using the relation

$$\begin{bmatrix} q_1 \\ q_2 \end{bmatrix} = \begin{bmatrix} 1 & 0 \\ 1 & 1 \end{bmatrix} \begin{bmatrix} \theta_1 \\ \theta_2 \end{bmatrix}. \quad (\text{A.3})$$

Substituting (A.3) in (2.17), we get

$$\begin{aligned} & \begin{bmatrix} m_1 \ell_1 + m_2 \ell^2 + m_2 \ell_3^2 + m_H \ell^2 & & \\ +2m_2 \ell \ell_3 \cos(\theta_2) + I_1 + I_2 & m_2 \ell_3^2 + m_2 \ell \ell_3 \cos(\theta_2) + I_2 & \\ m_2 \ell_3^2 + m_2 \ell \ell_3 \cos(\theta_2) + I_2 & & m_2 \ell_3^2 + I_2 \end{bmatrix} \begin{bmatrix} \ddot{\theta}_1 \\ \ddot{\theta}_2 \end{bmatrix} \\ & + \begin{bmatrix} -2m_2 \ell \ell_3 \sin(\theta_2) \dot{\theta}_2 & -m_2 \ell \ell_3 \sin(\theta_2) \dot{\theta}_1 \\ m_2 \ell \ell_3 \sin(\theta_2) \dot{\theta}_1 & 0 \end{bmatrix} \begin{bmatrix} \dot{\theta}_1 \\ \dot{\theta}_2 \end{bmatrix} \\ & + \begin{bmatrix} (m_1 g \ell_1 + m_H g \ell + m_2 g \ell) \cos(\theta_1) + m_2 g \ell_3 \cos(\theta_1 + \theta_2) \\ m_2 g \ell_3 \cos(\theta_1 + \theta_2) \end{bmatrix} = \begin{bmatrix} \tau_1 \\ \tau_2 \end{bmatrix} \end{aligned} \quad (\text{A.4})$$

Setting  $m_H = I_{1,2} = 0$  and rotating the reference of  $\theta_1$  by  $-\pi/2$  in Equation (A.4), we obtain the double pendulum equation of [47].

The coordinates of the bipedal robot of Figure A.1a are found in [2]. Also, it is noted that the  $(\theta_1, \theta_2)$ -coordinates in Figure A.1b are very common in robotics literature [6].

# Appendix B

## Necessary and sufficient conditions on $k_1$ resulting in $k_1 > k_2$

This appendix presents an argument that explains the statement: Equation (4.15) is a necessary and sufficient condition for  $k_1 > k_2$ .

Define the constants  $a = j_{21}\Delta^b$ ,  $b = j_{22}\Delta^b$ ,  $c = j_{11}\Delta^b$  and  $d = j_{12}\Delta^b$  where the matrix  $j$  defined in (2.43).

### Sufficiency

Consider the quadratic equation

$$\hat{m}(k_1) := dk_1^2 + (c - b)k_1 - a \quad (\text{B.1})$$

The constant  $d$  is always negative since

$$\begin{aligned} d &= j_{12}\Delta^b \\ &= J_{22}^b J_{12}^a \Delta^b \\ &= (m_1 \ell_2^2 + I_1) (I_2 - m_2 \ell_3 \ell_4) \\ &= \left( m_1 \ell_2^2 + \frac{1}{12} m_1 \ell^2 \right) \left( \frac{1}{12} m_2 \ell^2 - m_2 \ell_3 \ell_4 \right) \quad (\text{since legs are assumed to be rigid rods}) \\ &= \left( m_1 \ell_2^2 + \frac{4}{12} m_1 \ell_2^2 \right) \left( \frac{4}{12} m_1 \ell_2^2 - m_1 \ell_2^2 \right) \quad (\text{since } m_1 = m_2 \text{ and } \ell_1 = \ell_2 = \ell_3 = \ell_4 = \ell/2 \\ &\hspace{10em} \text{by assumption}) \\ &= -\frac{8}{9} m_1^2 \ell_1^4 < 0 \end{aligned}$$

$d < 0 \Rightarrow$  Equation (B.1) is concaved down. Since  $\frac{b-c+\sqrt{(c-b)^2+4ad}}{2d} < k_1 < \frac{b-c-\sqrt{(c-b)^2+4ad}}{2d}$  (by hypothesis) and  $\hat{m}(k_1)$  is concaved down, then  $\hat{m}(k_1) > 0$ . Now, we have

$$\begin{aligned}
dk_1^2 + (c-b)k_1 - a &> 0 \\
\Rightarrow \frac{a+bk_1}{c+dk_1} &< k_1 \\
\Rightarrow \frac{j_{21}+j_{22}k_1}{j_{11}+j_{12}k_1} &< k_1 \quad (\text{since } \Delta_b \neq 0, \text{ look page 32}) \\
\Rightarrow k_2 &< k_1 \quad (\text{by definition of } k_2)
\end{aligned}$$

## Necessity

We have,

$$\begin{aligned}
k_1 &> k_2 \quad (\text{by hypothesis}) \\
\Rightarrow \frac{j_{21}+j_{22}k_1}{j_{11}+j_{12}k_1} &< k_1 \quad (\text{by definition of } k_2) \\
\Rightarrow \frac{a+bk_1}{c+dk_1} &< k_1 \\
\Rightarrow dk_1^2 + (c-b)k_1 - a &> 0 \\
\Rightarrow \hat{m}(k_1) &> 0
\end{aligned}$$

The roots of  $\hat{m}(k_1)$  are  $k_1 = \frac{b-c \pm \sqrt{(c-b)^2+4ad}}{2d}$ . The roots exist since  $(c-b)^2 + 4ad > 0$ . Since roots of  $\hat{m}(k_1)$  exist,  $\hat{m}(k_1) > 0$ ,  $\hat{m}''(k_1) < 0$  and  $d < 0$ , then  $\frac{b-c+\sqrt{(c-b)^2+4ad}}{2d} < k_1 < \frac{b-c-\sqrt{(c-b)^2+4ad}}{2d}$ .

# References

- [1] R. Goebel, R. Sanfelice, and A. Teel, “Hybrid dynamical systems,” *IEEE Control Systems Magazine*, vol. 29, no. 2, pp. 28–93, 2009.
- [2] M. Maggiore and L. Consolini, “Virtual holonomic constraints for Euler-Lagrange systems,” *IEEE Transactions on Automatic Control*, vol. 58, no. 4, pp. 1001–1008, 2013.
- [3] T. McGeer, “Passive dynamic walking,” *The international journal of robotics research*, vol. 9, no. 2, pp. 62–82, 1990.
- [4] V. I. Arnold, *Mathematical methods of classical mechanics*. Springer, 1978.
- [5] J.-C. Latombe, *Robot Motion Planning: Edition en anglais*. Springer, 1991.
- [6] M. W. Spong, S. Hutchinson, and M. Vidyasagar, *Robot Modeling and Control*. John Wiley & Sons New York, 2006.
- [7] A. Tanwani, B. Brogliato, and C. Prieur, “Passivity-based observer design for a class of lagrangian systems with perfect unilateral constraints,” in *Proceedings of the 52nd IEEE Conference on Decision and Control*. IEEE, 2013, pp. 3338–3343.
- [8] T. McGeer, “Passive walking with knees,” in *IEEE International Conference on Robotics and Automation*,. IEEE, 1990, pp. 1640–1645.
- [9] —, “Passive bipedal running,” *Royal Society of London Proceedings Series B*, vol. 240, pp. 107–134, 1990.
- [10] A. Goswami, B. Thuilot, B. Espiau *et al.*, “Compass-like biped robot part i: Stability and bifurcation of passive gaits,” *Institut National De Recherche En Informatique Et En Automatique*, 1996.

- [11] A. Goswami, B. Espiau, and A. Keramane, “Limit cycles in a passive compass gait biped and passivity-mimicking control laws,” *Autonomous Robots*, vol. 4, no. 3, pp. 273–286, 1997.
- [12] A. Goswami, B. Thuilot, and B. Espiau, “A study of the passive gait of a compass-like biped robot symmetry and chaos,” *The International Journal of Robotics Research*, vol. 17, no. 12, pp. 1282–1301, 1998.
- [13] M. Vukobratović and J. Stepanenko, “On the stability of anthropomorphic systems,” *Mathematical Biosciences*, vol. 15, no. 1, pp. 1–37, 1972.
- [14] M. Vukobratović and B. Borovac, “Zero-moment point: thirty five years of its life,” *International Journal of Humanoid Robotics*, vol. 1, no. 01, pp. 157–173, 2004.
- [15] F. Asano, M. Hashimoto, N. Kamamichi, and M. Yamakita, “Extended virtual passive dynamic walking and virtual passivity-mimicking control laws,” in *IEEE International Conference on Robotics and Automation*, vol. 3. IEEE, 2001, pp. 3139–3144.
- [16] F. Asano, M. Yamakita, N. Kamamichi, and Z. Luo, “A novel gait generation for biped walking robots based on mechanical energy constraint,” *IEEE Transactions on Robotics and Automation*, vol. 20, no. 3, pp. 565–573, 2004.
- [17] E. R. Westervelt, J. W. Grizzle, C. Chevallereau, J. H. Choi, and B. Morris, *Feedback control of dynamic bipedal robot locomotion*. CRC press Boca Raton, 2007.
- [18] A. Shiriaev, J. W. Perram, and C. Canudas-de Wit, “Constructive tool for orbital stabilization of underactuated nonlinear systems: Virtual constraints approach,” *IEEE Transactions on Automatic Control*, vol. 50, no. 8, pp. 1164–1176, 2005.
- [19] A. Shiriaev, J. Perram, A. Robertsson, and A. Sandberg, “Explicit formulas for general integrals of motion for a class of mechanical systems subject to virtual constraints,” in *Proceedings of the 43rd IEEE Conference on Decision and Control*, vol. 2. IEEE, 2004, pp. 1158–1163.
- [20] J. Perram, A. Shiriaev, C. Canudas-de Wit, and F. Gognard, “Explicit formula for a general integral of motion for a class of mechanical systems subject to holonomic constraint,” in *Proceedings of the 2nd IFAC Workshop Control Methods for Lagrangian and Hamiltonian Systems*, 2003, pp. 87–92.
- [21] A. Shiriaev, A. Robertsson, J. Perram, and A. Sandberg, “Periodic motion planning for virtually constrained Euler-Lagrange systems,” *Systems & control letters*, vol. 55, no. 11, pp. 900–907, 2006.

- [22] L. B. Freidovich, U. Mettin, A. S. Shiriaev, and M. W. Spong, “A passive 2-DOF walker: hunting for gaits using virtual holonomic constraints,” *IEEE Transactions on Robotics*, vol. 25, no. 5, pp. 1202–1208, 2009.
- [23] ———, “A passive 2DOF walker: Finding gait cycles using virtual holonomic constraints,” in *Proceedings of the 47th IEEE Conference on Decision and Control*. IEEE, 2008, pp. 5214–5219.
- [24] L. Freidovich, A. Shiriaev, and I. Manchester, “Stability analysis and control design for an underactuated walking robot via computation of a transverse linearization,” in *Proceedings of the 17th IFAC World Congress, Seoul, Korea*, 2008, pp. 10–166.
- [25] J. Grizzle, G. Abba, and F. Plestan, “Asymptotically stable walking for biped robots: Analysis via systems with impulse effects,” *IEEE Transactions on Automatic Control*, vol. 46, no. 1, pp. 51–64, 2001.
- [26] B. Morris and J. Grizzle, “A restricted poincaré map for determining exponentially stable periodic in systems with impulse effects: Application to bipedal robots,” in *Proceedings of the 44th IEEE Conference on Decision and Control*. IEEE, 2005, pp. 4199–4206.
- [27] J. Grizzle, J. Hurst, B. Morris, H.-W. Park, and K. Sreenath, “Mabel, a new robotic bipedal walker and runner,” in *American Control Conference*. IEEE, 2009, pp. 2030–2036.
- [28] H. won Park, K. Sreenath, J. W. Hurst, and J. W. Grizzle, “Identification of a bipedal robot with a compliant drivetrain: Parameter estimation for control design,” *Control Systems Magazine*, 2011.
- [29] H. Park. (2010) First attempt at walking over rough ground for bipedal robot mabel. [Online]. Available: <http://youtu.be/IIWIWf4daNs>
- [30] H.-W. Park, A. Ramezani, and J. Grizzle, “A finite-state machine for accommodating unexpected large ground-height variations in bipedal robot walking,” *Robotics, IEEE Transactions on*, vol. 29, no. 2, pp. 331–345, 2013.
- [31] H. Park. (2011) 8 inch (20 cm) blind step-down experiment on bipedal robot mabel. [Online]. Available: <http://youtu.be/fFILLvOl7jo>
- [32] A. Ames, “Human-inspired control of bipedal robots,” *IEEE Transactions on Automatic Control*, vol. 59, no. 5, pp. 1115–1130, May 2014.

- [33] J. Zhang, K. H. Johansson, J. Lygeros, and S. Sastry, “Zeno hybrid systems,” *International Journal of Robust and Nonlinear Control*, vol. 11, no. 5, pp. 435–451, 2001.
- [34] C. J. Tomlin, “Hybrid systems,” University Lecture Notes, 2005.
- [35] M. Broucke, “A geometric approach to bisimulation and verification of hybrid systems,” in *Hybrid Systems: Computation and Control*. Springer, 1999, pp. 61–75.
- [36] A. Filippov, *Differential Equations with Discontinuous Righthand Sides*. Kluwer, 1988.
- [37] J. Ginsberg, *Advanced engineering dynamics*. Cambridge University Press, 1998.
- [38] M. Garcia, A. Chatterjee, A. Ruina, M. Coleman *et al.*, “The simplest walking model: Stability, complexity, and scaling,” *Journal of Biomechanical Engineering*, vol. 120, no. 2, pp. 281–288, 1998.
- [39] J. Meriam and L. Kraige, *Engineering mechanics: dynamics*. John Wiley & Sons Incorporated, 2012, vol. 2.
- [40] H. K. Khalil, *Nonlinear systems*. Prentice Hall, 2002.
- [41] M. Hirsch, R. Devaney, and S. Smale, *Differential Equations, Dynamical Systems, and Linear Algebra*, ser. Pure and Applied Mathematics. Elsevier Science, 1974.
- [42] F. Wu and C. Desoer, “Global inverse function theorem,” *IEEE Transactions on Circuits and Systems*, vol. 19, no. 2, pp. 199–201, 1972.
- [43] I. W. Sandberg, “Global inverse function theorems,” *IEEE Transactions on Circuits and Systems*, vol. 27, no. 11, pp. 998–1004, 1980.
- [44] R. L. Tedrake, “Applied optimal control for dynamically stable legged locomotion,” Ph.D. dissertation, Massachusetts Institute of Technology, 2004.
- [45] M. J. Coleman, *A stability study of a three-dimensional passive-dynamic model of human gait*. Cornell University, May, 1998.
- [46] C. Nielsen, “Robot dynamics and control,” University Lecture Notes, 2011.
- [47] H. Nijmeijer and A. Van der Schaft, *Nonlinear dynamical control systems*. Springer, 1990.